Experimental Investigation of Greenhouse Coffee Beans Drying System Using Solar Air Heater Enhanced with Reverse Absorber Flat-Plate Collector and Nanofluid coated Absorber

Merdokiyos Amare Ante

A Thesis Submitted to the Department of Mechanical Engineering

School of Mechanical, Chemical, and Materials Engineering

Presented in Partial Fulfillment of the Requirement for the Degree of Master of science in Thermal Engineering

Office of Graduate Studies

Adama Science and Technology University

June 2022

Adama, Ethiopia

Experimental Investigation of Greenhouse Coffee Beans Drying System Using Solar Air Heater Enhanced with Reverse Absorber Flat-Plate Collector and Nanofluid coated Absorber

Merdokiyos Amare Ante

Advisor: Dr. Dawit Gudeta

A Thesis Submitted to the Department of Mechanical Engineering

School of Mechanical, Chemical and Materials Engineering

Presented in Partial Fulfillment of the Requirement for the Degree of Master of science in Thermal Engineering

Office of Graduate Studies

Adama Science and Technology University

June 2022

Adama, Ethiopia

DECLARATION

I hereby declare that this Master Thesis entitled "Experimental Investigation of Greenhouse Coffee Beans Drying System Using Solar Air Heater Enhanced with Reverse Absorber Flat-Plate Collector and Nanofluid coated Absorber "is my original work. That is, it has not been submitted for the award of any academic degree, diploma or certificate in any other university. All sources of materials that are used for this thesis have been duly acknowledged through citation.

Merdokiyos Amare Ante	____________________	_____________
Name of student	Signature	Date

RECOMMENDATION

I/we, the advisor(s) of this thesis, hereby certify that I/we have read the revised version of the thesis entitled "Experimental Investigation of Greenhouse Coffee Beans Drying System Using Solar Air Heater Enhanced with Reverse Absorber Flat-Plate Collector and Nanofluid coated Absorber." prepared under my/our guidance by Merdokiyos Amare submitted in partial fulfillment of the requirements for the degree of Mater's of Science in Thermal engineering. Therefore, I/we recommend the submission of revised version of the thesis to the department following the applicable procedures.

Dr. Dawit Gudeta	______________________	_______________
Major Advisor/Supervisor	Signature	Date

APPROVAL PAGE OF M.SC. THESIS

I, the advisors of the thesis entitled "Experimental Investigation of Greenhouse Coffee Beans Drying System Using Solar Air Heater Enhanced with Reverse Absorber Flat-Plate Collector and Nanofluid coated Absorber." and developed by Merdokiyos Amare hereby certify that the recommendation and suggestions made by the board of examiners are appropriately incorporated into the final version of the thesis.

Dr. Dawit Gudeta	______________________	_______________
Major Advisor/Supervisor	Signature	Date

We, the undersigned, members of the Board of Examiners of the thesis by Merdokiyos Amare have read and evaluated the thesis entitled **"**Experimental Investigation of Greenhouse Coffee Beans Drying System Using Solar Air Heater Enhanced with Reverse Absorber Flat-Plate Collector and Nanofluid coated Absorber.**"** and examined the candidate during open defense. This is, therefore, to certify that the thesis is accepted for partial fulfillment of the requirement of the degree of Master of Science in Thermal Engineering.................................. ... ...
....

________________________	______________________	____________________
Chairperson	Signature	Date
________________________	______________________	____________________
Internal Examiner	Signature	Date
________________________	______________________	____________________
External Examiner	Signature	Date

Finally, approval and acceptance of the thesis is contingent upon submission of its final copy to the Office of Postgraduate Studies (OPGS) through the Department Graduate Council (DGC) and School Graduate Committee (SGC).

________________________	__________________	__________________
Department Head	Signature	Date
________________________	__________________	__________________
School Dean	Signature	Date
________________________	__________________	__________________
Office of Postgraduate Studies, Dean	Signature	Date

ACKNOWLEDGEMENTS

First of all, I would like to give my deepest gratitude to the almighty God for giving me the patience, courage, and strength to do this thesis. I would like to express my sincere gratitude to my advisor Dr. Dawit Gudeta for his continued support and guidance throughout this thesis work. Without his precious help, this thesis could have never achieved its current form. I would like to thank Dr. Addisu Bekele for sharing instruments and for his encouragement, suggestion, and guidance during my study. I would also like to thank Dr. Gezahegn Habtamu for his encouragement and guidance since my proposal work and Mr. Sintayhu for his help and sharing thermocouple wires. I would also like to express my deep feeling of happiness to all my families and my friends, who encourages me to finish this study with full of commitment and everyone who helped me finish this thesis. Finally, I would like to thank Adama science and technology university for giving me the chance to join the master's program with full sponsorship.

Contents

Page

LIST OF FIGURES

LIST OF TABLES

ABERRATIONS

HTF	Heat-Transfer Fluid
OSD	Open Sun Drying
PCM	Phase Changing Materials
RAFPC	Reverse Absorber Flat-Plate Collector
SAH	Solar Air Heater
SHS	Sensible Heat Storage
TES	Thermal Energy Storage
LHS	Latent Heat Storage
TCS	Thermo-Chemical Heat Storage

NOMENCLATURES

A_{ap}	Aperture area of the parabolic trough reflector (m^2)
I_b	Beam radiation (W/m^2)
η_{th}	Thermal efficiency (%)
Q_u	Useful energy (W)
Ac	Area of the cover material (m^2)
Af	Area of the concrete floor (m^2)
Ain	Cross-section area of the air inlet (m^2)
Aout	Cross-section area of the air outlet (m^2)
Ap	Area of the product (m^2)
Cpa	Specific heat of air (J/kg –K)
Cpc	Specific heat of cover material (J/kg –K)
Cpl	Specific heat of liquid (J/kg –K)
Cpp	Specific heat of product (J/kg –K)
Cpw	Specific heat of water vapour (J/kg –K)
D	Average distance between the floor and the cover (m)
Dp	Thickness of the product (m)
Fp	Fraction of solar radiation falling on the product (decimal)
H	Humidity ratio of air inside the dryer (kg/kg)
Hin	Humidity ratio of air entering the dryer(kg/kg)
Hout	Humidity ratio of the air leaving the dryer (kg/kg)
hc,c-a	Convective heat transfer between the cover and the air (W/m^2-K)
hc,f-a	Convective heat transfer between the floor cover and the air (W/m^2-K)
hc,p-a	Convective heat transfer between the product and the air (W/m^2-K)
hr,c-s	Radiative heat transfer between the cover and the sky (W/m^2-K)
hr,p-c	Radiative heat transfer between the product and the cover (W/m^2-K)
hw	Convective heat transfer between the cover and the ambient (W/m^2-K)
hD,f-g	Conductive heat transfer between the floor and the underground (W/m^2-K)
It	Incident solar radiation (W/m^2)
ka	Thermal conductivity of air (W/m-K)

kf	Thermal conductivity of floor material (W/m-K)
kc	Thermal conductivity of the cover (W/m-K)
Lp	Latent heat of vaporization of moisture from product (J/kg)
M	Moisture content of product (db, decimal)
Mdry	Annual production of dried product (kg)
Me	Equilibrium moisture content of product (db, decimal)
Mf	Mass fresh product (kg)
Mo	Moisture content of product (db,decimal)
Mp	Moisture content of dry product (db,decimal)
ma	Mass f air inside the dryer (kg)
mc	Mass of the cover (kg)
mf	Mass of floor (kg)
mp	Mass of product (kg)
Nu	Nusselt number (dimensionless)
Re	Reynolds number (dimensionless)
M	Moisture content (%)
Ta	Air Temperature in the dryer (K)
Tam	Ambient temperature (K)
Tc	Cover temperature (K)
Tf	Floor temperature (K)
Tin	Temperature of the inlet air of the dryer(K)
Tout	Temperature of the outlet air of the dryer (K)
Tp	Temperature of product (K)
Ts	Sky temperature (K)
t	Time (s)
Uc	Overall heat loss coefficient from air inside the dryer through the cover to ambient air (W/m2-K)
V	Volume of the drying chamber (m3)
Va	Air speed in the dryer (m/s)
Vin	Inlet air flow rate (m3/s)
Vout	Outlet air flow rate (m3/s)

Vw	Wind speed (m/s)
v	Air speed (m/s)
vin	Inlet air speed (m/s)
vout	Outlet air speed (m/s)
W	Width of the dryer floor (m)
W	Mass of water removed(kg)
X	exergy (J)
αc	Absorptance of the cover material(decimal)
αf	Absorptance of floor (decimal)
αp	Absorptance of product (decimal)
δc	Thickness of the cover (m)
ν	Viscosity of air (m^2/s)
σ	Stefan -Boltzmann's constant (W/m^2-K^4)
ρa	Density of air (kg/m3)
ρc	Density of the cover material (kg/m^3)
ρd	Density of the dry product (kg/m^3)
ρp	Density of the product (kg/m^3)
τc	Transmittance of the cover material(decimal)
εc	Emissivity of the cover material(decimal)
εp	Emissivity of the product (decimal)

GREEK SYMBOLS

α	Absorptance (decimal)
δc	Thickness of the cover (m)
ν	Viscosity of air (m^2/s)
σ	Stefan -Boltzmann's constant (W/m^2-K^4)
ρ	Density of air (kg/m3)
τc	Transmittance of the cover material(decimal)
εc	Emissivity of the cover material(decimal)
εp	Emissivity of the product (decimal)
η_{th}	Thermal efficiency

SUBSCRIPTS

a	Air
am	Ambient
c	Cover
ch	Charging
disch	Discharge
f	final
f	Fluid/Floor
I	initial
in	Inlet
m	Melting
out	Outlet
p	Product
pcm	phase changing material
th	Thermal

ABSTRACT

Coffee bean is one of high commodity from Ethiopia. The drying process is an important step in its production. The process is to determine the moisture level of the coffee bean which also affects the quality of the coffee. However, this process takes a long time. The drying process of coffee cherries by sun drying needs two to three weeks to produce dry coffee beans. To facilitate the drying process solar thermal system is designed. The main aim of this study is to develop and experimentally test the performance of solar greenhouse washed coffee dryer. The dryer is designed based on requirements to dry 5kg of washed coffee beans and the study set up consists of solar collector and greenhouse with their axillary components. The greenhouse consists six equally spaced tray having dimensions of 60 cm x 60cm and to enhance the out temperature of solar collector black ink with 3% concentrated nanofluid paint/coat, double pass, and reverse back reflector are used. Since coffee needs continuous drying thermal energy storage is provided to store heat and release when it is need. Tube and shell type heat exchanger is designed and manufactured to store 9 kg of paraffin wax. A comparative study of the performance of a greenhouse with and without enhanced solar collector with reverse absorber and nanofluid absorber coat and thermal energy storage was conducted, and the result shows that integrating the reverse absorber and nanofluid coted absorber collector to greenhouse increases change in inlet air temperature, thermal and exergy efficiency of the greenhouse by *an average value of 6 ℃, 7% and 0.53%, respectively. The addition of thermal energy storage reduces the air temperature fluctuation in afternoon. Washed coffee beans was dried within 16 h and 24 h, reducing the moisture content from an initial value of 61% (wet basis) to a final value of 11.6% (wet basis) and 12.1%(wet basis), in the greenhouse integrated with enhanced solar collector and solo greenhouse, respectively. The Computational Fluid Dynamics analysis was performed and their model validation lies in acceptable range. Finally, an economic analysis was carried out and the pay-back period of the dryer was found to be 2.04 years.*

Key-words: Coffee beans, Moisture level, Greenhouse, Nanofluid coated absorber, *Reverse absorber, Computational Fluid Dynamics*

CHAPTER ONE

1. INTRODUCTION

1.1 Background

We have an abundant amount of solar energy, which may be extensively used as an energy source. So among research community in the world, solar energy utilization for society has become one of the most important issues. A Solar heater is one among solar thermal systems which are extensively used for heating purposes like drying of crops, spa, winter home heating, seasoning of timber, etc. In many countries of the world, the use of solar thermal systems in the agricultural area to conserve vegetables, fruits, coffee, and, other crops have shown to be practical, economical and the responsible approach environmentally. Solar heating systems to dry food and other crops can improve the quality of the product while reducing wasted produce and traditional fuels.

In Ethiopia, the drying of agricultural products usually relies on direct exposure to sunlight. Obviously, this traditional method for the drying of agricultural products requires a long drying period and has sanitary problems that lower the quality of dried products. For mass production of agricultural products, it is essential to have a drying device or facility, but this greatly increases the cost of dried agricultural products due to high-energy consumption for the drying process.

Solar dryers are widely used in agricultural sections due to the consumption of free and clean energy, especially in countries with suitable solar radiation, and using this type of energy for drying agricultural products is increasing. For the fields with higher agricultural production (especially in summer season) this is very important to decrease the moisture content of the harvested product. Thus the waste and losses rate of the products reduces considerably. In other words, due to lack of processing systems near to the farm lands, most of the products are spoiled. Moreover, the dried products are used in other seasons when the crop is not available. Therefore, farmers try to use different processing method to solve the mentioned problems and drying could be a best solution. Due to the environmental problems caused by the dryers (which use fossil fuels as a thermal energy source), in most countries solar dryers are considered as the proper method to dry the agricultural products. Moreover, with the reduction of fossil fuel sources, the price of this type of energies is increasing and this increases the price of the product (Shariah et al., 1996).

Drying is an operation that includes heat and mass transfer rates and some processes, such as physical or chemical transformations, which in turn causes change in the quality of the results as well as the mechanism of heat and mass transfer (Purohit, et al., 2006). Cereals are consumed worldwide as staple foods. Similar to other food materials, cereals have high moisture content therefore they are prone to biological, chemical and biochemical changes. In order to prevent deterioration, moisture content needs to be reduced by drying. Likewise, coffee is highly perishable and thus drying is required to extend its shelf life (Motahayyer et al., 2018). Sun drying has been practiced since long time ago to reduce moisture content but it has several issues including difficulty to control drying conditions, requirement of large drying area, high labor cost, poor hygiene and risks of insect infestation and contamination (Zhang, 2006 and Ho et al., 2008).

Heat transfer enhancement techniques in solar air heating systems topic on the research of solar energy has become a matter of great concern due to energy crisis all over the world. The direct applications of solar energy (i.e. thermal application of solar energy) are simpler and more feasible application compared to indirect applications (i.e. photoelectric application) to generate electricity by using solar radiation. Flat plate collector is the central component of any solar air heating system (Çomakli et al., 1996). The efficiency of a solar air heating system is based on the performance of flat plate collector. Flat-plate solar collectors are the devices which absorb the solar radiation, transform it into heat, and to heat passing media (usually air, water, or oil). Flat plate solar collectors are simpler than concentrating collectors to be used in domestic and industrial needs, which are constructed with the blackened absorber to transfer the absorbed energy to the flowing medium, transparent cover to reduce convection and radiation losses to atmosphere, and back and side insulation to reduce conduction losses. Hence, the most of the research works have been focused on the performance improvement of flat plate collector. The characteristics of solar air heating systems are based on the absorber plate and its design, selective coatings, thermal insulation, tilt angle of the collector and weather condition of the locality. Several designs of solar collectors have been analyzed by the researchers to enhance the thermal behavior of solar air heater such as fin, incorporating phase changing materials, nanoparticle paints, air jet impingement etc.

The focus of this thesis is to study theoretically and/or experimentally the performance of greenhouse enhanced with reverse absorber and nanofluid coated absorber solar thermal air heater for coffee beans drying system.

1.2 Problem Statements

Coffee beans equilibrium moisture content should be 12% or less and wet coffee beans moisture content ranges 55-62% by mass. For drying 1 ton of coffee beans the amount of moisture to be removed ranges 43% to 48% which amounts from 489 to 568 kg of water. Currently in Ethiopia coffee drying system is practiced by open sun drying which takes two to three weeks to produce dry coffee beans. Moreover, large-scale production limits the use of open sun drying because it suffers from several drawbacks such as it requires long drying time and inability to control the drying process properly, uncertainties of weather, need for large areas, infection by insects and other foreign matter which leads high beans losses. This need drying system; Greenhouse integrated with solar collector dryers are more suitable in remote areas as well as local coffee beans drying. However; the output temperature from the collector is the major demerit that need to be enhanced or improved. To improve this reverse absorber flat plate collector, and Nanofluid paint/coating are used. Since coffee drying needs continues drying at day and night there must be some mechanism to store energy for night time thermal energy storage materials are used to solve this problem.

1.3 Objectives

1.3.1 General Objective

The general objective of the study is to Experimental investigation of greenhouse coffee beans drying system using solar air heater enhanced with reversed absolver plate and Nanofluid coat /paint under Adama weather condition.

1.3.2 Specific Objectives

The specific objectives of this study are

- To conduct laboratory experimentation for identifying the energy required to dry coffee beans to the desired moisture percent in a laboratory for different quantities of coffee beans.
- To study analytically and numerically the heat and mass transfer performance of a solo greenhouse coffee drying system under Adama weather condition.
- To study analytically and numerically the performance of greenhouse coffee drying system integrated with solar air drier with Nanofluid coated absorber and back reversed absorber plate.
- To study the experimentally performance of greenhouse coffee drying system integrated with enhanced solar air drier under Adama weather condition.

1.4 The Significance of the Research

This research has the following significance,

- Protection of the coffee product from insects, birds, dust, and rain.
- Reduction of the grand postharvest losses.
- Long-term storage without deterioration.
- Production of the hygienic marketable coffee product.

1.5 Expected outcomes

This study is expected to achieve efficient and reliable solar coffee drying system for coffee drying local companies as well as local coffee farmers.

1.6 The Scope of the Study

The scope of this study will be investigation on improve the thermal efficiency of greenhouse integrated with solar air heater by using nanofluid coat, and revere absorber flat plate. Further; to investigate numerically the performance of solar coffee beans draying system for coffee cultivated areas and obtaining the optimum parameters and to develop prototype based on optimum design parameters and finally conduct experimentation.

CHAPTER TWO

2. LITERATURE REVIEW

2.1 Introduction

A solar thermal collector collects heat by absorbing sunlight. The term "solar collector" commonly refers to a device for solar hot water heating, but may refer to large power generating installations such as solar parabolic troughs and solar towers or non-water heating devices such as solar air heaters. Solar dryers are widely used in agricultural sections due to the consumption of free and clean energy, especially in countries with suitable solar radiation, and using this type of energy for drying agricultural products is increasing (Shariah et al., 1996).

This chapter concerns about information on Greenhouse heater, Solar Air-heater, Enhancement technique, Solar dryer and thermal energy storage. In addition, previous research works on different solar air heaters, enhanced solar air heater with Nanoparticle coat, double pass, and reverse back reflector will be discussed.

2.2. Solar Air Heater (SAH)

A solar air heater (SAH) is a device that absorb solar energy from the sun by absorbing material and extracts the thermal energy by the air flowing over the surface of the absorbing material .A conventional solar air heater is essentially a flat-plate collector with a blackened absorber plate having α as absorptivity, a transparent cover having τ as a transmissivity at the top, and insulation at the bottom and on the sides. The whole assembly is encased in a sheet-metal container, and the system is referred to as a “solar flat-plate air collector.” The working fluid is air, instead of water, which is blown either below or above the absorber plate. The solar flat-plate air collector is used for the heating of living spaces and drying of crops/vegetables. Solar flat-plate air collectors are advantageous compared with other solar thermal collectors using liquid as working fluid.

The applicability of a solar air collector depends on various factors, namely, thermal efficiency, fabrication cost and installation, operational and maintenance costs, and the specific use. Solar air heaters have been extensively investigated both experiment ally as well as theoretically. A variety of geometries have been proposed to enhance the heat- transfer proper ties of the system.

2.2.1 Solar Air Heater Components

The main components of solar air heater are cover plate, absorbing plate and insulation. As the

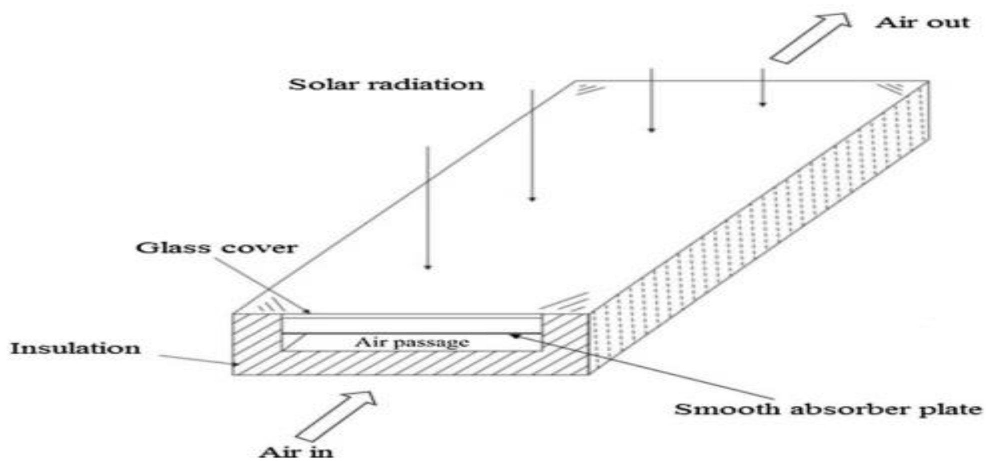

Figure 2. 1 Schematic diagram of a solar air heater (Ghritlahre et al., 2019)

solar radiation passes through the translucent cover of solar air heater, its absorbed by the absorbing plate and this absorbing plate transfers this heat to the air.

2.2.2 Factors that affect the performance of flat plate solar air heaters

The performance of flat plate solar air heaters can be affected by many factors like (Dessie ,2019):

a) Thickness of glazing.
b) Glazing material and number of glazing.
c) Air gap between plate and glazing.
d) Absorber plate coating and emissivity.
e) Ambient temperature.
f) Air flow rate.
g) Collector tilt angle.
h) Transmittance of the glazing.
i) Insulation.
j) Configuration of the collector (double pass or single pass).
k) Air flow arrangement inside the collector (parallel flow or counter flow)

Duct aspect ratio

The duct aspect ratio (W/H) is the ratio of duct width to duct height. The selection of the duct aspect ratio is depended upon many factors and mainly depended on output temperature requirement. Generally, a high duct aspect ratio causes a high heat transfer rate with a rapid increase in factor increases rapidly, which does not ensure that it would provide higher thermo hydraulic performance (Tabish and Man-Hoe ,2017).

Glass cover emissivity

Low-emissivity glass covers help to reduce the heat losses to the environment, leading to improved collector performance. Heat losses can be reduced up to 50% by using low emissivity glass covers.

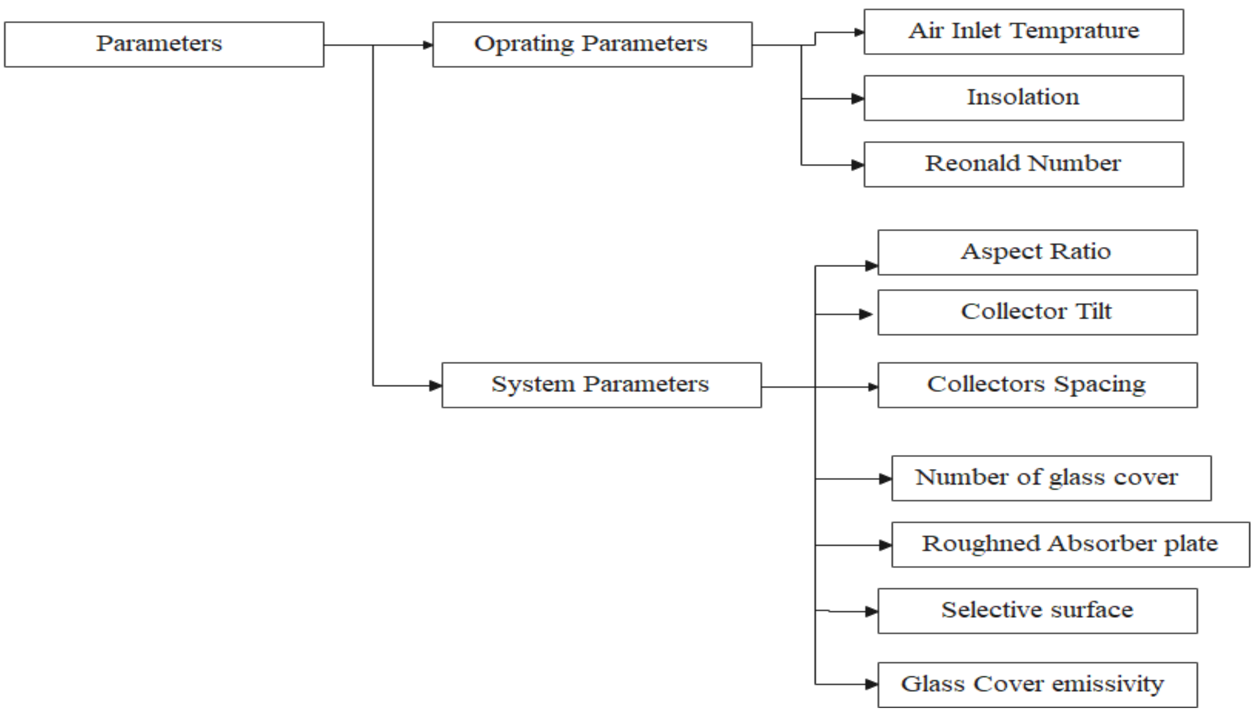

Figure 2. 2 Classification of factors affecting performance.

Collector tilt

In order to capture the maximum amount of solar energy, the tilt angle of the collector is optimized based on many factors such as location, path of sun, weather and so on. Generally, the recommended collector tilt angles for summer and winter operation are φ-(10–15°) and φ+(10–15°), respectively. For the entire year, a tilt angle of approximately 0.9 time of latitude has been recommended for maximum solar energy collection.

Collector pacing

Design of the collector is depended mainly on the requirement of output air temperature and heating capacity. Additionally, other factors are also taken into account, such as operating conditions; tilt angle and air inlet temperature. Therefore, optimized spacing between collector and glass cover is not fixed, however, typical value of spacing is used in the range of 1–6 mm (Tabish and Man-Hoe ,2017).

Number of glass covers

Thermal losses can be reduced using large number of glass cover, although, insolation reaching to absorber plate is also decreased due to decrease in overall transmittance-absorption product (ια). Selections of number of covers depend on the absorber temperature. For selective surface, one cover is sufficient for optimum performance. Two covers are recommended for non-selective surfaces (Tabish and Man-Hoe ,2017).

Selective surfaces

Characteristics of selective surface are to absorb maximum insolation without exhibit much more radiative losses. Selective surface is obtained by coating the layer of such materials which have high value of absorptivity and low value of emissivity without affecting the life of collector. Black chrome on bright nickel is considered to be as the best selective surface which have 0.96 absorptivity and 0.07 emissivity.

Roughened absorber

Roughness creates flow turbulence near surfaces and promotes flow mixing in low-turbulence regions, which effectively enhances the convective heat transfer coefficient and lowers the absorber plate temperature leading to lower thermal losses. Roughness also causes to increase pressure drop penalty

2.3. Classification of solar air heater

Solar dryers can be classified as high and low temperature dryers based on operating temperature, direct, indirect, mixed, greenhouse, tunnel, open sun drying and hybrid dryers based on utilization of solar energy, forced and natural convection dryers based on the mode of air flow, bare plate, single cover and double cover SAH based on the collector cover (glass), based on absorber materials as metallic nonmetallic, and matrix, according to shape of absorbing surface with slat, with porous and with fin, based on absorber flow pattern, over, under, and on both sides, based on the flow shape, single pass flow ,double pass flow ,parallel pass flow and triple pass flow, and based on application, drying, preheating, space heating and cooling(Oztop et al., 2013).

2.3.1. Classification Based on Utilization of Solar Energy

According to the utilization of solar power, the drying system is also classified into two groups; open sun drying (OSD) and controlled solar drying (Lingayat *et al*., 2020). Further controlled classified in to direct, indirect, mixed, greenhouse, tunnel, and hybrid dryers (Abdu, 2020).

2.3.1.1 Open sun drying

In open sun drying (OSD), the crop is spread in a thin layer on the ground and exposed directly to solar radiation, wind and other ambient conditions. The working principle of OSD is illustrated in Fig. 2.3. The solar radiation falling on the crop surface is partly reflected and partly absorbed. The absorbed radiation and surrounding heated air heat up the crop surface. A part of this heat is utilized to evaporate the moisture from the crop surface to the surrounding air. The part of this heat is lost through radiation (long wavelength) to the atmosphere and through conduction to the ground surface. The process of heat and mass transfer occurs simultaneously in OSD. The rate of drying depends on a number of external parameters (solar radiation, ambient temperature, wind velocity, and relative humidity) and internal parameters (initial moisture content, type of crops, crop absorptivity and mass of product per unit exposed area). (Jain and Tiwari.2003).


Figure 2. 3 Open sun drying (Wikipedia ,2021)

It is well known that the task of modeling heat transfer between crops and surrounding air in the presence of solar energy is a complex phenomenon. Several researchers have presented the various numerical models for moisture migration considering diffusion as the primary transport mechanism (Jain and Tiwari.2003).

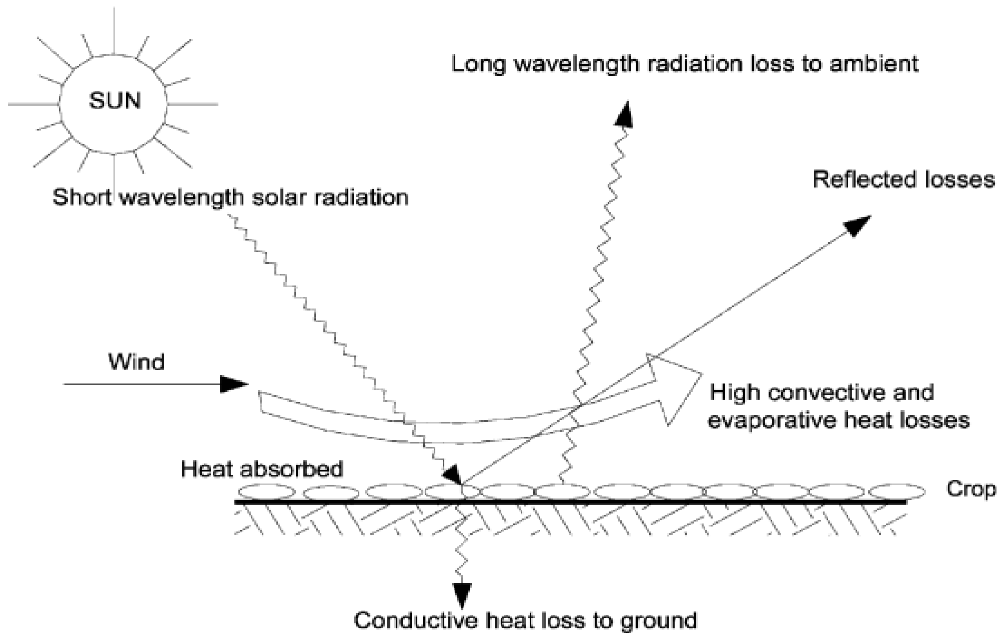

Figure 2. 4 Working principle of OSD (Jain and Tiwari.2003).

2.3.1.2 Direct solar dryers

In these systems the substance to be dehydrated is exposed to direct sunlight. The dryer consists of a cover material, drying trays and frame as shown in Figure 2.5. The dryer has inlet and outlet air vents and solar drying is assisted by the movement of the air in and out of the dryer. The products are placed at the drying trays and dried by the incoming solar radiation (Bolaji, 2005).

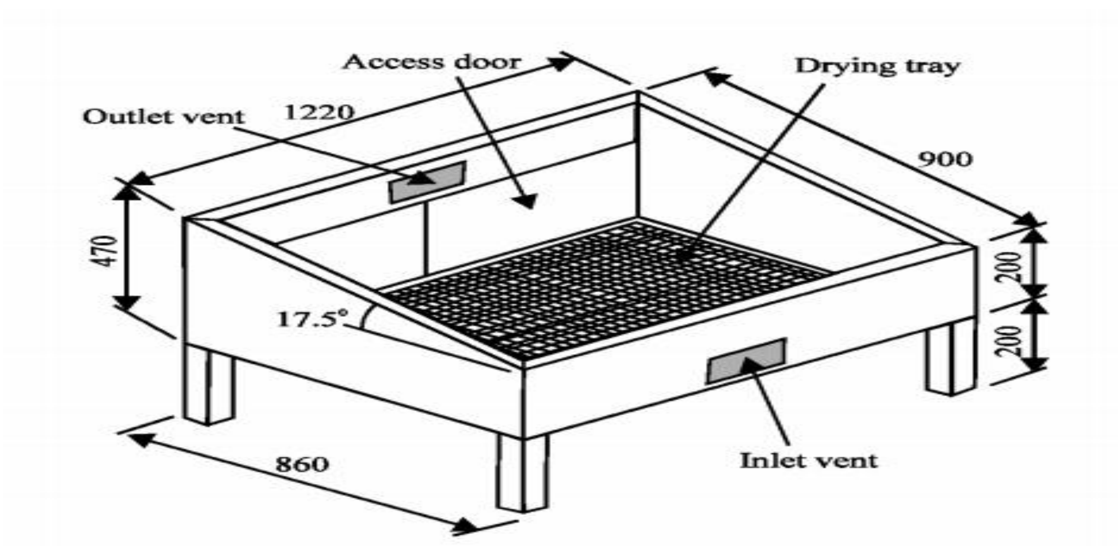

Figure 2. 5 Direct solar dryer (Bolaji, 2005)..

Tefera *et al*., (2013) evaluated the performance of a pyramidal and wooden direct solar dryer for drying potatoes and compared it to drying in the sun. The result showed that 2-3 h was saved compared to open sun drying. From the two dryers, pyramid dryer was better in creating conducive drying environment and in economic feasibility than box dryer. Similarly, Dissa *et al*., (2011) experimentally studied drying characteristics of Amelie and Brooks mangoes using a direct solar dryer with final moisture content of 24.83% and 66.32%, respectively. Results showed that, drying rate and efficiency were observed to decrease with drying time progression.

Eke and Arinze, (2011) developed a prototype natural convection direct solar dryer for drying maize. The result shows that moisture content was drop from 29% to 12% on a wet basis. The dryer diminishes 55% of drying time compared to drying in the open sun. Drying efficiency of 45.6 % and 22.7 % were found for the dryer and open sun drying, respectively. Similarly, Gbaha *et al*., (2007) designed and tested experimentally a direct, natural convection type solar dryer for drying cassava, bananas, mango. The moisture content of cassava and sweet banana reduced to 13% from 80% in 19 and 22 h, respectively. The newly developed dryer had achieved better thermal performance compared to open sun drying.

2.3.1.3. Indirect solar dryers

These dryers consist of a solar air heater with black absorber plate, a transparent cover plate, insulation and a drying chamber. The black surface heats incoming air, rather than directly heating the substance to be dried. This heated air passes through the drying chamber and exits upward often through a chimney, taking moisture released from the substance with it (Bolaji, 2005).

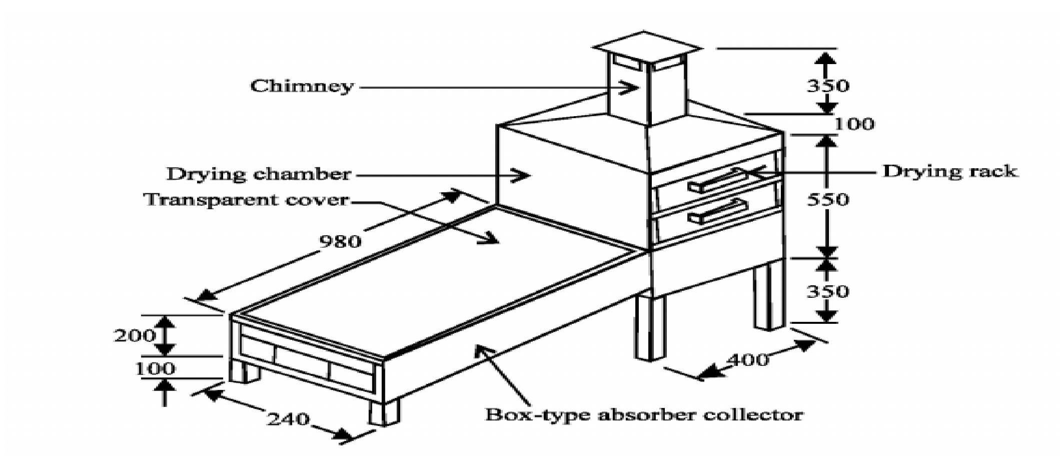

Figure 2. 6 Indirect solar dryer (Bolaji, 2005).

Hubackova *et al*., (2014) made a solar drying model for Cambodian fish species and compared it with the electric oven dryer. The solar dryer is assisted with blower. The result shows that the average drying temperature and relative humidity in the solar dryer were 55.6 ℃ and 19.9%, respectively. The overall efficiency of the solar dryer corresponding to 15% of final product moisture content was 12.37% and the average evaporative capacity of the dryer is 0.049 kg/h. It was also concluded that, the drying rates were higher in the solar drying process compared to control drying in an electric oven.

Lingayat *et al*., (2017) conducted an experiment by designing and developing indirect type solar dryer. The dryer is composed of flat plate air collector with V corrugated absorption plate, insulated drying chamber, and chimney for exhaust air. The result showed that, the average thermal efficiency of the collector and drying chamber efficiency were 31.50% and 22.38%, respectively. It was also observed that, the temperature of drying air, humidity of air and air velocity highly affect the drying rate.

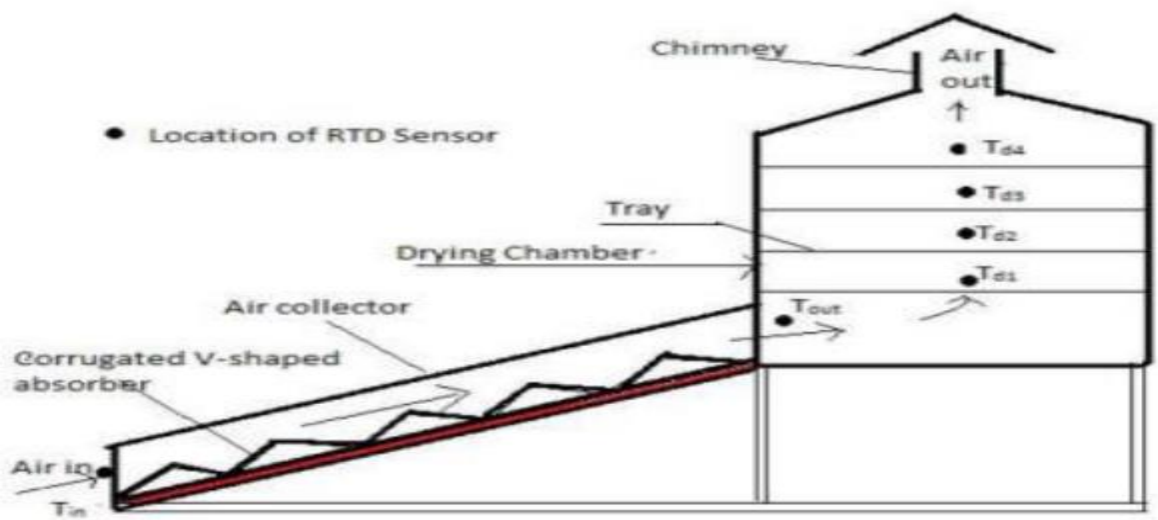

Figure 2. 7 indirect solar dryer consists of V corrugated absorption plate ***(***Lingayat et al., 2017)

Goud *et al*., (2019) developed an indirect solar dryer (ISD) for green chilli and okra and fans that operated by solar photovoltaic (PV) panels were used. The moisture content of green chilli and okra were reduced from 8.3984 and 10.1234 kg/kg (db) to 0.01001 and 0.12675 kg/kg (db) in 18 and 9 h, respectively. Solar air collector efficiency of 74.13 % and 78.30 % and drying efficiency of 9.15 % and 26.06 % were achieved for green chilli and okra, respectively. The total heat supplied to the drying chamber was 817.08 W and 885.03 W during complete drying of green chilli and okra, respectively.

Al-Juamily *et al.*, (2007) developed and tested an indirect mode forced convection solar dryer for drying fruit and vegetable. The dryer consisted of a solar collector, blower, and a solar drying cabinet. Two identical solar collectors with V-groove absorber plates and two air passes were used. Grapes, apricots and beans with initial moisture contents of 80%, 80% and 65% respectively, were dried. The result shows that the final moisture content of apricot was 13% within one day and a half of drying, 18% for grapes in two and a half days of drying and 18% for beans in 1 day only. Similarly, **Afriyie *et al.*, (2009)** experimentally tested the performance of a solar chimney crop dryer. A cabinet dryer using a normal chimney was tested first and repeated with a solar chimney and the roof of the drying chamber was inclined further to form a tent dryer to carry out the trials. The result shows that the solar chimney dryer can be designed with the appropriate angle of drying chamber roof to increase the airflow rate.

2.3.1.4. Mixed mode solar dryers

The structural features of these dryers are the same as indirect type solar dryers except that the drying chamber is made from transparent walls. The products are heated by both the solar radiation transmitted through the transparent walls and the hot air from the solar air heater.

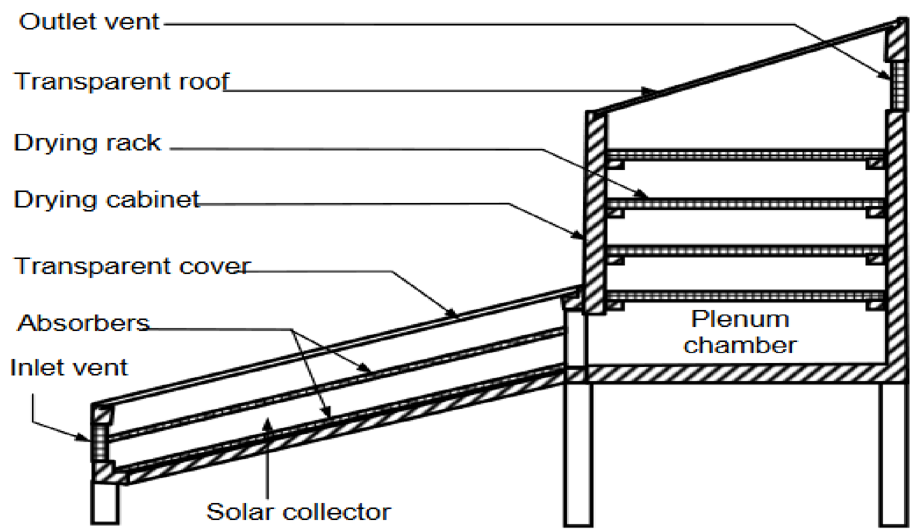

Figure 2. 8 Mixed mode solar dryer (Bolaji and Olalusi, 2008)

Bolaji and Olalusi, (2008) designed and built a mixed mode solar dryer using local materials. The temperature rises inside the drying cabinet reached 24 °C (74%) for about three hours just after solar noon. Drying rate, collector efficiency and percentage of moisture removed (in terms of dry matter) when drying the yam were 0.62 kg / h, 57.5 and 85.4%, respectively.

2.3.1.5. Hybrid solar dryer

Solar energy with a conventional or some auxiliary source of energy such as electricity, biomass, etc. can be used in combined or single mode. It combines both the actions, direct solar radiation heating as well as preheating of air using an auxiliary energy source (Kumar *et al*., 2016)

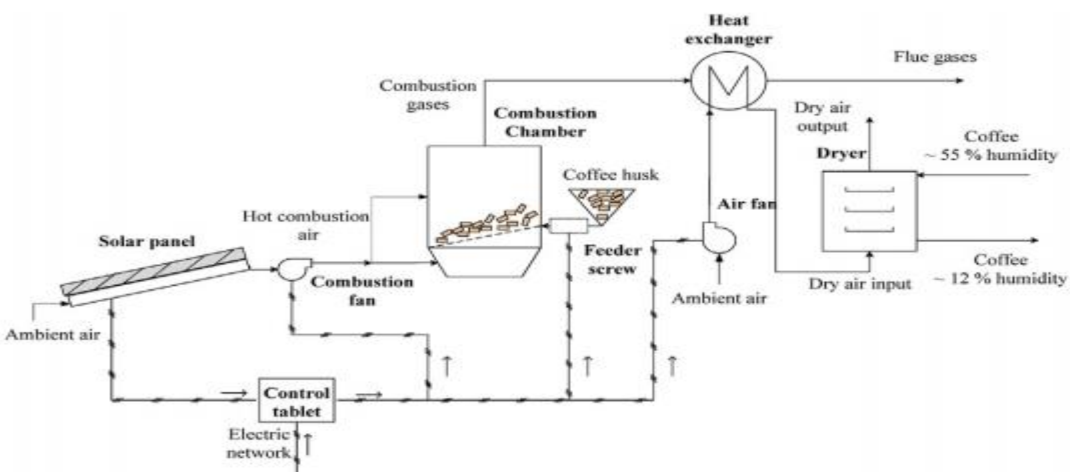

Figure 2. 9 Hybrid solar biomass coffee dryer (Raiza et al.,2020)

Bena and Fuller, (2002) combined a direct natural convection solar dryer and a simple biomass burner for drying fruits and vegetables where no electricity is used. The overall drying efficiency was found to be 9% with a capacity of the dryer about 20–22 kg fresh pineapple (Ananas comosus) arranged in a single layer of 0.01 m thick slices. Similarly, **Tarigan and Tekasakul (2005)** developed a mixed mode solar dryer with natural convection and integrated with biomass burner for drying agricultural products. Drying efficiency of 23% and 40% were observed for the solar component with and without the heat storage, respectively. uniform drying across the drying tray and acceptable thermal efficiency were achieved for the combined unit.

2.3.1.6. Greenhouse dryer:

Greenhouse is basically an enclosed structure covered with stabilized UV resistant polythene sheets, acts itself as a solar collector and drying chamber. Such dryers are used for drying of multiple agricultural products at low cost. Several designs of solar dryer Greenhouse have been studied from a simple small scale to a large scale solar dryer. Based on airflow, structure, floor types, north wall type, and covering material solar Greenhouse dryer can be classified as shown in Figure 2.10. The advantage of Roof Even Span type solar Greenhouse dryer is the mixing of air inside dryer efficiently. The Dome type solar Greenhouse dryer is to maximize the utilization of global solar radiation.

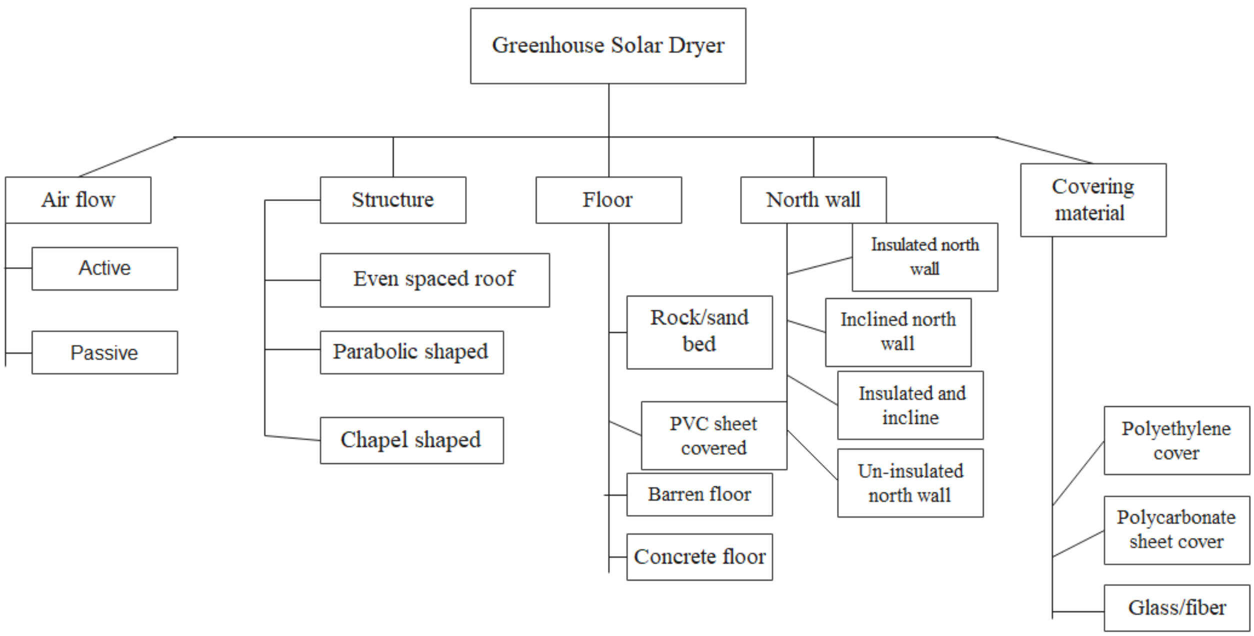

Figure 2. 10: Classification of Greenhouse solar dryers(Singh et al., 2018)

Koyuncu et al., (2006) designed, constructed and tested the performance of two different types of natural circulation Greenhouse type crop dryers i.e. dryer with chimney and without chimney. The results of the study show that the solar Greenhouse dryers increase the ambient air temperature by 5 to 9 ^{o}C and these dryers are 2 to 5 times more efficient than plastic mesh platform type open sun dryer. The dryers with a drying air outlet chimney give a better value of air mass flow by increasing the air velocity.

Sengar *et al.*, (2009) designed a low-cost solar dryer to dry products under hot and humid conditions. The main parts of the dryer were collector, drying chamber, inlet and outlet openings. UV stabilized 200micron plastic film was used for the collection of solar energy and mosquito net was used as trays with a capacity of 0.6kg. The result from this study shows that, this solar dryer is suitable for domestic drying of prawns' fish up to10 kg capacity. Salted fish inside the dryer required 8h to reach a moisture content of 16.15% whereas unsalted fish required 15 h to reach 15.15% in open conditions. Overall collection efficiency was 70.97% and average drying efficiency was 14% and 11% whereas pickup efficiency was 10 and 9% for salted and unsalted fish respectively.

Purusothaman et al., (2018) conducted Computational fluid dynamics (CFD) analysis of solar Greenhouse dryer for both natural and forced convection processes. The variation has been made in the thickness of shut material & mass flow rate. It is concluded that solar radiation increased shapely from 10 am to noon. A higher temperature is observed in forced convection then natural convection by 41%.

Bereket, (**2019**) performed numerical analysis for three different shapes of solar greenhouse dryers and to evaluate the placement of the Thermal Energy Storage by using CFD software (ANSYS Fluent). Three different forms are Gable-even-span shape, Pyramidal Greenhouse solar dryer shape and Half-spherical (Quonset) shape. The total temperature distribution obtained from the previous data reveals that the Gable Even Span solar dryer, Pyramidal Greenhouse solar dryer shape and Half-spherical (Quonset) shape is 36℃, 33℃ and 31 ℃ respectively. The most convenient dryer is Gable Even Span solar dryer since it gave high gain solar energy, high fluid temperature, and highest efficiency during the numerical simulation.

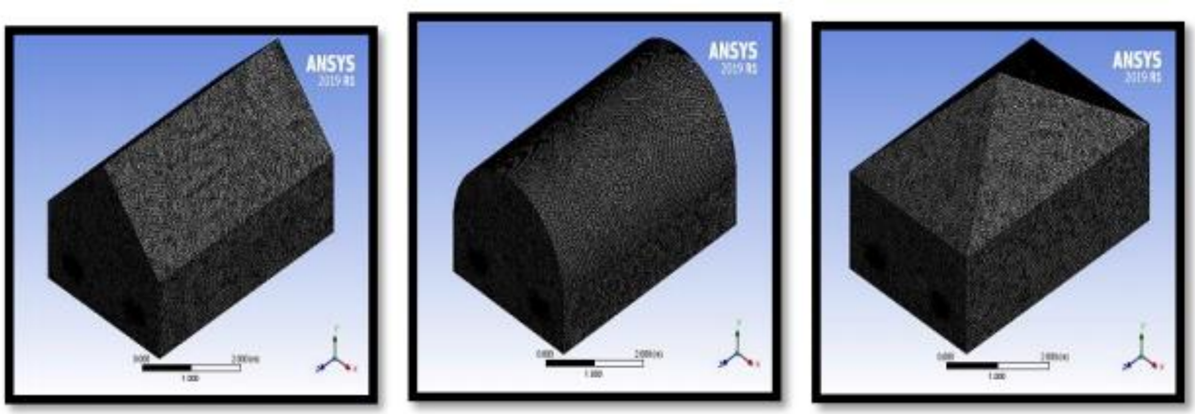

(a) (b) (c)

Figure 2. 11Models after the meshing process. (a) Gable-even-span shape, (b) Pyramidal Greenhouse solar dryer shape, (c) Half-spherical (Quonset) shape (Bereket, ***2019)***

2.3.1.7. The solar tunnel drying system

Is simple in construction and consists of a collector as well as drying tunnel connected in series. Both collector and drying tunnel are covered with transparent glasses or plastic sheets. The collector element contains black color metallic absorber plate while drying chamber has number of trays for loading the product to be dried.

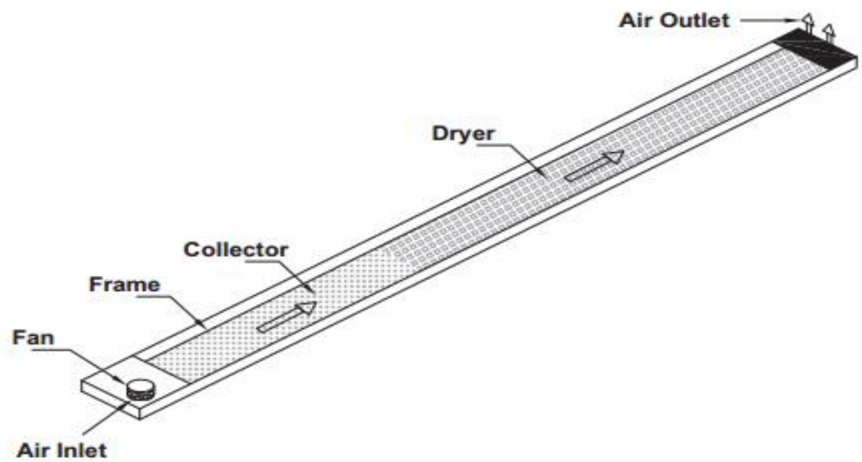

Figure 2. 12 Solar tunnel dryer (Rajendra and Rupesh ,2016)

Sablani *et al*., (2003) investigated the performance of three different solar dryers, namely open rack consisted of perforated rack, convection cabinet made with wooden walls with wire mesh and multi-rack dome dryer consisted of three layers with ten racks per layer. The result shows that, the air temperatures generated and relative humidity within the cabinet unit were 11 to 53 ℃ and 20 to 87% depending upon the time of day respectively. For the multi-rack dome unit, the air temperature and relative humidity varied from 11 to 37 ℃ and 22 to 96% respectively. The initial moisture content of sardine was 2.33 kg water/kg dry solids and at the end of drying the final moisture contents were 0.166 and 0.111 kg water/kg solids for open rack and cabinet dryers, respectively and 0.219 and 0.228 kg water/kg solids at the top and bottom layer of the multi-rack dome dryer respectively.

Reza *et al*., (2009) carried out a study in a solar tunnel dryer to produce safe and high-quality dried fish products. The dryer consists of a flat plate collector, a tunnel drying unit and four small fans. Five fish species such as silver Jewfish, Bombay duck, big-eye tuna, Chinese pomfret and ribbonfish were used. The result shows that, moisture content of the fish samples reached 16%

after 36 and 32 h of drying at temperature ranges of 45 to 50 °C and 50 to 55 °C, respectively. Products produced at 45 to 50 °C were found to have excellent flavor, color and texture.

2.3.2. Classification Based on the Mode of Air Flow

2.3.2.1. Active solar energy dryers

Active solar energy dryers are usually suitable for larger amounts of material and often they are hybrid units using auxiliary sources of energy as conventional fuels to operate during cloudy weather and/ or nighttime. These are more complicated and more expensive than the passive system s as they require fans (Kalogirou,2014).

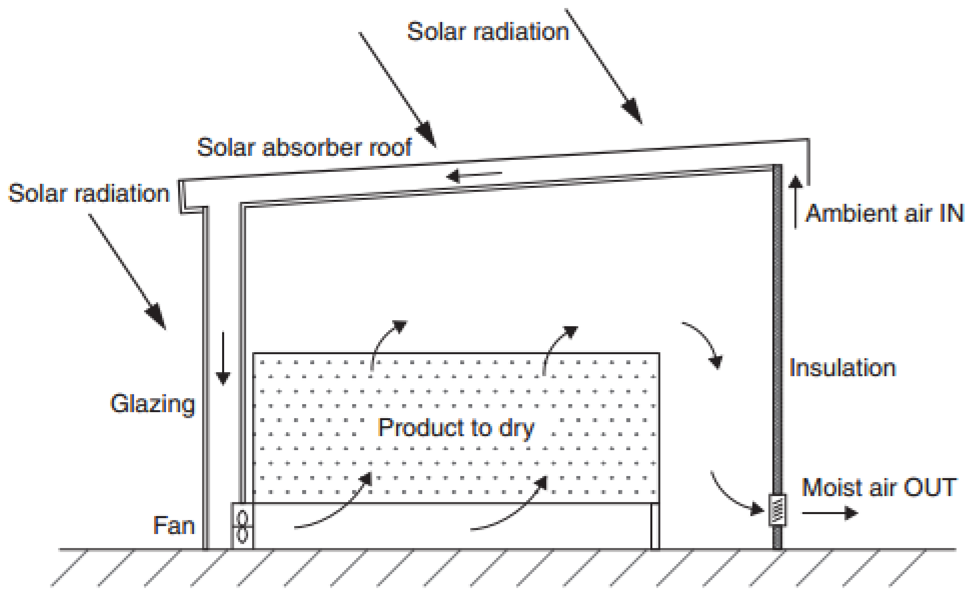

Figure 2. 13 Active collector roof solar energy dryer (Kalogirou,2014*)*.

2.3.2.2. Passive solar energy dryers

Passive or direct drying of crops is still in com mon practice in many Mediterranean, tropical, and subtropical regions, especially in Africa and Asia or in small agricultural communities. Passive solar dryers are “hot box” units where the product in the hot b ox is exposed to the sola r radiation through a transparent cover. Heating takes place by natural convection, through the dryer transparent cover or in a solar air heater.

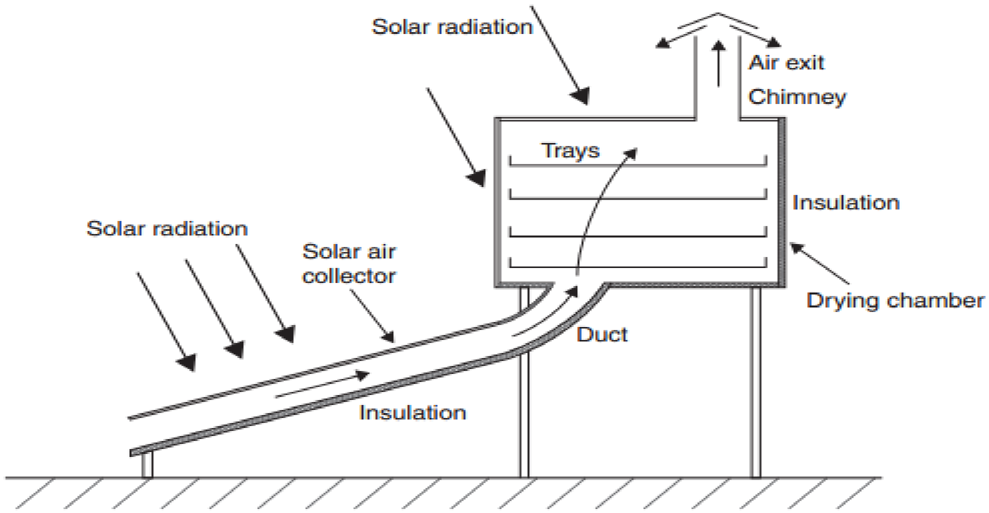

Figure 2. 14 Natural circulation, mixed-mode solar energy dryer (Kalogirou,2014).

The passive-type solar dryer s are primitive inexpensive constructions, easy to install and operate, especially at sites where no electrical grid exists. Passive or natural circulation solar energy dryers operate by using entirely renewable sources of energy, such as solar and wind (Kalogirou,2014).

2.3.3. Classification According to Shape of Absorbing Surface

2.3.3.1 With slat (nonporous)

Nonporous absorbers are flat and an air stream flows as follows:

(I) **Above the blackened absorber plate**: In this case, absorbed solar radiation, after transmission from the glass cover, heats the blackened absorber plate. Thermal energy from the blackened absorber plate is then convicted to the flowing air above blackened absorber plate (hot surface facing upward), and then it is heated (Figure 2.16a).

(II) **Below the blackened absorber plate**: In this case, absorbed solar radiation, after transmission from the glass cover, heats the blackened absorber plate. Thermal energy from the blackened absorber plate is then convicted to the flowing air below the blackened absorber plate (hot surface facing downward), and then it is heated (Figure 2.16b).

(III) **Both sides of the blackened absorber plate**: In this case, air flows from both sides (above and below) of the blackened absorber plate (Figure 2.16c). The temperature of hot air is much less compared with cases (i) and (ii) respectively. Because there is more heat transfer in the case of the hot surface facing upward (double) compared with the hot surface facing downward.

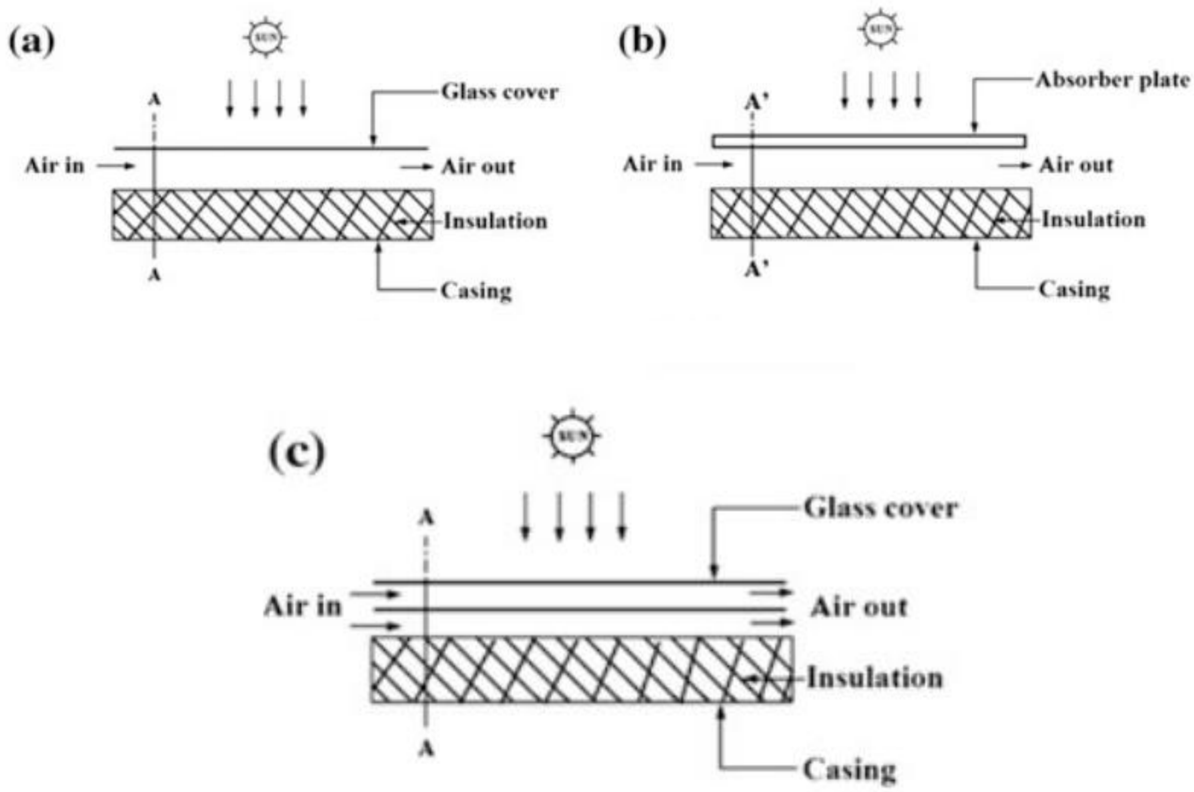

Figure 2. 15 Nonporous absorber-type air heaters (Tiwari ,2016*)*

2.3.3.2. With Porous

In the porous absorber solar air heater, porous absorbers of different configurations such as wire mesh, honeycomb, or glass plates are used as shown in Figure 17.

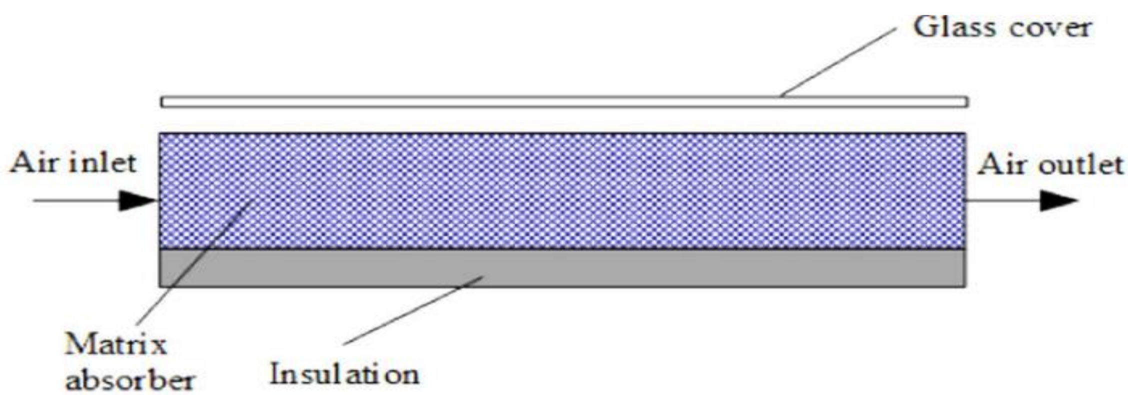

Figure 2. 16 Solar air collectors with matrix absorber (Razak et al., 2016)

The porosity and thickness of the absorber must be optimized for higher thermal efficiency. It should be optimized in such a way that it transfers more thermal energy to the air flowing in the solar air heater (Tiwari ,2016).

2.3.3.3. With Fin

The heat-transfer rate (and hence the thermal efficiency of the solar air heater) from the fixed area of the absorber plate to the air stream can be increased by increasing the contact area between the air stream and the absorber plate. This can be achieved by introducing fins on the rear side of the absorber plate as shown in Figure 2.18. The inclusion of fines causes an additional pressure drop across the solar air heater. The number and design of additional fins are limited to the additional power requirement to run the fan for air circulation.

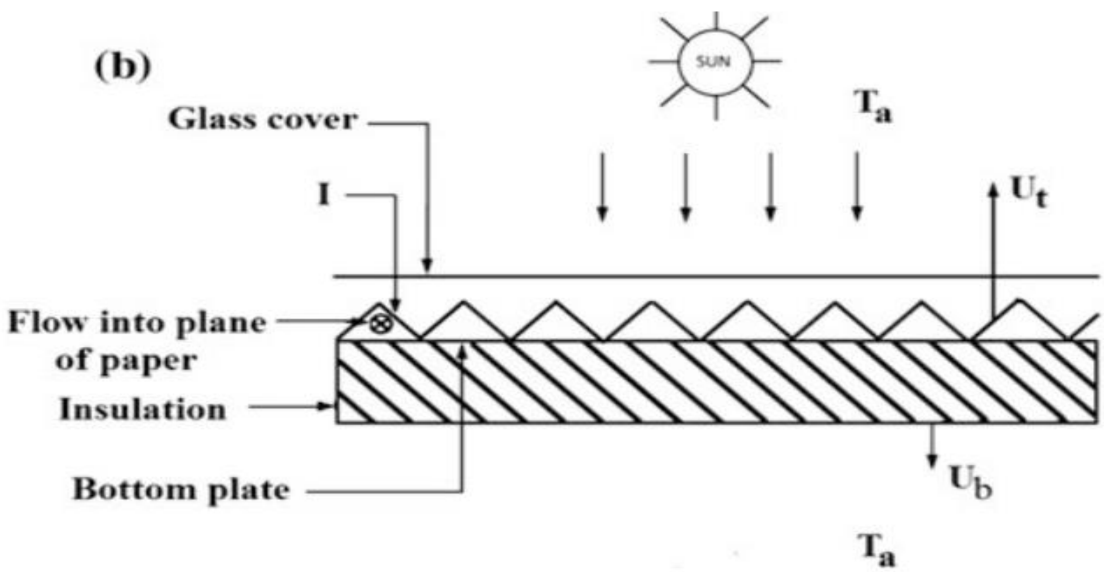

Figure 2. 17 Solar air heater with triangular fins (Tiwari ,2016)

2.4. Solar Air Heater Performance Enhancement Techniques

Many scholars try to found different enhancement techniques for solar heaters. Among them some of them discussed below.

2.4.1. Reverse-Absorber Air Heater

A nonporous conventional air heater/collector can provide hot air at a temperature of 15– 30 °C above the ambient temperature. Furthermore, the rise in temperature say (100 ^{o} C) can be obtained by reducing the convective and radiative top-heat losses from the absorber to the ambient air through the top glass cover. This is feasible in a new type of solar air collector known as a “reverse absorber flat-plate collector” (RAFPC). It can collect solar energy at a high temperature of 200 ^{o}C (Kalogirou,2014).

Working principle

Solar radiation is reflected by the polished curved cylindrical surface after transmission from the glass cover toward the glazed reverse-absorber plate. After absorption, the absorber plate emits long-wavelength radiation. The long-wavelength radiation is then trapped between the absorber

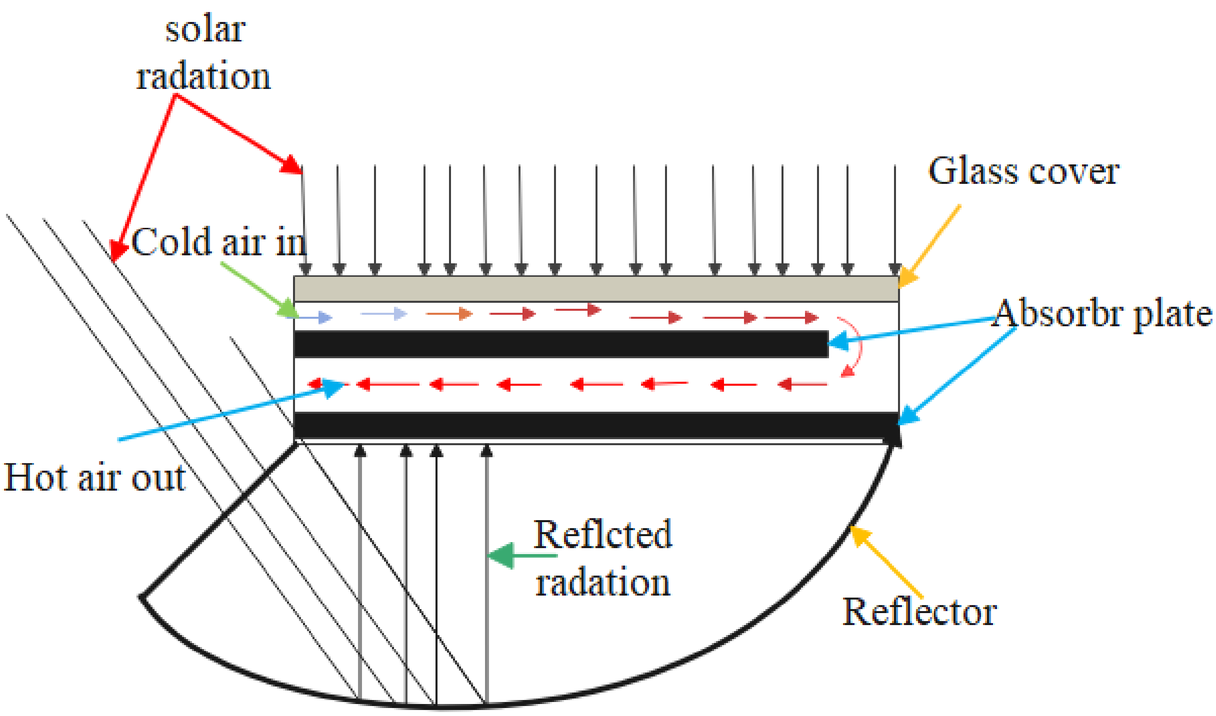

Figure 2. 18 Double pass, glass cover on top, metallic absorber plates on bottom and metallic absorber plate as separator for air channels

plate and the glazed cover. In this case, the convection and radiation heat losses are suppressed due to the hot absorber plate facing downward. The air passing above the absorber is heated. The aperture area of the RAFPC collector is equal to the absorber plate area. The concentration ratio is 1 (Tiwari ,2016). Configurations of the RAFPC are shown in Figure 2.19.

Vijay and Shashank, (2018) investigates experimentally solar crop dryer coupled with reversed absorber type solar air heater. Red chill is used as crop for this experiment Excel software is used to analyze the raw data obtained from the drying experiment to develop a model. The result shows that moisture content will be rapidly reduced in solar dryer with reversed absorber due to higher drying temperatures. To determine drying rate three models are used Newton model, Page and Henderson and Pabis model to fitting drying rate. the values of the coefficient of determination (R^2=0.997), mean bias error (MBE=0.00026) and root mean square error (RMSE=0.016) were used to determine the goodness or the quality of the fit. Also this study compares solar air heater with and without reversed absorber type. The experimental set up as shown in Figure 2.20.

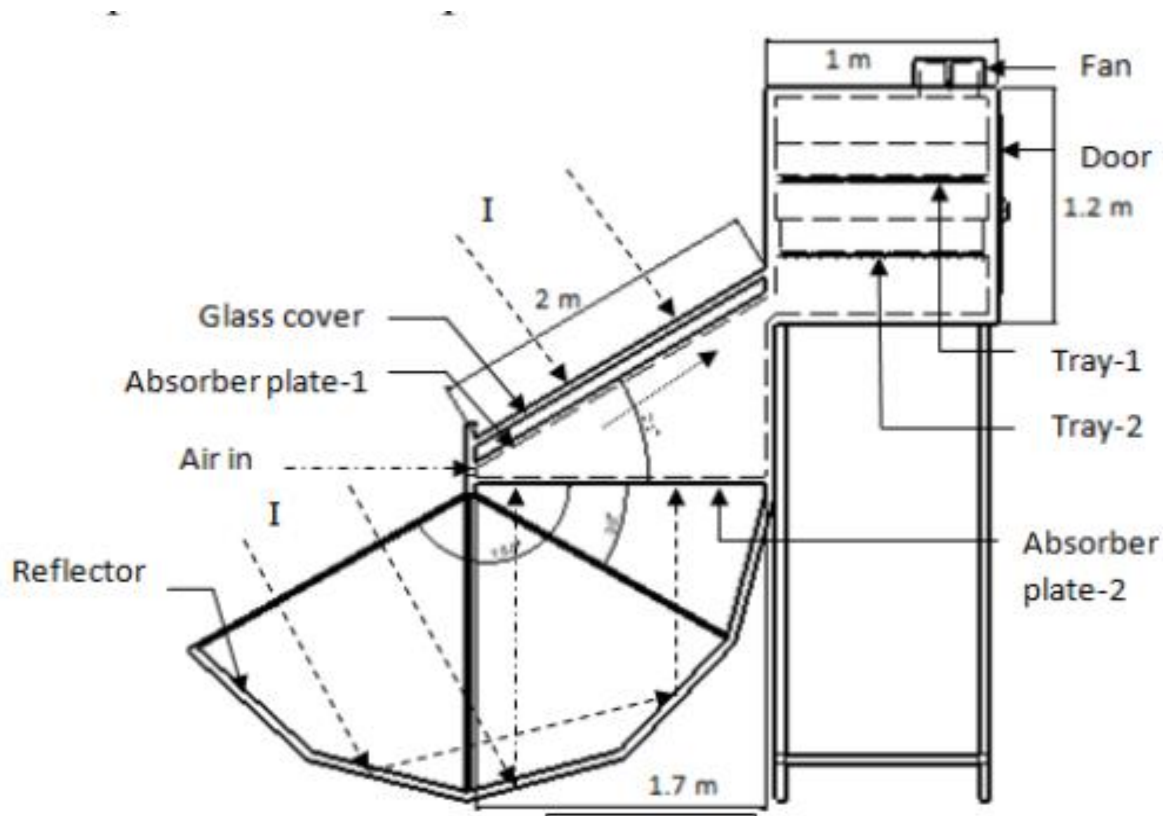

Figure 2. 19: Schematic diagram of solar crop dryer with reversed absorber plate and reflector (Vijay and Shashank,2018)

The maximum thermal efficiency obtained is 30% and 21% for solar air heaters with reversed absorber and single absorber respectively for air mass flow rate of 0.0269 kg/s.

2.4.2. Nanofluids Paint

Characteristics of selective surface are to absorb maximum insolation without exhibit much more radiative losses. Selective surface is obtained by coating the layer of such materials which have high value of absorptivity and low value of emissivity without affecting the life of collector. Black chrome on bright nickel is considered to be as the best selective surface which have 0.96 absorptivity and 0.07 emissivity. The list of different properties of selective surfaces has been given in Table 2.1.

Table 2. 1 Properties of different selective surfaces (Tabish and Man-Hoe ,2017).

Coating	Substrate	Emissivity	Absorptivity
Black nickel	Zn/Fe	0.09	0.94
Black nickel on bright nickel	Fe,Cu	0.07	0.96
Black chrome nickel on bright nickel	Fe,Cu	0.09	0.095
CuO	Al	0.11	0.93
CuO	Fe	0.16	0.90
CuO	Cu	0.11	0.90
CuO/ZnO	Zn/Al	0.20	0.88
Co_2O	Ni	0.08	0.92
Co_2O	Zn/Fe	0.08	0.93

2.4.3 Double Pass

The double pass concept was first introduced to reduce the top heat losses to environment. Double pass arrangement is designed in which air flows along the underside of the absorber plate and extracts heat from the absorber plate, thereafter, air flows in the reverse direction above the absorber plate (Tabish and Kim, 2017). When the air passes along the upper side of the absorber plate, it recovers some of the heat that was lost to the environment because of the high temperature of the absorber plate. The second air pass causes the glass cover to have a temperature similar to the atmospheric temperature. A typical double pass SAH has a 10–15% higher efficiency than a single-pass SAH. Figure 2.21 shows a conventional double-pass SAH. Basically there are two types of double pass SAH, parallel pass and counter pass.

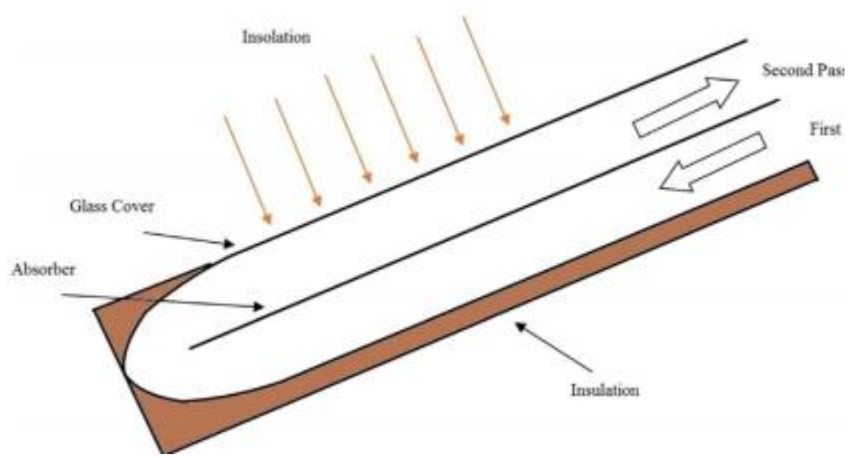

Figure 2. 20 Conventional double-pass SAH *(Tabish and Kim, 2017)*.

2.4.3.1 parallel pass

The configurations of a parallel air pass SAH consists of an absorber plate, glass cover, and back insulation One air pass is located between the back insulation and the absorber plate; other air pass is located above the absorber plate i.e. between the absorber plate and the glass cover. Figure 2.22 shows a diagram of this configuration. In this configuration, airflow directions are in same direction. presented theoretical model for a double-pass SAH in parallel air pass mode. The model was capable of predicting the mean air temperature, mean airflow, heat transfer coefficient, and relative humidity of outlet air.

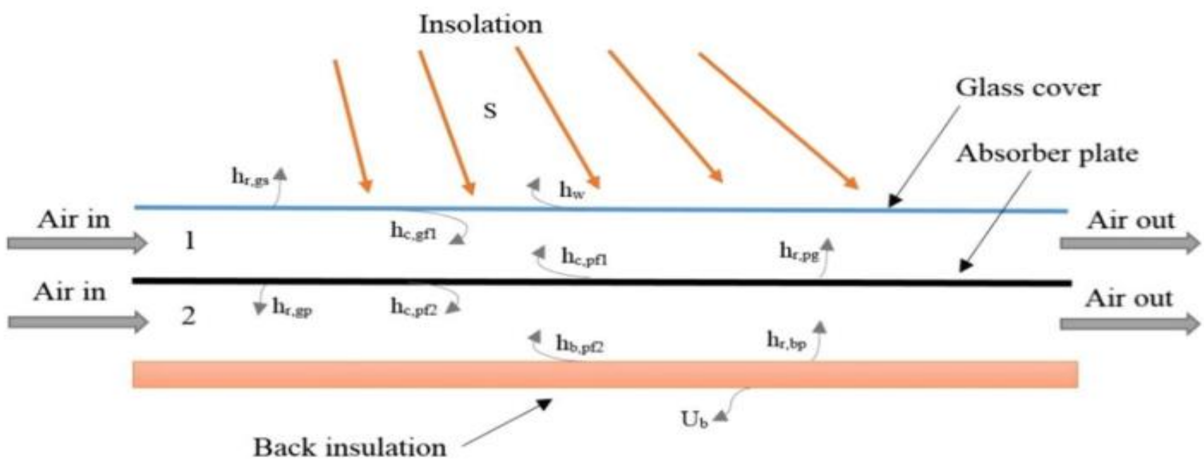

Figure 2. 21 Parallel-flow, double-pass SAH *(Tabish and Kim, 2017)*..

2.4.3.2 Counter air pass

Counter-flow air pass design is attractive design because it allows to extract more heat, leading to improvement in thermal performance. A counter-flow, double-pass SAH consists a glass cover, absorber plate, and back insulation. The design is quite similar to the parallel-flow air pass SAH. In this configuration, air flows above the absorber plate (i.e. in between the absorber and glass cover), and then air is diverted to underside of the absorber plate. This configuration has been shown in Figure 2.23

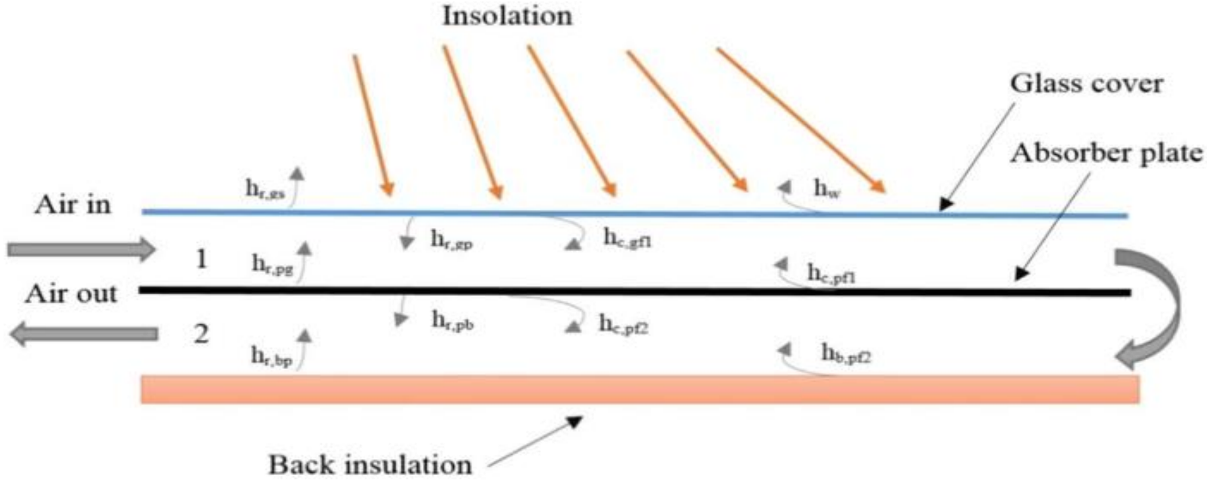

Figure 2. 22 Counter-flow, double-pass SAH.

2.4.3.3 Recycle

Know days, it was proved that air mixing and strength of forced heat convection played an important role in heat transfer enhancement. Double pass SAH utilized same concept in which part of heated outlet air is diverted to inlet channel, thereby, mixed with fresh inlet air by means of blower. Blower regulates the mass flow rate of heated air before it enters into the recycle channel. The schematic diagram of double pass SAH with recycle has been shown in Fig. 2.19. (Tabish and Kim, 2017).

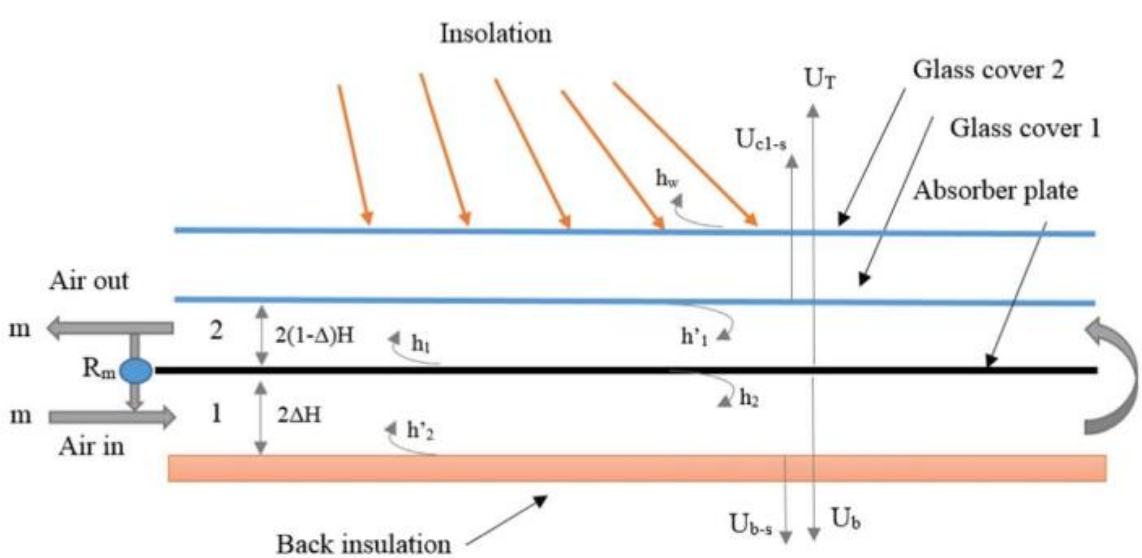

Figure 2. 23 Double-pass SAH with recycle operation (Tabish and Kim, 2017).

2.4.4 Thermal energy storage (TES)

Thermal energy storage (TES) allows excess thermal energy to be stored and used hours, days, months later, at scales ranging from the individual process, building, multiuser-building, district, town, or region. They are important in balancing of energy demand between daytime and nighttime, storing summer heat for winter heating, or winter cold for summer air conditioning (Seasonal thermal energy storage). Storage media include water or ice-slush tanks, masses of native earth or bedrock accessed with heat exchangers by means of boreholes, deep aquifers contained between impermeable strata; shallow, lined pits filled with gravel and water and insulated at the top, as well as eutectic solutions and phase-change materials (Ioan ,2018).

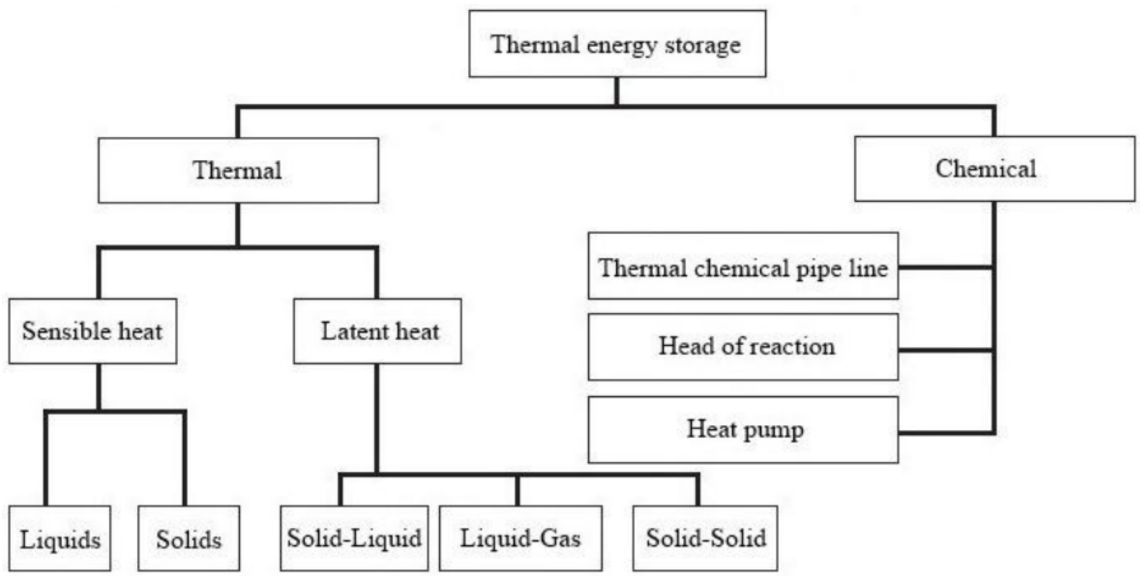

Figure 2. 24 Types of thermal energy storage (TES) (Ioan ,2018)

Thermal energy storage can be divided into three separate categories: sensible heat, latent heat, and thermo-chemical heat storage.

2.4.4.1 Sensible Heat Storage

In the sensible heat storage, thermal energy is accumulated by increasing the temperature of a liquid or solid using the heat capacity and changing the temperature of the material during the process of charging and discharging without undergoing phase change (Sonar, 2021). The specific heat of the material and temperature difference during heating decides the amount of heat storage

(Solomon *et al*., 2020). Molten salts, oils and liquid metals, rocks etc. are used as sensible heat storage. However, water appears to be the best SHS liquid available because its high specific heat and inexpensiveness.

2.4.4.2 Latent Heat Storage

Latent heat storage (LHS) is the absorption or release of heat when a storage material undergoes a phase change from solid to liquid or from liquid to gaseous or vice versa at a more or less constant temperature. LHS also known as phase change materials and offers the possibility of storing higher amounts of energy per unit storage material mass compared to SHS systems.

Any latent heat energy storage system possesses at least the following three components (Bal *et al*., 2010):

- A suitable PCM with its melting point in the desired temperature range.
- A suitable heat exchange surface.
- A suitable container compatible with the PCM

Classification of phase change materials

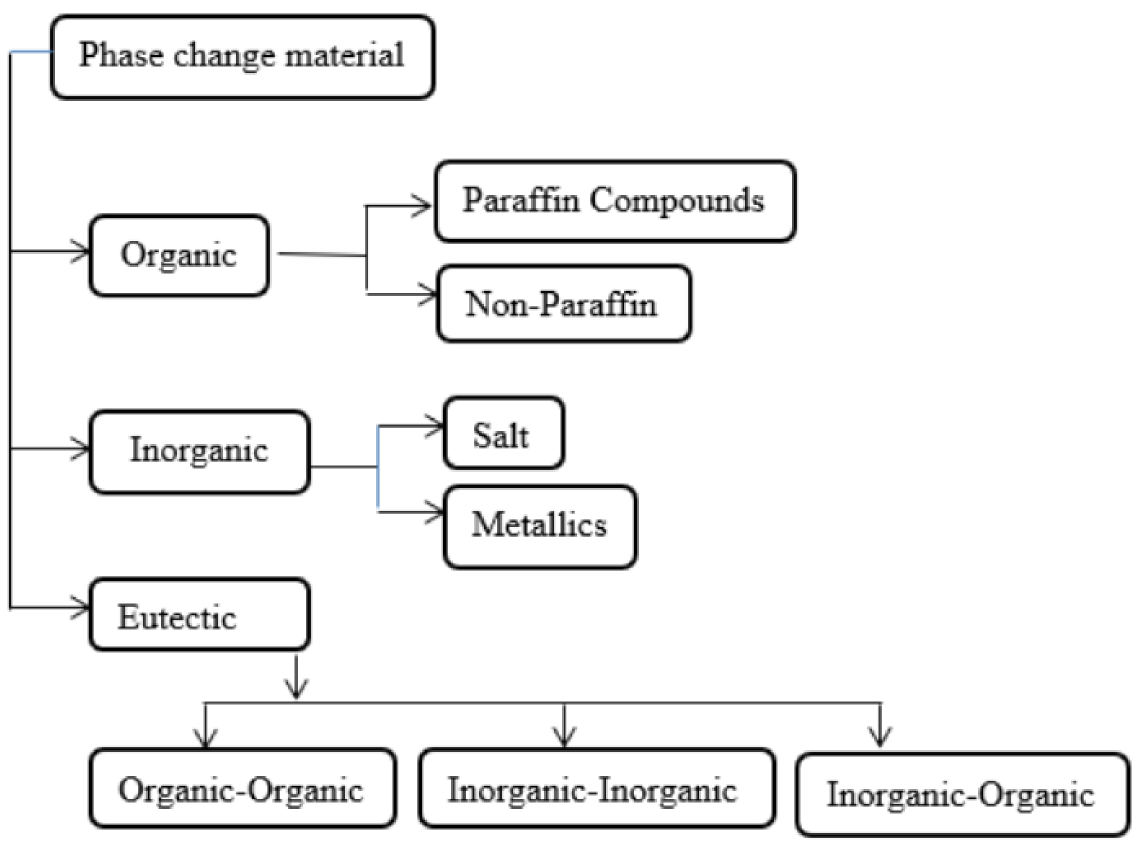

Figure 2. 25: Classification of PCMs (Ali and Deshmukh, 2020)

There are three types of phase change materials used in application: Organic, Inorganic and Eutectic. Organic materials are further described as paraffin and non-paraffin. Paraffins consist saturated hydrocarbon chains of C_nH_{2n+2} and are known to be safe, reliable, predictable, less expensive, and non-corrosive. However, they also have low thermal conductivity. The non-paraffin organics are the most numerous of the phase change materials with highly varied properties. They include a wide range of organic materials such as fatty acids, esters, alcohols, and glycols (Fufa *et al*., 2019 and Soares, 2016).

Salt hydrates are inorganic PCMs that consist of salt and water in a crystal matrix when they solidify. They can have wide range of latent heat and phase change temperatures depending on the mixture. Other branch of inorganic PCMs are metallic, which includes the low melting metals and metal eutectics.A eutectic is a minimum-melting composition of two or more components, each of which melts and freezes congruently forming a mixture of the component crystals during crystallization (Tyagi and Buddhi, 2007). Eutectic PCMs are subdivided into organic-organic, organic-inorganic and inorganic-inorganic.

Alkilani *et al.*, (2009) predicted the outlet air temperature of a solar air heater integrated with a thermal energy storage system with mass flow rates in the range of 0.05 to 0.19 kg/s. 0.5% mass fraction of aluminum powder was added with paraffin wax to enhance the conduction heat transfer process. The freezing time of the PCM has been predicted for the investigated mass flow rate. The result shows that the freezing time of the PCM is inversely proportional to the mass flow rate; it took approximately 8 h with a flow rate of 0.05 kg/s and the outlet air temperature was predicted as 42 °C at this flow rate. Similarly, **Tyagi *et al.*, (2012)** presented a comparative experimental study of a solar air heater with and without thermal energy storage material. Paraffin wax and hytherm oil were used as thermal storages and the study was based on energy and exergy analysis. First and second law efficiencies were determined for three different arrangements, one arrangement without thermal energy storage and two arrangements with thermal energy storage. The result shows that both efficiencies were higher for the solar air heater with thermal storage material than those without thermal storage material. It was also revealed that both efficiencies of the solar air heater that uses paraffin wax were higher than that of hytherm oil. Later, **Bouadila *et al.*, (2013)** experimentally evaluate the thermal performance of a new solar air heater using a packed bed of PCM spherical capsules. The packed bed absorber was formed of spherical capsules with a black coating and it is fixed with a steel matrix. The result shows that, the daily energy and exergy efficiency of the solar air heater varied between 32% and 45% and 13% and 25%, respectively.

2.4.4.3 Thermo-chemical Energy Storage

Thermo-chemical systems rely on the energy absorbed and released in breaking and reforming molecular bonds in a completely reversible chemical reaction. In this case, the heat stored depends on the amount of storage material, the endothermic heat of reaction, and the extent of conversion (Bal *et al*., 2010). Amongst above thermal heat storage techniques, latent heat thermal energy storage is particularly attractive due to its ability to provide high-energy storage density per unit mass and per unit volume in a more or less isothermal process.

2.5. Conclusion from Literatures and Research Gap

Several studies have been review about the existing conventional solar air heater and some modified dryer and heat transfer enhancement technique has been studied briefly so far. From the works of literatures, it can be concluded that solar air heater can be used in a number of field of area. However; the incorporation of solar energy in the air heater may affect the process stability, which results from the daily fluctuate and unpredictable nature of solar energy. Thermal energy storage is a key issue to be addressed toward the intermittent nature of solar energy. Open solar drying is so far well-known but it is exposed to insects, contaminations and reduce the quality of product. Therefore, control methods are having to be used. The collector must be enhanced to get better quality and dry product in short time. On another hand it can be conclude that the efficiency and heat gain for most solar dryer is low. To overcome this problem a number of researchers have been dedicated to study the enhancement technics i.e., integrating storage material, using reverse back reflector, Nanofluid coating of absorber plate, integration of greenhouse with enhanced solar collector, and double pass solar collector increases the efficiency of the system.

To cope up the mentioned problems, this thesis work presents experimental and numerical evaluation of solar air heater enhanced with reverse back reflector, Nanofluid coat of absorber plate, and double pass solar air collector, and phase changing materials used in integration with greenhouse. Finally, the experimentation of solo greenhouse and integrated with enhanced solar collector will be studied.

CHAPTER THREE

3. METHODOLOGY

3.1 Introduction

In this chapter, the methodology used to meet the objectives stated in the Chapter one, collected data required for this study, data sources, collection techniques, materials and equipment's used have been discussed. Both theoretical and experimental approaches are used; The theoretical approach is described by using governing equations for the analysis of each component of the system. Related literatures are studied to gain an insight to the area of interest background and other influencing factors. The literatures are obtained from academic literatures, articles, websites etc. The experimental approach is used to test the performance of the system. The prototype of the dryer has been developed after the sizing and selection of materials for each component was completed. Estimation of solar radiation intensity by applying empirical formulas for Adama city using the weather data which was collected from National Metrological Agency(NMA), Adama branch is presented and analyzed by using empirical formulas. For numerical analysis, each system configuration was modeled and Microsoft excel or matlab program code was developed to perform the analysis.

3.2 Methodology

Both theoretical and experimental analysis are approaches that were used as a methodology in this thesis study. The theoretical approach uses governing equations for the analysis of the system components. For the experimental performance analysis, the prototype was constructed after sizing of each component and selecting the materials to be used. Greenhouse stand alone is tested firstly then enhanced solar air heater assisted greenhouse is tested and finally experimental result is validated with similar previous works.

3.3 Materials and Equipment's

Materials, measuring devices, and system components required for developing the experimental prototype and measuring the system parameters are obtained by purchasing from the local market in Adama and Addis Ababa. Materials used to construct the experimental setup were selected based on local availability and cost-effectiveness. The main materials used are presented below with their uses.

- **Rectangular Iron**: used for constructing of greenhouse, and enhanced solar collector supporter.
- **Transparent Glass**: used for covering solar collector and greenhouse.
- **Paraffin:** used as a thermal storage medium due to its better thermal properties.
- **Stainless Steel:** due to its corrosion resistance property at high temperature, used for construction of storage container walls and parabolic trough shape and to make absorber plates.
- **Cooper oxide:** nanoparticle used for enhancing the performance of solar air heater.
- **Black paint:** used to paint absorber plates to increase absorbance of absorber plate.
- **Glass Mirror:** used for the fabrication of the reflector surface of the parabolic reflector system by using adhesive tape.
- **Insulator**: used for covering pipelines and system components to reduce thermal heat loss.
- **Blower**: used to force air in to greenhouse.

3.4 Research Design

Both analytical and experimental research design procedures are used and both qualitative and quantitative research techniques are employed. Solar collector assisted greenhouse is evaluated based on the existing hypothesis and experiential testing of the hypothesis. The general process layout of the methodology followed in the research is presented in Figure 3.1.

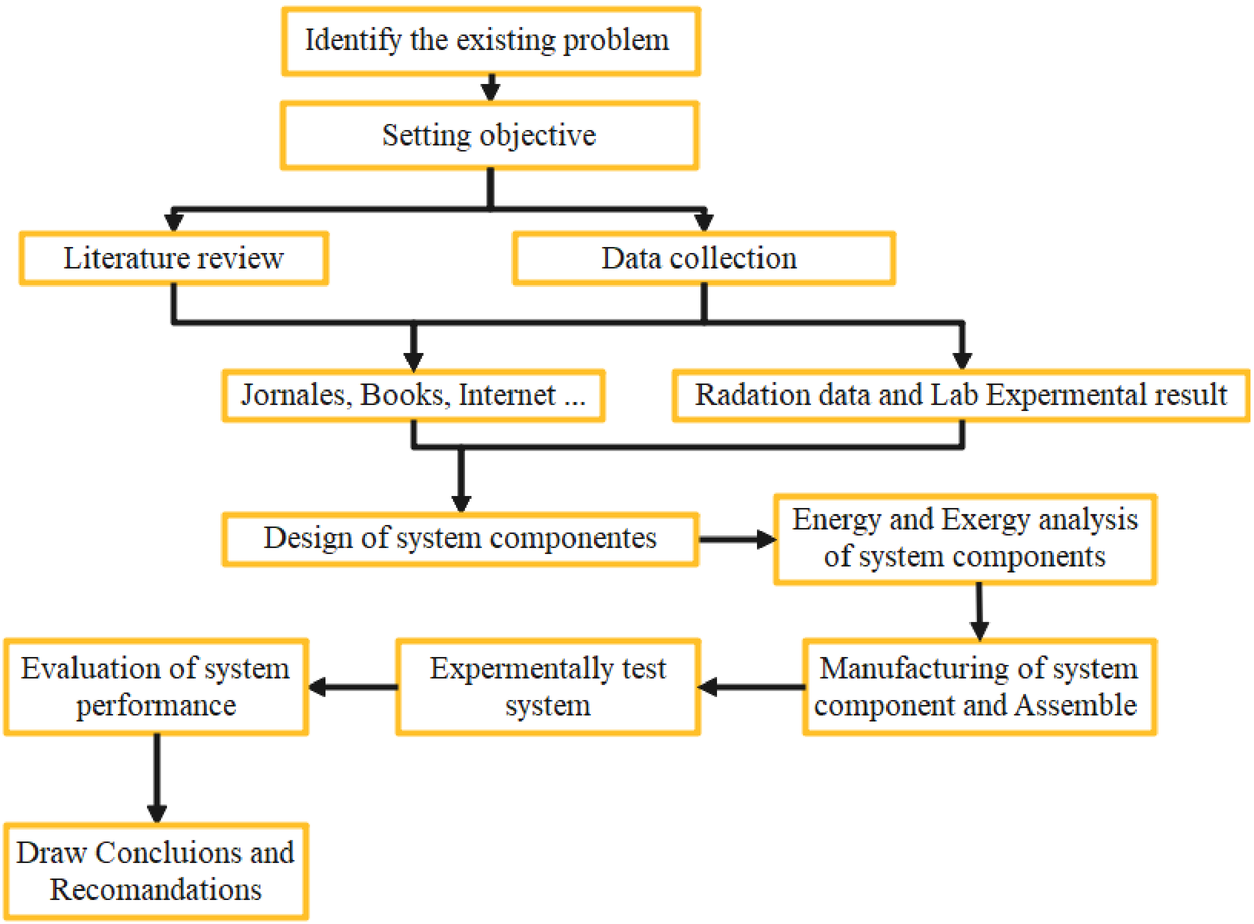

Figure 3. 1: Methodology of the study

3.5 Data Collection

Primary and secondary sources are used when collecting data. The primary sources of data are meteorological data of the test site obtained from nearby meteorological station and moisture content of the coffee beans which is evaluated using oven for different sample in chemical laboratory as seen in Table:3.1. The secondary source of data are data obtained from literature review of different books, journals and from websites.

Primary data collected from National Metrological Agency and lab experiment are discussed as below.

Table 3. 1: Chemical laboratory result of oven dryer

Sample number	Initial mass coffee (grams)	Final mass of coffee (grams)	Mass of water removed (grams)
1	20	9.1	10.9
2	30	13.6	16.4
3	50	22.7	27.3
4	100	45.45	54.55
5	150	68.2	81.8
6	210	94.08	115.92

The coffee is originated from Sidama region. The above sample results in initial moisture content of coffee sample is identified as 61% w.b and the final moisture content is 11.7 %w.b.

a b c

Figure 3. 2: Laboratory experimentation procedure to measure moisture rate a) calibration of Petri dish mass b) mass of coffee before draying c) mass of coffee after dry.

Major data obtained ten years of data from 2011 to 2021 for Adama city from metrology are presented in Figure 3.3 and 3.4.

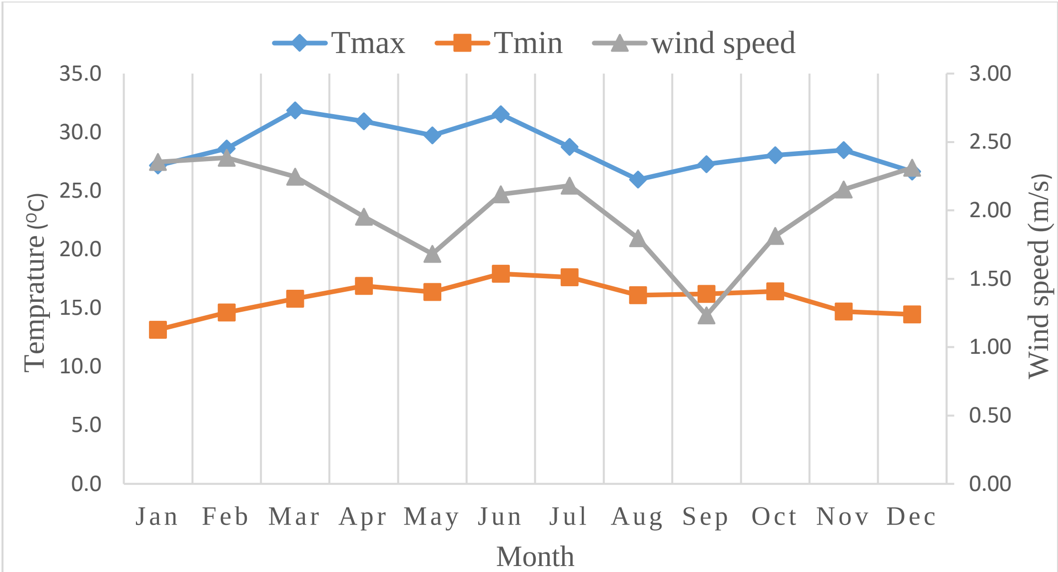

Figure 3. 3: Daily maximum, minimum temperature and daily average wind speed for Adama

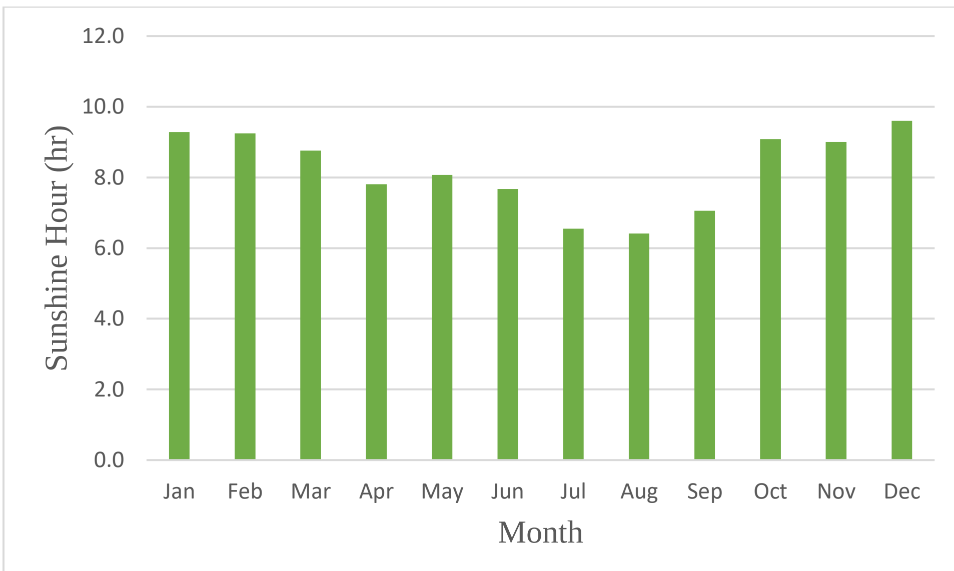

Figure 3. 4:Monthly average daily sunshine hour of Adama

3.6 Preliminary Terminology and Sign Conventions for Estimation of Solar Radiation

3.6.1 Basic Solar Angles

Latitude angle (ϕ): is the angular geographical location that is made in between the line joining location with a center of the earth and its projection on equatorial plane. northern is positive.$-90° \leq \phi \leq 90°$(Tiwari, 2016).

Declination angle (δ): is the angular position of the sun at solar noon (that is, when the sun is on the local meridian) concerning the plane of the equator, north positive;$-23.45 \leq \delta \leq 23.45°$

(Duffie and Beckman, 2013). The declination, **δ**,in degrees for any day of the year (n) can be calculated approximately by the equation (Cooper, 1969).

$$\delta = 23.45 \sin\left[\frac{360}{365}(284+n)\right] \qquad (3.1)$$

Where, n is day of the year which is counted starting from January 1.

Table 3. 2: Recommended average days for months and the values of n by months (Duffie and Beckman, 2013).

Month	n for *i*th Day of Month	Representative day of Month	
		Date	N
January	i	17	17
February	31+i	16	47
March	59+i	16	75
April	90+i	15	105
May	120+i	15	135
June	151+i	11	162
July	181+i	17	198
August	212+i	16	228
September	243+i	15	258
October	273+i	15	288
November	304+i	14	318
December	334+i	10	344

Hour angle (ω): the angular displacement of the sun east or west of the local meridian due to rotation of the earth on its axis at 15° per hour; morning negative, afternoon positive. The hour angle, ω ,in degrees for any time of the solar time(ST) can be calculated approximately by the equation (Duffie and Beckman, 2013).

$$\omega = (ST - 12) * 15^o \qquad (3.2)$$

3.6.1 Derived Solar Angles

Zenith angle (θz): The angle between Sun's rays; the line perpendicular to a horizontal plane is known as the "zenith angle".

$$\cos\theta z = \cos\phi\cos\delta\cos\omega + \sin\phi\sin\delta \qquad (3.3)$$

Solar altitude angle (αs) the angle between the horizontal and the line to the sun, that is, the complement of the zenith angle.

$$\sin\alpha s = \cos\phi\cos\delta\cos\omega + \sin\phi\sin\delta \qquad (3.4)$$

Surface azimuth angle (γ): the deviation of the projection on a horizontal plane of the normal to the surface from the local meridian, with zero due south, east negative, and west positive; $-180^o \leq \gamma \leq 180^o$.

Solar azimuth angle(γs): the angular displacement from south of the projection of beam radiation on the horizontal plane. Displacements east of south are negative and west of south are positive. The sign function in equations (3.4) is equal to +1 if ω is positive and is equal to −1 if ω is negative (Duffie and Beckman, 2013)

$$\gamma s = sign(\omega)\left[\cos^{-1}\left(\frac{\cos\theta z\sin\phi - \sin\delta}{\sin\theta z\cos\phi}\right)\right] \qquad (3.5)$$

Tilt angle or slope angle(β):- the angle between the plane of the surface in question and the horizontal. $0° \leq \beta \leq 180°$**.** The yearly optimum slope angle of the solar collector is presented by (Duffie and Beckman, 2013)**.**

$$\beta_{opt} = \phi + (10-15)^o \qquad (3.6)$$

For Adama optimal slope/tilt angle will be obtained by equation(3.6b) (Ahmad and Tiwari, 2009)

$$\beta_{opt} = \phi + 15 \qquad (3.7)$$

Angle of incidence (θ): The angle made between normal to the inclined surface and the solar beam radiation falling on the inclined surface is known as the "angle of incidence" In general, the angle of incidence, θ, can be expressed as equation (3.7) (Duffie and Beckman, 2013)**.**

$$\cos\theta = \sin\delta\sin\phi\cos\beta - \sin\delta\cos\phi\sin\beta\cos\gamma + \cos\delta\cos\phi\cos\beta\cos\omega$$

$$+\cos\delta\cos\phi\sin\beta\cos\gamma\cos\omega + \cos\delta\sin\beta\sin\gamma\cos\omega \qquad (3.8)$$

And

$$\cos\theta = \cos\theta z\cos\beta + \sin\theta z\sin\beta\cos(\gamma s - \gamma) \qquad (3.9)$$

Sunrise and sunset angles (ωs): The sun is said to rise and set when the solar altitude angle is 0. So, the hour angle at sunset, ωs, can be found by solving Eq. (3.4) for ω when αs = 0 (Duffie and Beckman, 2013)**.**

$$\cos \omega s = -\tan \delta \tan \phi \quad \text{...(3.10)}$$

The sunrise hour angle is the negative of the sunset hour angle. It also follows that the number of daylight hours is given by (Duffie and Beckman, 2013).

$$Ns = \frac{2}{15}(\omega s) \quad \text{... (3.11)}$$

Where Ns =daylight hours

ωs = sunrise hour angle

3.7 Estimation Solar Radiation

3.7.1 Estimation of the Extraterrestrial Solar Radiation on a Horizontal Surface

the solar radiation (Io) incident on a horizontal plane in the extraterrestrial region/outside the atmosphere in W/m^2, which is equivalent to being in the absence of atmosphere, is a component of Iext along the normal to horizontal surface and can be obtained from Eq.(3.10) (Duffie and Beckman, 2013).

$$I_o = I_{ext} \cos \theta z \quad \text{...(3.12)}$$

$$I_{ext} = I_{sc}\left(1 + 0.033\cos\left(\frac{360 * n}{365}\right)\right) \quad \text{...(3.13)}$$

where I_{SC} is the solar constant (1367 W/m^2), and n is nth day of the year

θz is zenith angle

n is number of day starting from January one

Substitution of cos(θz) from Eq. (3.3) in the previous equation gives

$$I_o = I_{sc}\left(1 + 0.033\cos\left(\frac{360 * n}{365}\right)\right)\left(\cos\phi\cos\delta\cos\omega + \sin\phi\sin\delta\right) \quad \text{...(3.14)}$$

The extraterrestrial radiation on a horizontal surface for a given period from hour angles ω_1 to ω_2 (where ω_2 is larger) can be calculated by integrating Eq. (3.12) for a period, and it is given by (Duffie and Beckman, 2013).

$$I_o\left(\frac{J}{m^2}\right)=\frac{12*3600}{\pi}I_{sc}\left(1+0.033\cos\left(\frac{360*n}{365}\right)\right)\left(\cos\phi\cos\delta\left(\sin\omega_2-\sin\omega_1\right)+\frac{2\pi\left(\omega_2-\omega_1\right)}{360}\sin\phi\sin\delta\right)$$
....(3.15)

Integrating the equation above over the period from sunrise to sunset the daily total extraterrestrial radiation on a horizontal surface gives

$$H_o\left(\frac{J}{m^2}\right)=\frac{24*3600}{\pi}I_{sc}\left(1+0.033\cos\left(\frac{360*n}{365}\right)\right)\left(\cos\phi\cos\delta\sin\omega s+\frac{2\pi\omega s}{360}\sin\phi\sin\delta\right) \quad ....(3.16)$$

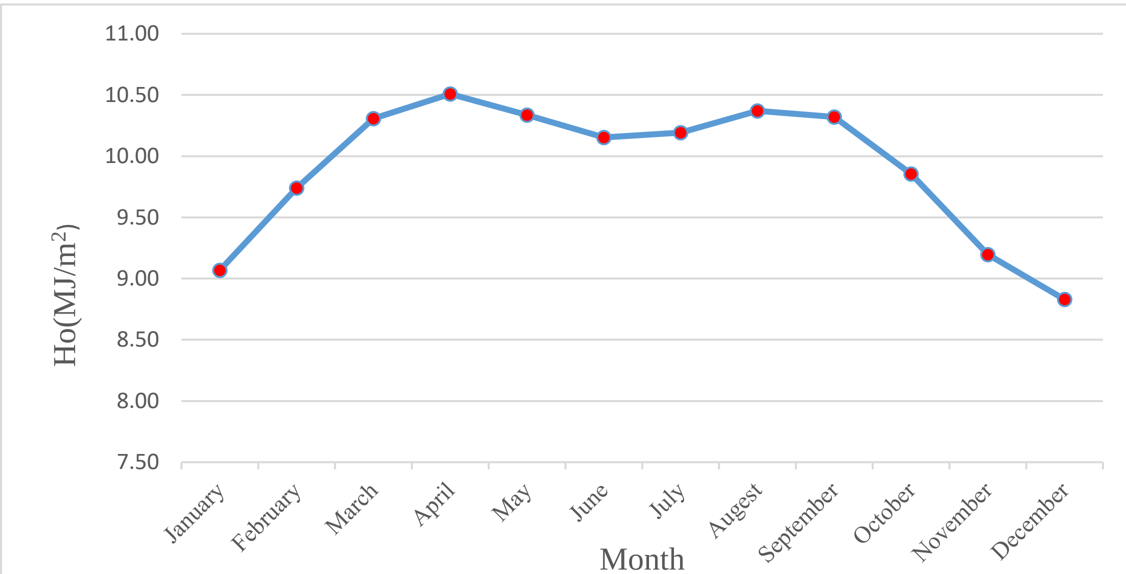

Figure 3. 5: Monthly average daily extra-terrestrial solar radiation for Adama 2022 (Ho)

3.7.2 Terrestrial Region

3.7.2.1 Estimation of Monthly Average Daily Global Radiations on a Horizontal Surface

The first correlation proposed for estimating the monthly average daily global radiation is based on the method of Angstrom (1924). The original Angstrom-type regression equation-related monthly average daily radiation to clear day radiation in a given location and average fraction of possible sunshine hours and expressed with 10 % accuracy using as follow (Duffie and Beckman, 2013).

$$\frac{\overline{H}}{\overline{H}_o}=a+b\left(\frac{\overline{n}}{\overline{N}}\right) \quad ....(3.17)$$

where $\overline{n}$ and $\overline{N}$ are the observed monthly average of daily bright sunshine hours and the total length of average day of month. $\overline{H}$ and $\overline{H_o}$ are the monthly average of daily total solar radiation on a horizontal surface in the terrestrial and extraterrestrial region, respectively.

The regression coefficients a and b are given by

$$a = -0.110 + 0.235\cos\phi + 0.323\left(\frac{\overline{n}}{\overline{N}}\right)$$

$$b = 1.449 - 0.553\cos\phi - 0.694\left(\frac{\overline{n}}{\overline{N}}\right) \quad \text{.......(3.18)}$$

Estimation of Monthly Average Daily Diffuse and Beam Radiations

The monthly average daily diffuse radiation on a horizontal surface $(\overline{H_d})$ in kw/m^2 day can be determined from the monthly average daily global radiation on a horizontal surface and the number of bright sunshine hours (Tiwari and Tiwari, 2016).

$$\frac{\overline{H_d}}{\overline{H}} = 0.931 - 0.814\left(\frac{\overline{n_s}}{\overline{N_s}}\right) \quad \text{.......(3.19)}$$

The monthly average daily beam radiation $\left(\overline{H_b}\right)$ on a horizontal surface is the difference between the monthly average daily global and diffuse radiations.

$$\overline{H_b} = \overline{H} - \overline{H_d} \quad \text{.......(3.20)}$$

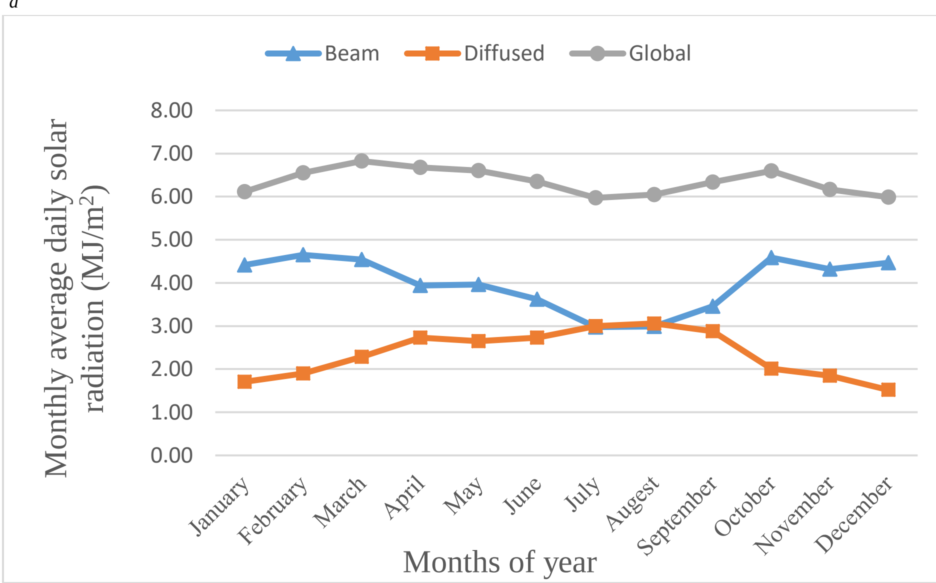

Monthly average daily solar radiation

Estimation of Hourly Radiation from Daily Data

Statistical studies of the time distribution of total radiation on horizontal surfaces through the day using monthly average data for a number of stations have led to generalized charts of **rt** the ratio of hourly total to daily total radiation, as a function of day length and the hour. The hours are designated by the time for the midpoint of the hour, and days are assumed to be symmetrical about solar noon (Duffie and Beckman, 2013)**.** Thus, knowing day length (a function of latitude φ and declination δ) and daily total radiation, the hourly total radiation for symmetrical days can be estimated.

$$r_t = \frac{I}{H} \quad (3.21)$$

$$r_t = \frac{\pi}{24}\left(a + b\cos\omega s\right)\frac{\cos\omega - \cos\omega s}{\sin\omega s - \frac{\pi\omega s}{180}\cos\omega s} \quad (3.22)$$

The coefficients a and b are given by

$$a = 0.409 + 0.5016\sin\left(\omega s - 60\right)$$

$$b = 0.6609 - 0.4767\sin\left(\omega s - 60\right) \quad (3.23)$$

Diffused component is estimated by the formula from (Liu and Jordan 1960):

$$r_d = \frac{\overline{I_d}}{\overline{\overline{H_d}}} \quad (3.24)$$

Where r_d is given by

$$r_d = \frac{\pi}{24}\frac{\cos\omega - \cos\omega s}{\sin\omega s - \frac{\pi\omega s}{180}\cos\omega s} \quad (3.25)$$

In these equations ω is the hour angle in degrees for the time in question (i.e., the midpoint of the hour for which the calculation is made) and ωs is the sunset hour angle.

The monthly average hourly beam radiation on a horizontal surface $\left(\overline{I_b}\right)$ is the difference between the monthly average hourly global and diffuse radiations.

$$\overline{I_b} = \overline{I} - \overline{I_d} \quad (3.26)$$

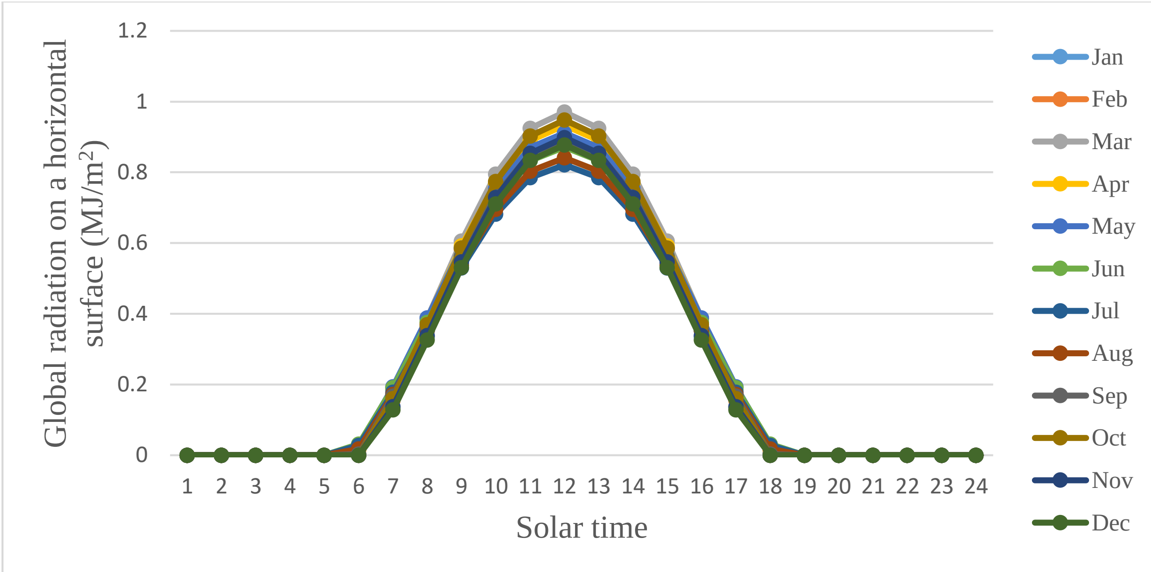

Figure 3. 6: Global radiation on a horizontal surface

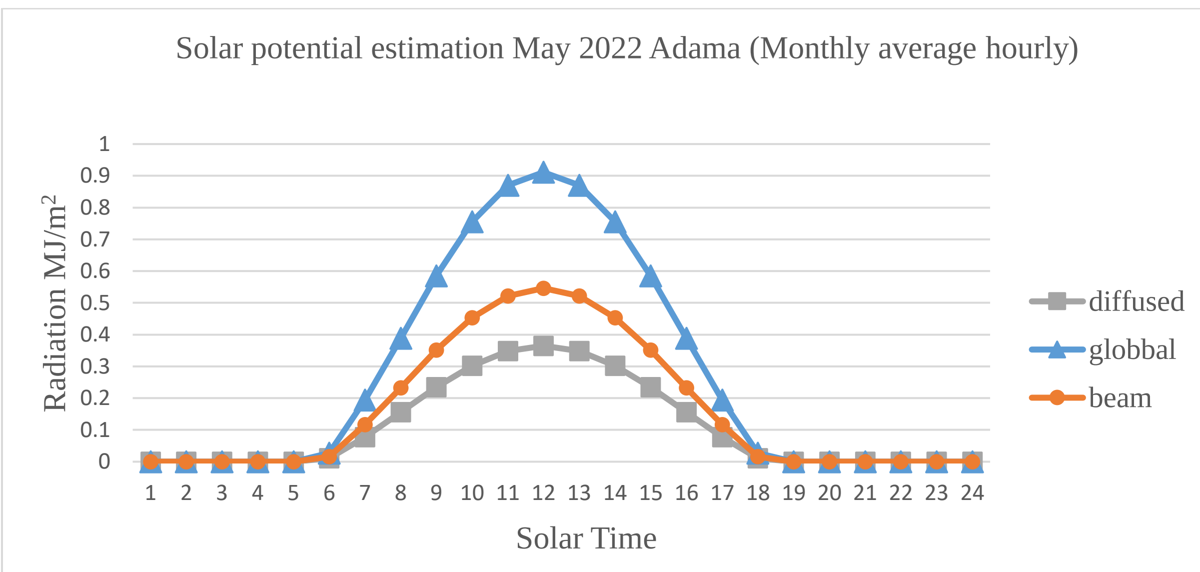

Figure 3. 7: Solar potential estimation May 2022 Adama

3.7.3 RADIATION ON SLOPED SURFACES

The incident solar radiation on an inclined (tilted) surface is the sum of the beam, diffuse and reflected solar radiation from various surfaces (from a horizontal surface and surfaces surrounding it). Therefore, the total incident solar radiation on a surface tilted at an angle β can be expressed in terms of the global, beam, diffuse and the total reflected radiation to the tilted surface (Duffie and Beckman, 2013).

$$I_T = I_b R_b + I_d\left(\frac{1+\cos\beta}{2}\right) + \left(I_b + I_d\right)\rho\left(\frac{1-\cos\beta}{2}\right) \qquad (3.27)$$

Where I_T is total hourly irradiance on a tilted surface (W/m^2)

I_b is beam hourly irradiance on a tilted surface (W/m^2)

I_d is diffused hourly irradiance on a tilted surface (W/m^2)

β is tilt angle (^{0})

R_b is the beam radiation factor which can be defined as the ratio of the incident beam radiation on a tilted surface to that on a horizontal surface. for location found in northern hemisphere using artificial latitude $(\phi - \beta)$ (Tiwari and Tiwari, 2016).

$$R_b = \frac{\cos\theta}{\cos\theta z} = \frac{\cos(\phi-\beta)\cos\delta\cos\omega + \sin(\phi-\beta)\sin\delta}{\cos\phi\cos\delta\cos\omega + \sin\phi\sin\delta} \qquad (3.28)$$

where ρ is reflectivity of ground and its value is 0.2 for ordinary ground (Tiwari and Tiwari, 2016).

It is generally known that for a collector installed in the northern hemisphere, the optimum collector orientation is south facing ($\gamma = 0$) and the optimum tilt depends upon the latitude of the site and the day of the year (Tiwari and Tiwari, 2016) and optimal tilt angle will be found using Equation (3.7).

Estimation of hourly variation of atmospheric temperature

Hourly variation of atmospheric temperature can be estimated from the daily maximum and minimum temperatures. A sin-exponential model proposed by Parton and Logan (1981) is used and it describes the diurnal cycle by a sine function during daytime and a decreasing exponential function during nighttime. The major assumption of the model is the maximum temperature will occur sometime during the daylight hours before sunset and the minimum temperature will occur during the early morning hours. The mathematical description for day and night time, respectively are expressed as (Parton and Logan, 1981), (Abdu,2021), (Dessie,2020):

$$T_i = (T_{\max} - T_{\min})\sin\left(\frac{\pi m}{Y+2a}\right) + T_{\min} \qquad (3.29)$$

$$T_i = (T_{sunset} - T_{\min})\exp\left(-\frac{bn}{Z}\right) + T_{\min} \qquad (3.30)$$

Where T_i is temperature at the *i*th hour, Y and Z are the length of the day and the night in h respectively, m is the number of hours after the minimum temperature occurs until sunset and n is the number of hours after sunset until the time of the minimum temperature. The input variables required by the model include maximum and minimum temperatures and Julian date. The day and night lengths (Y and Z) are determined as functions of Julian date and latitude. The temperature at sunset (Tsunset) is calculated with Equation 3.29, while m and n are functions of time of day, day length, and the lag coefficient for the minimum temperature. The coefficients a and b vary as functions of soil depth or height above the soil surface and could also vary as functions of soil type and soil water content. Values for these coefficients were determined for different soil depths and air temperatures. a is the lag coefficient for maximum temperature = 1.8 h and b is the night time temperature coefficient =2.2 for Adama.

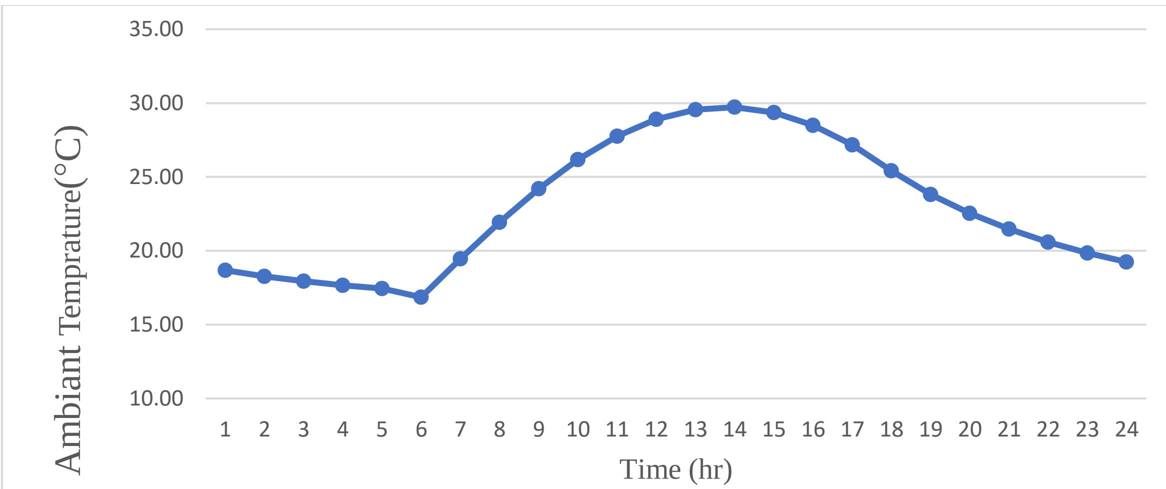

Figure 3. 8: Daily Ambient Temperature

CHAPTER FOUR

4. THEORETICAL ANALYSIS OF GREENHOUSE INTEGRATED WITH ENHANCED SOLAR COLLECTOR

4.1 Introduction

This chapter presents the theoretical analysis of greenhouse integrated with enhanced solar air collector which has double pass solar air heater enhanced by absorber plate painted black color mixed with copper oxide, reverse back reflector and latent heat storage between greenhouse and enhanced solar air heater. The analysis includes overall design of the collector and greenhouse which is sizing of the components of the system components. Selection of material for solar air heater is presented in detail. Energy and exergy analysis of the solar dryer and greenhouse components are also discussed in detail.

4.2 Design of the system

The main design specifications for the dryer includes the moisture to be removed from the product, quantity of energy and mass of air required for the drying process, the mass flow rate and volumetric air flow, the output temperature of the collector, and sizing of the components of the dryer.

4.2.1 Design of Components of the Greenhouse

To design the system amount of moisture to be removed from the product, amount of energy and air required for drying, daily solar radiation to determine energy received by the greenhouse per day, daily sunshine hours for the selection of total drying time, and wind speed to determine air vent dimensions are considered. These parameters can be determined from the principle of psychometric relation and energy balance equation. Before calculating and designing the solar dryer component values specification of initial parameters (assumptions) are mandatory based on the collected data.

Initial assumptions

To perform the numerical calculation some initial assumptions are required. those are as follow

Table 4. 1 initial assumptions

Parameter	Values and assumptions
Average ambient temperature	28 ^oC
Average daily relative humidity	60%
Initial moisture content of coffee	61%wb (laboratory Result)
Final moisture content	11.7%wb (laboratory Result)
Average solar radiation	645 W/m^2
Sample weight	5 kg
Critical coffee drying temperature	50 ^OC

The quality of the coffee beans may change due to changes in drying parameters such as temperature difference, drying time and remaining water content in coffee beans. The purpose of drying coffee beans is to reduce the water content contained in coffee beans from the initial moisture content of about 61% wb to reach the standard water content of about 11.7% w.b. The rate of drying of coffee beans is strongly influenced by seed temperature, water content in seeds, drying fluid temperature, fluid velocity and relative humidity. Critical temperature drying coffee beans is 50 °C. This is because the drying temperature above 50 °C can lead to case hardening. Case hardening phenomenon caused damage to coffee beans (Hendrarsakti and Firmansyah,2017).

The amount of water removed from the product (W)

The mass of water removed from a wet product (W) was calculated by using amount of initial mass product (mo), the initial and final moisture content of product (Mi , Mf) which were shown as (Poolsak and Serm ,2011).

$$W = \frac{m_o\left(M_i - M_f\right)}{100 - M_f} \quad \text{...} (4.1)$$

The moisture content of product (M) was calculated by referring equations (4.2) and (4.3) in wet basis and dry basis, respectively. The mass of products samples (w) and dry mass of products samples (d) were determined.

$$M = \frac{(w-d)}{w}100 \quad (4.2)$$

$$M = \frac{(w-d)}{d}100 \quad (4.3)$$

W=2.78 kg

4.2.1 Air flow requirement

The average drying air temperature rise over the ambient value is estimated using a modified form of an empirical formulae resulting from the study by (Macedo and Altemani, 1978).

$$\Delta T = 2\lambda(T_b - T_c)\frac{I_t}{I_{sc}} \quad (4.4)$$

Where $\Delta T = (T_o - T_{am})$, is the temperature difference between the expected mean temperature of the heated air at the collector outlet and the ambient air temperature, λ is a dimensionless parameter whose value is in the range 0.14–0.25. For an optimal design, a mean value of $\lambda = 0.20$ is assumed (Forson,1993) to allow for moderate drying air temperature and velocity for natural drying (Macedo and Altemani, 1978), (Tb-Tc) is the temperature difference between the boiling and freezing point of water at atmospheric pressure, It, is the intensity of radiation incident on the plane of the collector and Isc is the maximum intensity of the source of radiation or the solar constant the value of which is given as 1367 W/m^2.

T_o=51.4 ^{O}C

The total volume of air required (V_A) for removing the moisture is evaluated from the equation (Forson et al., 2007).

$$V_A = \frac{W L_h R_a T_a}{C_{pa} P_a (T_o - T_f)} \quad (4.5)$$

where Ra is the specific gas constant, Pa the partial pressure of dry air in the atmosphere, Cpa the specific heat capacity of air at constant pressure, T_f is the temperature of air leaving the drying bed, which value is given by

$$T_f = T_{am} + 0.25\Delta T \quad (4.6)$$

T_f =33.85 ^{O}C

The latent heat of vaporization was calculated using equation given by (Youcef-Ali *et al*., 2002)

$$L_h = 4.186\left(597 - 0.56T_{pr}\right) \quad (4.7)$$

Where; T_{pr} is maximum allowable temperature of the dried product in °C

The volume flow rate is calculated from the relation

$$\dot{V} = \frac{V_A}{t} \quad (4.8)$$

The mass flow rate of air needed to effect the drying is given by

$$\dot{m} = \dot{V}\,\rho_a \quad (4.9)$$

where t is the total time required to dry a given sample of moist material to safe storage level.

To find mass flow rate volume and volume flow rate in the equation 4.5-equation 4.9 by substituting the values of constants and calculated values i.e. W=2.78 kg, ρ_a = 1.2kg/m^3 , Ra=287 J/kg.K, To=51.4 ^{O}C, Tf=33.85 ^{O}C Tam=28 ^{O}C, Pa=101325 Pa, t=12h and Cpa=1005 J/kg.K. Then the design variables given as; L_h=2382.12 kJ/kg, Va=353.4 m^3, $\dot{V}$ =0.0082 m^3/s and $\dot{m}$ =0.02 kg/s.

4.2.2 Total area of the system for collecting incident energy

The effective total area surface of the dryer for collecting incident radiation is related to the overall system drying efficiency (η_d), which is given by

$$\eta_d = \frac{WL_h}{I_T A_t t} \quad (4.10)$$

where At is the total area of the dryer receiving incident radiation (the total surface area of the primary and secondary collectors), t the total time, Lt the latent heat of vaporization and I_T the intensity of radiation incident on a tilted surface. To achieve an optimal design, an average overall efficiency value of 12.5 can be assumed (Forson et al., 2007).

Substituting values to equation (4.10) gives

$$At=3m^2$$

Say area of collector be 1m^2 and area of greenhouse be 2m^2.let width of collector be 0.7m and the length will be 1.4 m.

4.2.3 Area of drying bed (tray)

The effective drying bed area Ada is obtained from first principles by relating the solid density of the wet material to its mass and the corresponding volume as (Forson et al., 2007).

$$A_d = \frac{M_o}{\rho_{pb} h_L \xi (1-\varepsilon_v)} \text{ ....(4.11)}$$

where M_o is the mass of the crop to be dried, ρ_{pb} the bulk density of the crop on wet basis, h_L the layer drying bed thickness, ξ the crop porosity, ε_v the loading bed void fraction. Putting M_o =5kg, ρ_{pb} =879kg/m^3, h_L = 0.01 m, ξ = 0.743, and ε_v =0.6 for coffee beans , the drying bed (Ad) area is given as 1.9 m^2. Assuming width of tray equals to l m then the length is 1.9 m.

4.2.4 Design of Reverse Back Reflector

Reverse back reflector is considered as parabolic trough. Geometry of parabolic trough will be discussed. The following four parameters are commonly used to characterize the form and size of a parabolic trough (Günther *et al*., 2011).

- Focal length
- Trough length
- Aperture width and
- Rim angle.

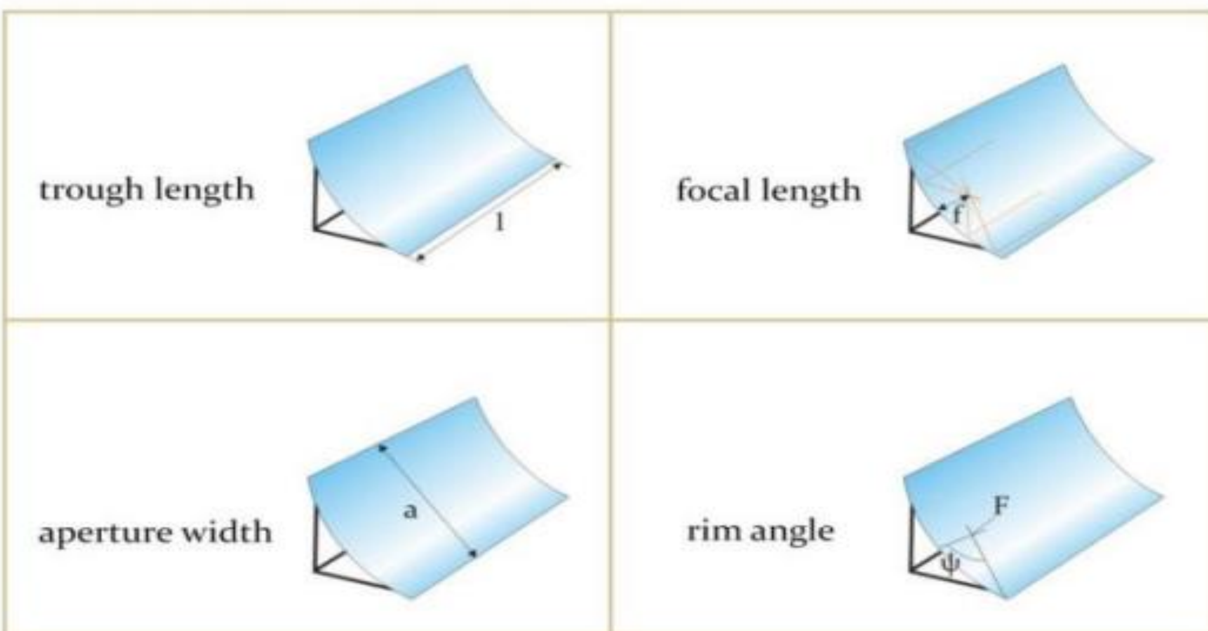

Figure 4. 1: Geometrical parabolic trough parameters (Günther et al., 2011)

A. **Reflector Aperture Area**

The aperture area is calculated as the product of the aperture width and the collector length (Günther *et al*., 2011).

$$A_{ap} = al \quad (4.12)$$

Where a is aperture width and l is aperture length. Aperture width is equals to length of solar air heater width plus 0.6 m for maximum reflection and length of aperture (l) is aperture area divided by aperture width (a).

Aperture area (A_{ap}) is calculated from the efficiency and solar radiation.

$$\eta_{th} = \frac{Q_u}{A_{ap} I_b} \quad (4.13)$$

where: Q_u is useful energy, I_b beam radiation A_{ap} is the aperture area of the parabolic trough reflector. thermal efficiency (η_{th}) assumed to be 50% (Padhy *et al.,* 2021). Average beam radiation (I_b) of Adama in Ethiopia sunshine hour is 645W/m^2.

Based on equation (4.14), the aperture area of the parabolic trough is:

$$A_{ap} = \frac{Q_u}{\eta_{th} I_b} \quad (4.14)$$

Substituting the value of I_b =500 W/m^2, η_{th} =50%, and Qu=1512.7 kJ/h gives A_{ap} =1.6 m^2, l=1.3 m, a=1.23 m.

B. **Focal length**

Focal point is the place where all radiations are meet at. Parabolic troughs have a focal line, which consists of the focal points of the parabolic cross-sections. Radiation that enters in a plane parallel

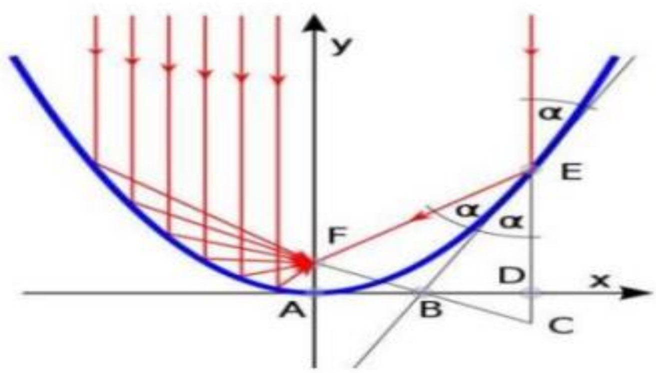

Figure 4. 2: Path of parallel rays at a parabolic mirror (Günther et al., 2011)

to the optical plane is reflected in such a way that it passes through the focal line. Focal length f is the distance between the vertex of the parabola and the focal point (Günther *et al.,* 2011).

$$f = \frac{a^2}{16h} \quad \text{.......(4.15)}$$

where: a is width of the parabolic trough h is the height of the parabolic trough. Assuming the height of parabola (h) is equals to 0.2 m. Then the focal length (f) is equals to 0.47 m.

C. **Rim Angle**

Rim angle is the angle between direct incident radiation on the reflective surface and the line joining focal point and extreme point of the reflective surface at the aperture width. The rim angle determines the shape of a parabolic trough and, ideally, it should neither be too small nor too large. If the rim angle is very small, then the parabolic trough is very narrow and this increases solar radiation incidence but at the same time increases the heat loss due to convection and radiation. Hence a small rim angle in the parabolic trough solar collector is not advantageous. It is calculated by using the width and focal length of the parabolic trough (Kumar and Shukla, 2016). The rim angle of real parabolic troughs is around 80°.

The rim angle ψ can be expressed as a function of the ratio of the aperture width to the focal length (Gnther *et al.*, 2011).

$$\tan\psi = \frac{\left(\frac{a}{f}\right)}{2 - \frac{1}{8}\left(\frac{a}{f}\right)^2} \quad \text{.......(4.16)}$$

Substituting the values of a=0.9 m and f =0.47 m into equation (4.16) gives $\tan\psi$ =2.29 , ψ =66.4^{O}

Parabola curvilinear length is given by:

$$l = 2f\left[a\sqrt{1+a^2} + \frac{1}{2}\ln\left(\frac{\sqrt{1+a^2}+a}{\sqrt{1+a^2}-a}\right)\right] \quad \text{.......(4.17)}$$

Substituting the values of a=1.23 m and f =0.47 m into equation (4.17) gives l=2.8 m

The surface area of a parabolic trough may be important to determine the material need for the trough. The area is calculated as follows (Günther *et al.*, 2011).

$$A = \left(\frac{a}{2}\sqrt{1+\frac{a^2}{16f^2}} + 2f\ln\left(\frac{a}{4f} + \sqrt{1+\frac{a^2}{16f^2}}\right)\right)l \quad \text{.......(4.18)}$$

Substituting the values of a=1.23 m and f =0.47 m into equation (4.18) gives A=1.8 m^2

Figure 4. 3: Summarized design parameters of reverse back reflector

Parameter	Symbol	Value
Aperture width	A	1.23 m
Aperture length	L	1.3 m
Aperture Area	A_{ap}	1.6 m^2
Focal length	F	0.47 m
Rim angle	ψ	66.3^O

4.2.5 Design of thermal energy storage

Thermal energy storages are introduced in solar drying system to keep uniform drying temperature and to continue the drying process at night; when solar radiation is not available. The shell and tube type LHS have a faster melting rate compared to rectangular LHS for the same heat transfer area and volume (Dessie,2020). The design includes selection of a storage material and sizing of heat storage unit. To fix the size of the storage required for the drying process, the appropriate PCM should be selected first. the main criteria for selecting PCMs for drying operation is their melting temperature. The minimum melting temperature of the PCM should be 5 to 10 ℃ higher than the desired temperature of the drying air (Lane *et al.*, 1983). The desired average air temperature of the solar drying system is 50 ℃. Therefore, paraffin wax of average melting temperature of 58-60 ℃ is selected as PCM since it is safe, non-toxic and easily available in the local market. Table 4.2 shows the physical property of paraffin wax.

Table 4. 2: Physical properties of paraffin wax RT58 (Bernardo et al.,2016)

Physical property	Symbol	Value
Density [Kg/m3]	ρ_{pcm}	840
Specific Heat solid[J/kg K]	$C_{p,s}$	2950
Specific Heat liquid [J/kg K]	$C_{p,l}$	2510
Thermal Conductivity [W/m K]	k_{pcm}	0.2
Latent Heat [J/Kg]	$L_{h,pcm}$	180000
Tsolidus[K]	Ts	321
Tliquidus [K]	T_L	335

The latent heat storage is a shell and tube heat exchanger. The drying air passes through the tubes and the shell is filled with paraffin wax. Heat is transferred from the hot air to the paraffin wax through the tubes during the charging process and the process is reversed during the discharging time. The heat was stored during the day time when the solar radiation was available to heat the air in the solar air heater and this stored heat will then be supplied to the drying chamber when there is no more heat supply from the solar air heater.

The quantity of heat needed to be stored in the thermal energy storage system can be estimated by assuming the storage will store the heat for 2 off-sunshine hours per day as follow:

The heat transfer fluid (HTF) passes through the tubes and the shell is filled with PCM. Heat is transferred from the hot HTF to the PCM through the tubes during the charging process and the process is reversed during the discharging time. The heat was stored during the daytime when the solar radiation was available to heat the HTF in the solar collector. The latent heat thermal energy storage system was designed for storing the heat needed in the drying system. Assuming the storage will store the heat for 2 off sunshine hours per day, the quantity of heat needed to be stored in the latent heat thermal energy storage system can be estimated by considering a safety factor of 1.5 for the change in temperature $\Delta T = T_d - T_a$ (Niyas *et al.*, 2017).

$$Q_s = \dot{m}_a C_{pa} \left(T_d - T_{am}\right) t \qquad (4.19)$$

The amount of PCM required was determined from the relationship (Gunjo, 2018) Qs equals to latent energy plus sensible energy.

$$Q_s = m_{pcm}\left(C_{pcm}\left(T_m - T_{am}\right) + L_{pcm}\right) \quad (4.20)$$

Where Tm is the melting temperature of PCM.

The volume of the PCM can be calculated from,

$$V_{pcm} = \frac{m_{pcm}}{\rho_{pcm}} \quad (4.21)$$

The volume of the tank is the sum of the volume of the PCM and the volume of the tubes

$$V_{tank} = V_{pcm} + V_{tube} \quad (4.22)$$

To find the volume of storage required, the tube volume V_{tube} should be determined

$$V_{tube} = \pi L n R_o^2 \quad (4.23)$$

Where L is length of the tube and n is number of tube used R_o is Radis of tube

To improve the heat transfer in the axial direction than in the radial direction, the length to diameter ratio of the storage can be taken as 5 (Niyas *et al.*, 2017; Velraj *et al.*, 1997 and Sharma *et al.*, 2005).

$$V_{tank} = \frac{1}{4} D^2 L \quad (4.24)$$

Substituting the values $\dot{m}$ =0.00983 kg/s Td=50 ^{O}C, Cpa= 1.005 kJ/kg,, t = 3 h, L_{pcm} =180 kJ/kg, Tam= 28 °C, Tm= 59 ^{O}C , Cpcm= 2510 (J/kg°C) ρ_{pcm} = 840 kg/m^3 in the Equation 4.19–Equation 4.24 gives Qs=2347.29 kJ, Mpcm=9 kg, Vpcm=0.0099 m^3. Assuming 4 tubes are used and their diameter is 24 mm and length of tube L=0.7 m. volume of tube V_{tube} =0.0016 m^3, V_{tank} =0.0115 m^3, D=0.144 m.

4.3 Energy and Exergy Analysis

Energy and exergy analysis of system components obtained by Appling the first law of thermodynamics for each component of the system.

4.3.1 Energy Analysis

The energy analysis of the drying system was performed based on the general mass and energy conservation equations by employing first law of thermodynamics for main components of the dryer. During the energy analysis, the flow in the drying system was assumed to be transient for numerical calculation. But for experimental evaluation we use steady state equation.

4.3.1.1 Energy Balance of Solar Air Heater

The energy-balance equations in this chapter are written under quasi-steady state and transient conditions with the assumptions given as follows:

[1]. There is no temperature gradient along the thickness of the glass cover and the absorber plate.

[2]. The convictive heat-transfer coefficients for the operating temperature range are assumed to be constant.

[3]. The mass -flow is stream-line flow and constant

[4]. The side- heat losses are neglected.

[5]. The temperature gradient along the depth of the duct is negligible; average air temperature changes along the direction of flow.

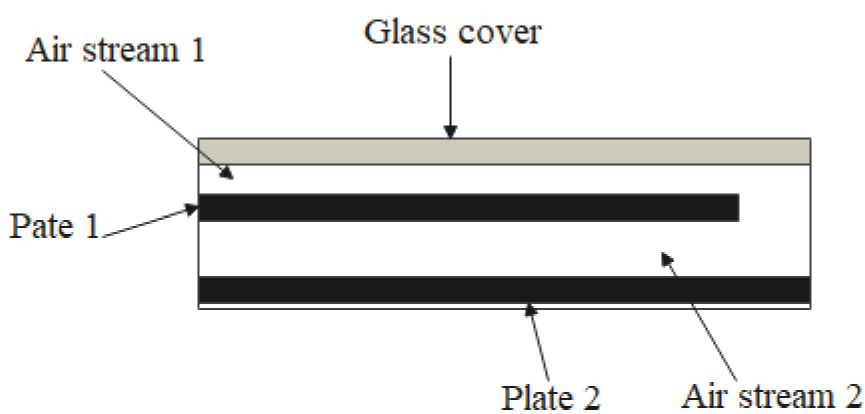

Figure 4. 4 Diagram of solar collector

Glass cover:

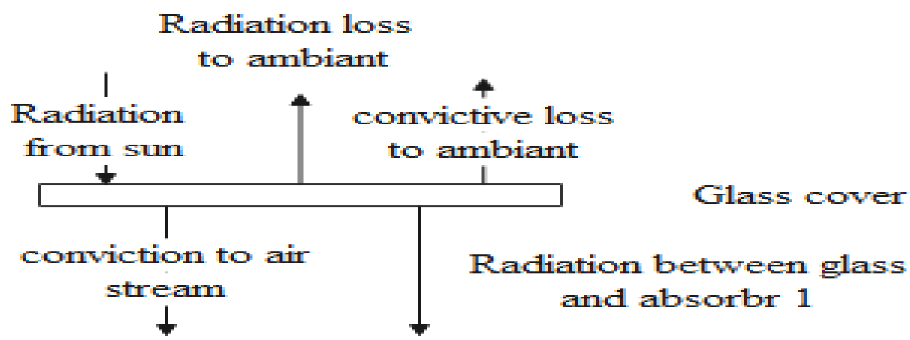

Figure 4. 5: Energy balance of glass cover

$$\alpha_g I_T + h_{r,p1g}(T_{p1} - T_g) + h_{c,f1g}(T_{f1} - T_g) = h_{c,ga}(T_g - T_a) + h_{r,gsky}(T_g - T_a) + (mC_p)_g \frac{\partial T_g}{\partial t} \qquad (4.25)$$

Where α_g is absorptance of glass, I_T is solar radiation in tilted surface, $h_{r,p1g}$ is radiative heat transfer from plate 1 to glass cover, $h_{c,f1g}$ convective heat transfer coefficient from fluid 1 to glass, $h_{c,ga}$ convictive heat transfer from glass to air, m mass of glass, C_p is specific heat capacity of glass.

Working fluid (air stream 1):

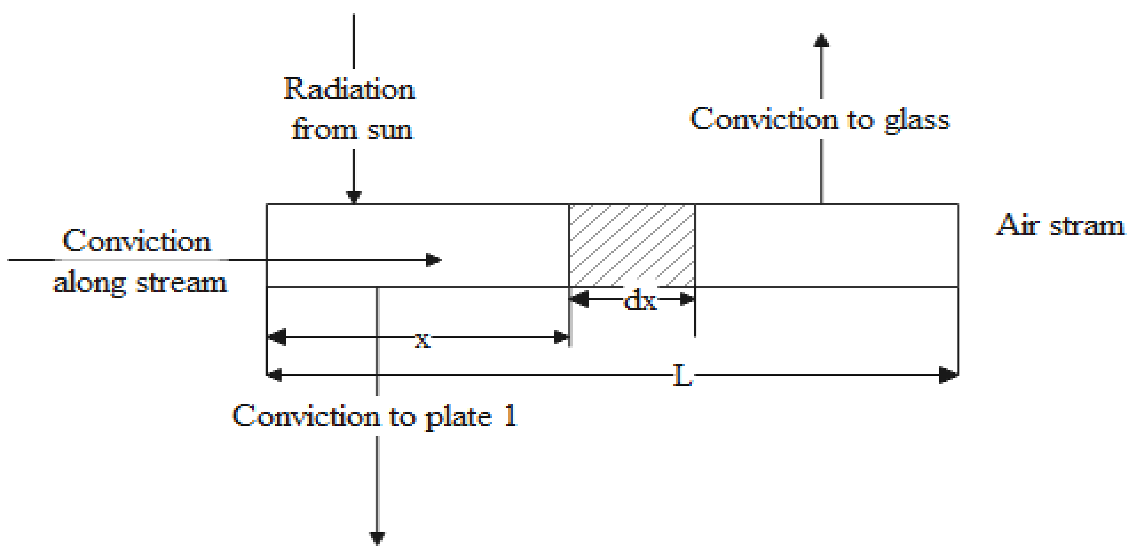

Figure 4. 6: Energy balance of air stream 1

$$(mC_p)_{f1} \frac{\partial T_{f,1}}{\partial t} = h_{c,f1p}(T_{p1} - T_{f1}) + h_{c,gf1}(T_g - T_{f1}) - \frac{(\dot{m}C_p)_{f2}}{w} \frac{\partial T_{f,1}}{\partial x} \qquad (4.26)$$

Where m is mass of air, C_P is specific heat capacity of air, $h_{c,f1p}$ is convictive heat transfer from fluid to plate 1, $h_{c,gf1}$ is convictive heat transfer from glass to fluid, w is width of collector, $\dot{m}$ is mass flow rate of air stream.

Working fluid (air stream 2):

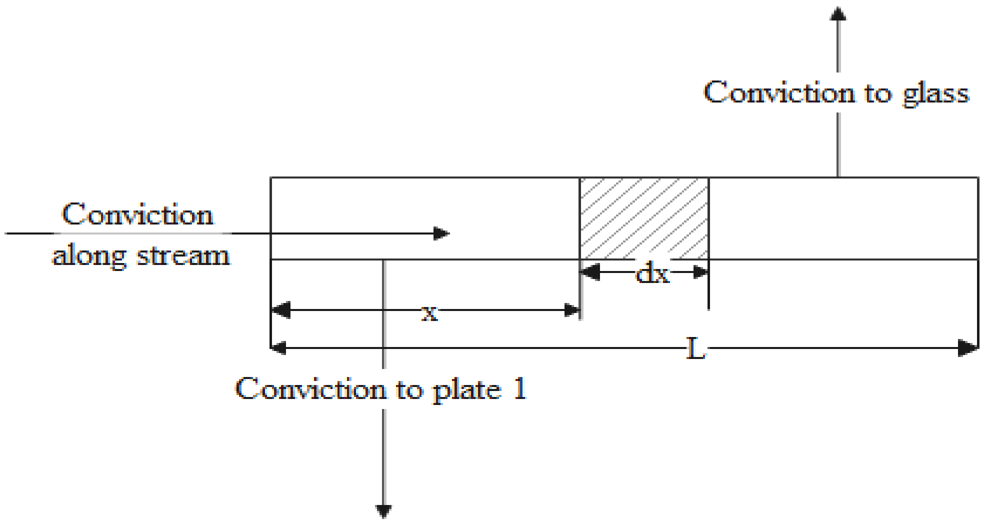

Figure 4. 7 : Energy balance of air stream 2

$$(mC_p)_{f2}\frac{\partial T_{f2}}{\partial t} = h_{c,p1f2}(T_{p1}-T_{f2}) - h_{c,f2p2}(T_{f2}-T_{p2}) - \frac{(\dot{m}C_p)_{f2}}{w}\frac{\partial T_{f2}}{\partial x} \quad \text{.......................................(4.27)}$$

Where m is mass of air, C_P is specific heat capacity of air, $h_{c,f1p}$ is convictive heat transfer from fluid to plate 1, $h_{c,gf1}$ is convictive heat transfer from glass to fluid, w is width of collector, $\dot{m}$ is mass flow rate of air stream.

Absorber plate 1:

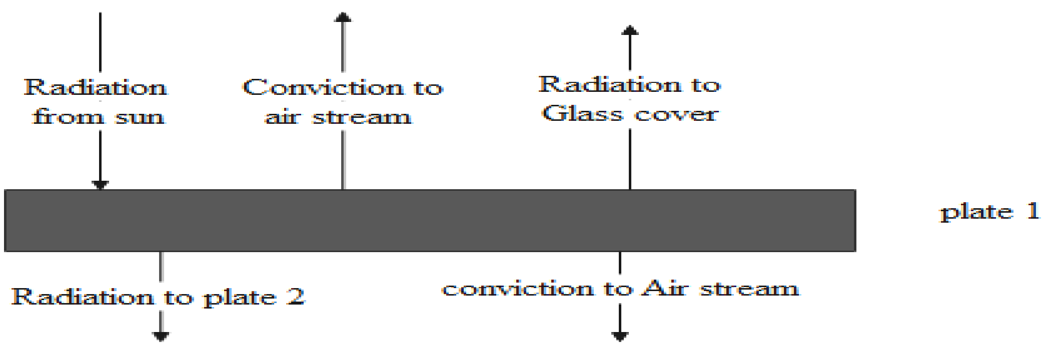

Figure 4. 8: Energy balance of air upper plate (plate 1)

$$\alpha_{p1}\tau_g I_T + h_{c,f1p1}(T_{f1} - T_{p1}) + h_{r,gp1}(T_g - T_{p1}) = h_{c,p1f2}(T_{p1} - T_{f2}) + h_{r,p1p2}(T_{p1} - T_{p2}) + (mC_p)_{p1}\frac{\partial T_{p1}}{\partial t}$$
....(4.28)

Where α_{p1} is absorptance of plate, τ_g is transmittance, $h_{c,f1p1}$ is convictive heat transfer from plate to fluid, m is mass of plate.

Absorber plate 2:

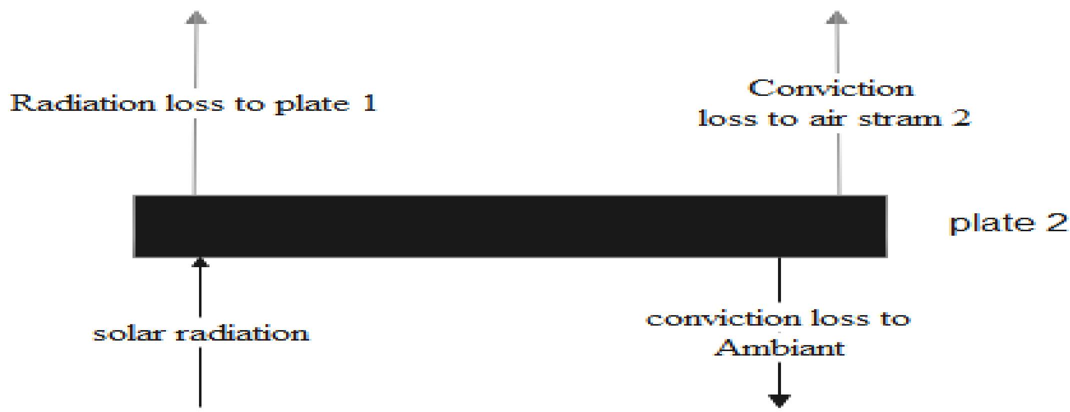

Figure 4. 9: Energy balance of air bottom plate (plate 2)

$$\alpha_{p2}\rho_R I_T - h_{c,ap2}(T_{p2} - T_a) = h_{c,p2f2}(T_{p2} - T_{f2}) + h_{r,p1p2}(T_{p2} - T_{p1}) + (mC_p)_{p2}\frac{\partial T_{p2}}{\partial t}$$ ....(4.29)

Where α_{p2} is absorptance of plate, τ_g is transmittance, $h_{c,f1p1}$ is convictive heat transfer from plate to fluid, m is mass of plate, ρ_R is reflectivity of reflector.

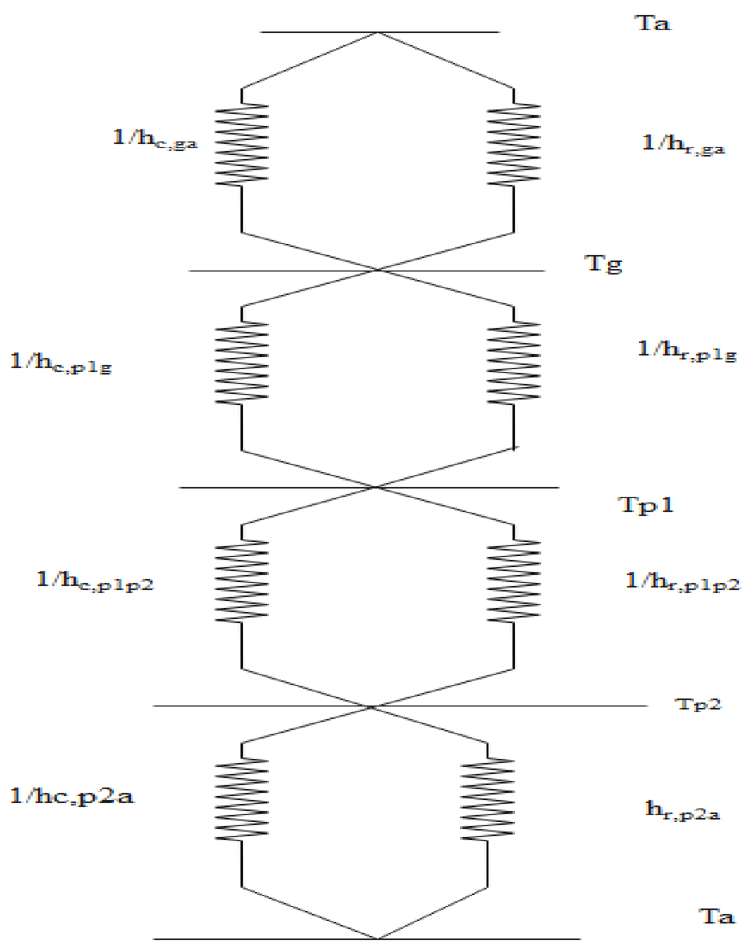

Figure 4. 10: Thermal resistance diagram of solar air heater

4.3.1.2 Energy analysis of energy storage

Performance Parameters of Latent Heat Storage System

Performance parameters of LHS include determination of melt fraction, charging, and discharging time. Most of the PCMs, especially a mixture of salts, often melt over a finite temperature range. This temperature range wherein, the melt exists in both solid and liquid phases is generally called mushy zone. The highest temperature at which, the material is completely in the solid state is called solidus temperature ($T_S = T_M - \Delta T_m$) and the lowest temperature at which, the material is completely in the liquid state is called liquidus temperature ($T_L = T_M + \Delta T_m$). Melt fraction is a non-dimensional parameter, which quantifies the percentage of liquid phase in the mushy region. Melt fraction of the PCM can be calculated based on the lever rule applied between the solidus and liquidus temperatures and it is given by equation (4.30). Charging is the process of storing heat energy in the latent heat storage material while it changes its phase from the solid state to the liquid state. Charging time implies the total time it takes for the LHS material or PCM to completely melt into the liquid state. The LHS is said to be fully charged when the entire PCM is completely melted, i.e., when the melt fraction reaches a value of one. Discharging is the process of releasing heat energy in the latent heat storage material while it changes its phase from the liquid state to the solid-state. Discharging time for LHS is defined concerning the temperature decrease of the PCM. The LHS is said to be fully discharged when the entire PCM is solidified, i.e., the melt fraction becomes zero (Niyas et al.,2017).

Melt fraction (θ_f) of the PCM was obtained from the relationship (Niyas et al.,2017).

$$\theta_f = \frac{T - Ts}{T_L - Ts} = \frac{T - T_m + \Delta T_m}{2\Delta T_m} = \begin{cases} 0 & for \quad T < Ts \\ 0-1 & for\, Ts \le T \le T_L \\ 1 & for \quad T > Ts \end{cases} \quad \text{.......(4.30)}$$

Where T_m is the melting point of PCM T is temperature recorded from thermocouple.

The total heat stored in the LHS system ($E_{T,Ch}$) consists of the sensible heat ($E_{S,Ch}$) and the latent heat ($E_{L,Ch}$). These can be obtained from the relationship (Niyas *et al.*,2017).

$$E_{T,Ch} = \underbrace{mC_{pa}(T - T_{in})}_{E_{S,Ch}} + \underbrace{mL_h\theta_f}_{E_{L,Ch}} \quad \text{.......(4.31)}$$

Energy recovered (discharged)

The total heat discharged from the LHS system ($E_{T,Dis}$) consists of the sensible heat ($E_{S,dis}$) and the latent heat ($E_{L,dis}$). These are expressed as (Niyas *et al.*, 2017).

$$E_{T,Dis} = \underbrace{mC_{pa}(T_{in} - T)}_{E_{S,dis}} + \underbrace{mL_h\left(1 - \theta_f\right)}_{E_{L,dis}} \quad \text{.......(4.32)}$$

Energy Efficiency of Latent Heat Storage System

Efficiency of latent heat storage is defined as the ratio of the net heat recovered during the discharging period to the net heat input during the charging period.

$$\eta_{LHS} = \frac{Q_{Dis}}{Q_{Ch}} \quad \text{.......(4.33)}$$

4.3.1.3 Greenhouse energy balance

The assumptions in developing the mathematical model for the solar greenhouse dryer are as follows:

- ✓ There is no stratification of the air inside the dryer.
- ✓ Drying computation is based on a thin layer drying model.
- ✓ Specific heat of air, cover and product are constant.
- ✓ Radiative heat transfers from the floor to the over and from the floor to the product are negligible

Energy Balance of the Cover

The balance of energy on the cover is considered as follows: Rate of accumulation of thermal energy in the cover = Rate of thermal energy transfer between the air inside the dryer and the cover due to convection + Rate of thermal energy transfer between the sky and the cover due to radiation + Rate of thermal energy transfer between the cover and ambient air due to convection + Rate of thermal energy transfer between the product and the cover due to radiation + Rate of solar radiation absorbed by the cover.

The energy balance of the cover gives:

$$m_c C_{cp} \frac{dT_c}{dt} = A_c h_{c,c-a}\left(T_a - T_c\right) + A_c h_{r,c-s}\left(T_s - T_c\right) + A_c h_w\left(T_{am} - T_c\right) + A_p h_{r,p-c}\left(T_p - T_c\right) + A_c \alpha_c I_t \quad ..(4.34)$$

Where m is mass, A_c is area of collector, C_p is specific heat capacity Ta is ambient temperature, Tp is product temperature, α_c is absorptance of collector.

Energy Balance of the Air inside the Dryer

This energy balance can be written as: Rate of accumulation of thermal energy in the air inside the dryer = Rate of thermal energy transfer between the product and the air due to convection + Rate of thermal energy transfer between the floor and the air due to convection + Rate of thermal energy gain of the air from the product due to sensible heat transfer from the product to the air + Rate of thermal energy gained in the air chamber due to inflow and outflow of the air in the chamber + Rate of over all heat loss from the air in the dryer to the ambient air.

The energy balance in the air inside the greenhouse chamber gives:

$$m_a C_{pa}\frac{dT_a}{dt} = A_p h_{c,p-a}\left(T_p - T_a\right) + A_f h_{c,f-a}\left(T_f - T_a\right) + D_p A_p C_{pw}\rho_p\left(T_p - T_a\right)\frac{dM_p}{dt} + \rho_a V_{out} C_{pa} T_{out}$$

$$-\rho_a V_{in} C_{pa} T_{in} + U_c A_c\left(T_{am} - T_a\right) \quad (4.35)$$

Where m is mass, A_c is area of collector, C_p is specific heat capacity Ta is ambient temperature, Tp is product temperature, α_c is absorptance of collector, D_p is depth of product A_p is area of product, ρ_a is density of air, V_{out} volume of air at outlet $h_{c,f-a}$ is convictive heat transfer from air to fluid, A_f is area of floor M_p is moisture percent.

Energy Balance of the Product

The energy balance of the product inside the greenhouse dryer can be written as: Rate of accumulation of thermal energy in the product = Rate of thermal energy transfer between air and product due to convection + Rate of thermal energy transfer between cover and product due to radiation + Rate of thermal energy lost from the product due to sensible and latent heat loss from the product + Rate of thermal energy absorbed by the product.

The energy balance on the product gives:

$$m_p(C_{pg} + C_{pl}M_p)\frac{dT_p}{dt} = A_p h_{c,P-a}\left(T_a - T_P\right) + F_p\alpha_p I_t A_c\tau_c + A_p h_{r,p-c}\left(T_c - T_p\right)$$

$$+ D_p A_p \rho_p\left[L_p + C_{pv}(T_a - T_p)\right]\frac{dM_p}{dt} \quad (4.36)$$

Where C_{pg} is specific heat capacity of product when water is in vapor, C_{pl} is specific heat capacity when water is liquid.

Energy Balances on the Floor

The energy balance on the floor of the greenhouse dryer can be written as: Rate of accumulation of thermal energy in the floor = Rate of convection heat transfer between air in the dryer and the floor + Rate of conduction heat transfer between the floor and the ground + Rate of solar radiation absorption on the floor.

$$m_f C_{pf}\frac{dT_f}{dt} = A_f h_{c,f-a}\left(T_a - T_f\right) + A_f h_{D,f-g}(T_g - T_f) + \left(1 - F_p\right)\alpha_f I_t A_f \tau_c \quad (4.37)$$

Mass Balance Equation

The accumulation rate of moisture in the air inside dryer = Rate of moisture inflow into the dryer due to entry of ambient air – Rate of moisture outflow from the dryer due to exit of air from the dryer + Rate of moisture removed from the product inside the dryer. The mass balance inside dryer chamber gives:

$$\rho_a V \frac{dH}{dt} = A_{in}\rho_a H_{in} V_{in} - A_{out}\rho_a H_{out} V_{out} + D_p A_p \rho_d \frac{dM_p}{dt} \quad \text{.......(4.38)}$$

Where H is relative humidity, A is Area , V is velocity ρ_a is air density, ρ_d is density of product, in is inlet and out is outlet

4.3.2 Heat Transfer and Heat Loss Coefficients

Radiative heat transfer coefficient from the cover to the sky ($h_{r,c-s}$) is computed according to (Duffie and Beckman,2013)

$$h_{r,c-s} = \varepsilon_c \sigma \left(T_c^2 + T_s^2\right)\left(T_c + T_s\right) \quad \text{.......(4.39)}$$

Radiative heat transfer coefficient between the product and the cover ($h_{r,p-c}$) is computed as (Duffie and Beckman,2013)

$$h_{r,p-c} = \varepsilon_p \sigma \left(T_p^2 + T_c^2\right)\left(T_p + T_c\right) \quad \text{.......(4.40)}$$

The sky temperature (Ts) is computed as (Duffie and Beckman,2013)

$$T_s = 0.552 T_{am}^{1.5} \quad \text{.......(4.41)}$$

Convective heat transfer coefficient from the cover to ambient due to wind (h_w) is computed as

$$h_w = 2.8 + 3V_w \quad \text{.......(4.42)}$$

Convective heat transfer coefficient inside the solar greenhouse dryer for either the cover or product and floor (hc) is computed from the following relationship (Duffie and Beckman,2013):

$$h_{c,f-a} = h_{c,c-a} = h_{c,p-a} = h_c = \frac{Nuk_a}{D_h} \quad \text{.......(4.43)}$$

Where D_h is given by:

$$D_h = \frac{4WD}{2(W+D)} \quad \text{.......(4.44)}$$

Nusselt number, (Nu) is computed from the following relationship (Kays and Crawford, 1980).

$$Nu = 0.0158\,\mathrm{Re}^{0.8} \quad \text{...}(4.45)$$

where Re is the Reynolds number which is given by:

$$\mathrm{Re} = \frac{D_h V_a \rho_a}{\upsilon} \quad \text{...}(4.46)$$

As the wind speed outside the dryer and the speed of drying air inside the dryer are very low, we assumed that the overall heat loss coefficient (U_c) of heat transfer from air inside the dryer to ambient air was approximately equal to the conductive heat transfer coefficient of the cover (Tiwari, 2003). This coefficient can be written as:

$$U_c = \frac{k_c}{\delta_c} \quad \text{...}(4.47)$$

The energy absorption of solar collector was evaluated according to ASHRAE standard ; fluid inlet, outlet temperature (Ti, To) and fluid flow rate ($\dot{m}$) were recorded accordingly. The amount of energy (Qu) is calculated by using the following equation.

$$Q_u = mC_p\left(T_o - T_i\right) \quad \text{...}(4.48)$$

The specific heat (C_p) was given by 1.005 kJ/kg K in these case. The thermal efficiency of the solar collector (ηc) which found from a general solar collector thermal efficiency equation was the ratio of useful energy (Qu) and the solar radiation incident on the plane of collector (AcI). The thermal efficiency of the solar collector was expressed that;

$$\eta_c = \frac{Q_u}{A_c I_t} = \frac{mC_p\left(T_o - T_i\right)}{A_c I_t} \quad \text{...}(4.49)$$

The efficiency of drying system was the ratio of the energy required to evaporated moisture (Wh_L) and the heat supplied to dryer. The heat suppliers were the solar radiation incident on the solar collector, heat energy of fan (Qf) and heat energy of fan (Qf). The efficiency of drying system was calculated as

$$\eta_d = \frac{Wh_L}{A_c I_t + Q_b + Q_f} \quad \text{...}(4.50)$$

The latent heat of vaporization (h_L) was given by 2,264.76kJ/kg. The mass of water removed from a wet product (W) was calculated by using amount of initial mass product (mo), the initial and final moisture content of product (Mi, Mf) as expressed in equation (4.1)

4.3.3 Exergy Analysis

Exergy is defined as the amount of maximum work, which can be produced by a system or a flow of matter or energy as it comes to equilibrium with a reference environment (El Khadraoui *et al.*, 2017). The exergy uses the conservation of the mass and the energy principles together with the second law of thermodynamics for the design and analysis of the energy systems.

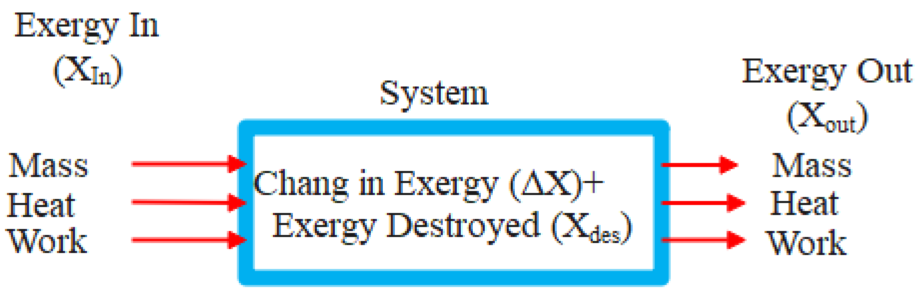

Figure 4. 11: Exergy balance

Exergy by Heat Transfer, Q

Exergy transfer by heat is appears between two heat sources at different temperatures is given by the following relation (Cengel and Boles, 2010):

$$X_{heat} = \left(1 - \frac{T_{si}}{T_{so}}\right) Q \quad \text{.....(4.51)}$$

Where Tsi is temperature at sink Tso temperature at source $T_{so} > T_{si}$, Q is heat transferred between the two reservoirs.

Exergy Transfer by Work, W

Exergy is the useful work potential, and the exergy transfer by work can simply be expressed as (Cengel and Boles, 2010):

$$X_{work} = p_o \left(V_2 - V_1\right) \quad \text{.....(4.52)}$$

*P*0 is atmospheric pressure, and *V*1 and *V*2 are the initial and final volumes of the system.

Exergy Transfer by Mass, *m*

Mass flow is a mechanism to transport exergy, entropy, and energy into or out of a system. When mass in the amount of *m* enters or leaves a system is given by (Cengel and Boles, 2010):

$$Xmass = m\psi \quad \text{.....(4.53)}$$

where $\psi = (h_2 - h_1) - T_o(s_2 - s_1) + \frac{V^2}{2} + gz$, h_1 and h_2 are enthalpy at inlet and outlet of system respectively, s_1 and s_2 are entropy at inlet and outlet of system. V is velocity of moving fluid, g is gravity and z is height of the system.

Exergy out and exergy in are the sum of exergy of heat (Q), exergy of mass (m) and exergy of work.

$$X_{in} = X_{work,in} + X_{heat,in} + X_{mass,in} \quad (4.54)$$

$$Xout = X_{work,out} + X_{heat,out} + X_{mass,out} \quad (4.55)$$

To perform exergy analysis, the following assumptions are considered

- The flow is assumed to be steady.
- The effects of the kinetic and the potential energy are neglected.
- The effect of moisture content on the heat capacity of the air is neglected.
- The exergy loss in the product is neglected.
- The change in the pressure between the inlet and out is neglected.

4.3.3.1 Exergy analysis of the solar air heater

Under steady state condition, the equation of exergy balance takes the following form (Jafarkazemi and Ahmadifard, 2013)

$$\sum \dot{X}_{In} - \sum \dot{X}_{Out} = \sum \dot{X}_{des} \quad (4.56)$$

Where, $\dot{X}_{In}$, $\dot{X}_{Out}$, $\dot{X}_{des}$ are the inlet, outlet, and destructed exergy rate, respectively.

The inlet exergy to the collector consists of the exergy of absorbed heat from sun ($\dot{X}_{rad}$) and the exergy of inlet fluid ($\dot{X}_{in,f}$). A major part of inlet exergy to the system is that solar radiation which is absorbed by the absorption plates and obtained using the expression (Yadav and Kaushal, 2014)

$$\dot{X}_{rad} = \left[1 - \frac{T_{am}}{T_s}\right]\dot{Q}_{in} \quad (4.57)$$

Where, T_s is the apparent sun temperature as exergy source which is approximately 3/4 of the blackbody temperature of the sun. It is assumed to be 4500 K in this analysis.

And the exergy of inlet fluid ($\dot{X}_{in,f}$) and outlet fluid ($\dot{X}_{out,f}$) expressed as:

$$\dot{X}_{in,f} = \dot{m}_a C_{pa}\left[\left(T_{i,SAH} - T_{am}\right) - T_{am} In\left(\frac{T_{i,SAH}}{T_{am}}\right)\right] \text{.......}(4.58)$$

$$\dot{X}_{out,f} = \dot{m}_a C_{pa}\left[\left(T_{out,SAH} - T_{am}\right) - T_{am} In\left(\frac{T_{out,SAH}}{T_{am}}\right)\right] \text{.......}(4.59)$$

The difference between these two components ($\dot{X}_{in,f}$ and $\dot{X}_{out,f}$) represents the amount of exergy loss in the collector and expressed as:

$$\dot{X}_{in,f} - \dot{X}_{out,f} = \left(1 - \frac{T_{am}}{T_s}\right)\dot{Q}_{in} - \dot{m}_a C_{pa}\left[\left(T_{out,SAH} - T_{out,SAH}\right) - T_{out,SAH} In\left(\frac{T_{out,SAH}}{T_{out,SAH}}\right)\right] \text{.......}(4.60)$$

The exergy destruction in the solar air heater is given by Equation (4.62)

$$\dot{X}_{des} = \left(1 - \frac{T_{am}}{T_s}\right)\dot{Q}_{in} - \dot{m}_a C_{pa}\left[\left(T_{out,SAH} - T_{out,SAH}\right) - T_{out,SAH} In\left(\frac{T_{out,SAH}}{T_{out,SAH}}\right)\right] \text{.......}(4.61)$$

The exergy efficiency of the solar air heater is expressed as follows (Akpinar and Koçyiğit, 2010)

$$\eta_{\dot{X},SHA} = 1 - \frac{\dot{X}_{des}}{\dot{X}_{in,SAH}} \text{.......}(4.62)$$

4.3.3.2 Exergy analysis of Greenhouse

The exergy inflow and outflow of the drying chamber are estimated by equations (4.64) and (4.65), respectively (Fudholi *et al*., 2014).

$$\dot{X}_{rad} = \left[1 - \frac{T_{am}}{T_s}\right]\dot{Q}_{in} \text{.......}(4.63)$$

$$\dot{X}_{in,gh} = \dot{m}_a C_{pa}\left[\left(T_{in,gh} - T_{am}\right) - T_{am}\ln\left(\frac{T_{in,gh}}{T_{am}}\right)\right] \text{.......}(4.64)$$

$$\dot{X}_{out,gh} = \dot{m}_a C_{pa}\left[\left(T_{out,gh} - T_{am}\right) - T_{am}\ln\left(\frac{T_{out,gh}}{T_{am}}\right)\right] \text{.......}(4.65)$$

During the solar drying process, the exergy destruction is determined as:

$$\dot{X}_{des} = \dot{X}_{rad} + \dot{X}_{in,gh} - \dot{X}_{out,gh} \text{.......}(4.66)$$

Substituting equation (4.63), (4.64) and (4.65) in to (4.66) gives

$$\dot{X}_{des} = \left(1 - \frac{T_{am}}{T_s}\right)\dot{Q}_{in} + \dot{m}_a C_{pa}\left[\left(T_{in,gh} - T_{out,gh}\right) - T_{am}\ln\left(\frac{T_{in,gh}}{T_{out,gh}}\right)\right] \quad (4.67)$$

The exergy efficiency of the drying cabinet is the ratio of the exergy outflow to the exergy inflow of the greenhouse is expressed as:

$$\eta_{\dot{X},gh} = \frac{\Delta\dot{X}_{air}}{\dot{X}_{in,gh}} = \frac{\dot{m}_a C_{pa}\left[\left(T_{out,gh} - T_{in,gh}\right) - T_{am}\ln\left(\frac{T_{out,gh}}{T_{in,gh}}\right)\right]}{\left(1 - \frac{T_{am}}{T_s}\right)\dot{Q}_{in}} \quad (4.68)$$

4.3.3.3 Exergy analysis of energy storage

During charging and discharging process, the instantaneous exergy input to the energy storage and exergy recovered from the storage, respectively, are expressed as (Dincer and Rosen, 2011):

$$\dot{X}_{ch} = \dot{m}_a C_{pa}\left[\left(T_{in,str} - T_{out,str}\right) - T_{am}\ln\left(\frac{T_{in,str}}{T_{out,str}}\right)\right] \quad (4.69)$$

$$\dot{X}_{dich} = \dot{m}_a C_{pa}\left[\left(T_{out,str} - T_{in,str}\right) - T_{am}\ln\left(\frac{T_{out,str}}{T_{in,str}}\right)\right] \quad (4.70)$$

The net exergy input and exergy recovered during the charging and discharging periods, respectively, are calculated as:

$$X_{ch} = \int_0^t \dot{X}_{ch}\,dt \quad (4.71)$$

$$X_{dich} = \int_0^t \dot{X}_{dich}\,dt \quad (4.72)$$

The exergy efficiency of the energy storage system is defined as the ratio of the net exergy recovered from the energy storage during the discharging period to the net exergy input to the storage during the charging period (Koca *et al*., 2008).

$$\eta_{X,str} = \frac{X_{dich}}{X_{ch}} \quad (4.73)$$

Exergy Stored During Charging

During the charging mode of operation, the exergy stored at any time instant is computed from the instantaneous heat transfer rate expressed as (Suresh *et al*., 2014):

$$\dot{X}_{ch} = mL_h\left(1-\frac{T_a}{T_m}\right)+\dot{m}C_{p,pcm}\left[(T_m - T_{in})-T_o \ln\left(\frac{T_m}{T_{in}}\right)\right]+\dot{m}C_{p,a}\left[(T_{in}-T_m)\right]-T_o \ln\left(\frac{T_{in}}{T_m}\right) \quad \text{............(4.74)}$$

Exergy Released During Discharging

Expressions for exergy stored during the discharging process can be obtained in the similar way corresponds to the charging process as (Suresh *et al*., 2014);

$$\dot{X}_{dis} = mL_h\left(1-\frac{T_a}{T_m}\right)+\dot{m}C_{p,pcm}\left[(T_{in,dis} - T_m)-T_o \ln\left(\frac{T_m}{T_{in,dis}}\right)\right]+\dot{m}C_{p,a}\left[(T_m-T_{in,dis})\right]-T_o \ln\left(\frac{T_m}{T_{in,dis}}\right)$$

....(4.75)

Exergy Efficiency of Latent Heat Storage System

The overall exergy efficiency of latent heat storage is expressed as;

$$\eta_{\dot{X},LHS} = \frac{\dot{X}_{dis}}{\dot{X}_{ch}} \quad \text{...(4.76)}$$

4.4 Numerical Formulation of the System Components

4.4.1 CFD Pre-Processing Stage for the system components

The pre-processing stage in the CFD simulation includes geometry creation, mesh development, physical properties set-up and the implementation of solving technique and parameters.

1. **Geometry creation.**

Geometry modeling in the ANSYS Workbench environment is highly automated and also provides users the flexibility to customize according to the type of analysis or application. The feature-based, parametric ANSYS Design Modeler software is used to create parametric geometry from scratch or to prepare an existing CAD geometry for analysis. It includes automated options for simplification, cleanup, and repair.

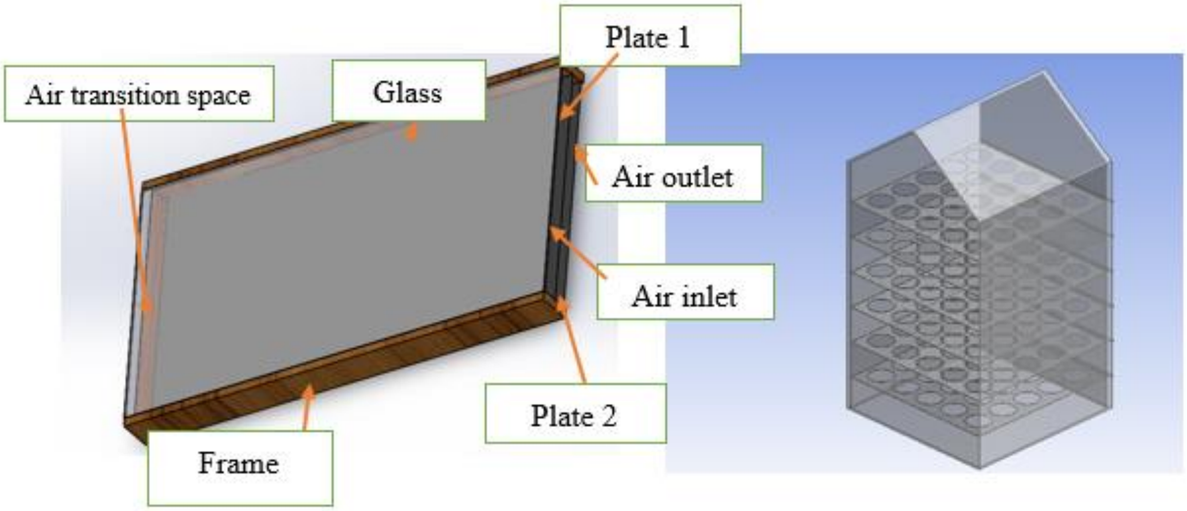

Figure 4. 12: The geometry of the solar collector and greenhouse

Solar heater and greenhouse were designed by using solid works 2018 based on the dimensions obtained by design parameters and initial conditions. The area obtained was $1m^2$ and $2m^2$ for solar collector and for greenhouse respectively, having length of 1.4 m and width of 0.72 m for collector and base area of 60 x60 cm^2 and height of 1.2m. The double pass solar collector and greenhouse generated from solid works 2018 were as shown in figure 4.11.

2. **Mesh development.**

The next step of CFD Analysis after creating geometry is importing geometry into Ansys and meshing and describing a model by Ansys fluent R19.2. Meshing is a key part of the quality and convergence of the solutions. The discretization of the domain was based on the finite volume method, by means of the decomposition of the domain into small control volumes, generating a three dimensional mesh of nodes. The finite volume method considers the principles of conservation of mass, momentum, and energy, which are the basis of fluid-dynamic mathematical modeling. The model consists of a glass cover, absorber plate, wooden box, and inlet and outlet sections for the fluid of solar collector and glass and, supporting structure as shown in figure 4.12

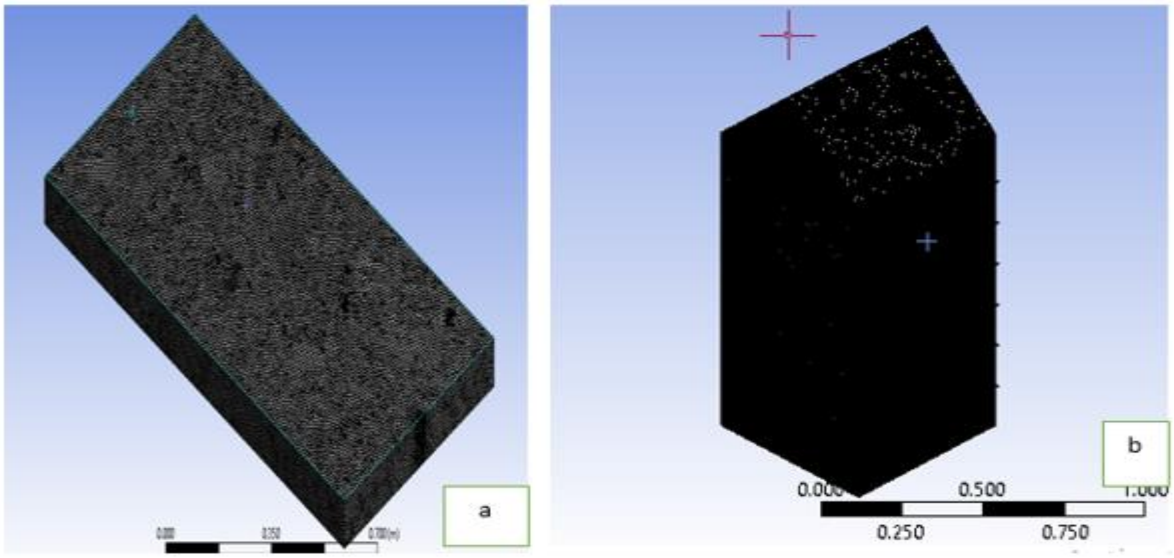

Figure 4. 13 Mesh genration a) collector b) greenhouse

3. **Setup**

A steady state implicit pressure-based simulation has been carried out using ANSYS FLUENT and a SIMPLE algorithm was used for the pressure velocity coupling. Discretization is made using second order upwind scheme and a standard k-epsilon model was used for the simulation. A residual convergence criterion of 10^{-6} is given for the solution to converge and a standard solution initialization technique is used to initialize the solution.

4. **Boundary conditions**

The momentum and energy equations are solved using finite volume method and appropriate boundary conditions are imposed on the computational domain. The inlet is specified as a "mass-flow inlet" with a mass flow rate of 0.02 kg/s and the outlet as pressure outlet with gauge pressure of 0 pa. A heat flux equivalent to the solar radiation falling on the surface on May is given on the top and the sides are insulated.

Governing equations for flat plate solar air heater and greenhouse

CFD methods consist of numerical solutions of mass, momentum, and energy conservation. The governing equation for the simulation is written based on the following assumptions.

1. The thermo-physical properties of components are constant
2. The flow is incompressible and continuous.

3. The material of duct wall and absorber plate are homogeneous and isotropic.
4. All the walls in contact with the fluid are assigned no-slip boundary condition.
5. Heat loss in the form of radiation is negligible.

Continuity equation is written as:

$$\nabla.\rho\vec{V}+\frac{\partial p}{\partial t}=0 \qquad (4.77)$$

Momentum equation is written as:

$$\frac{\partial\vec{v}}{\partial t}+\left(\vec{v}.\nabla\right)\vec{v}=\frac{1}{\rho}\left(-\nabla P+\mu\nabla^{2}\vec{v}\right) \qquad (4.78)$$

Energy equation is written as:

$$\left(\rho C_{p}u\frac{\partial T}{\partial x}+\rho C_{p}v\frac{\partial T}{\partial y}+\rho C_{p}w\frac{\partial T}{\partial z}\right)=K\nabla^{2}T \qquad (4.79)$$

4.4.2 Numerical modelling of the latent heat storage

For the simulation of the latent heat storage a finite element-based software COMSOL Multiphysics 5.3a is used.

1. Model description and meshing

A sectional view of a 3D shell and tube latent heat storage model filled with paraffin wax in the shell and air in the tubes is shown in Figure 4.8. The geometry of the storage has been created on COMSOL Multiphysics 5.3a using the dimension obtained from the design. The length and the diameter of the shell is 1 m and 0.2 m and the tubes are 1 m in length, 16 mm outer diameter and 14 mm inner diameter with a total of five tubes. Meshing is carried out using free tetrahedral and triangular meshes for the domains and boundaries as shown in Figure 4.13. A special meshing feature of COMSOL Multiphysics called boundary layer is used to have finer meshes near the critical zones of the model.

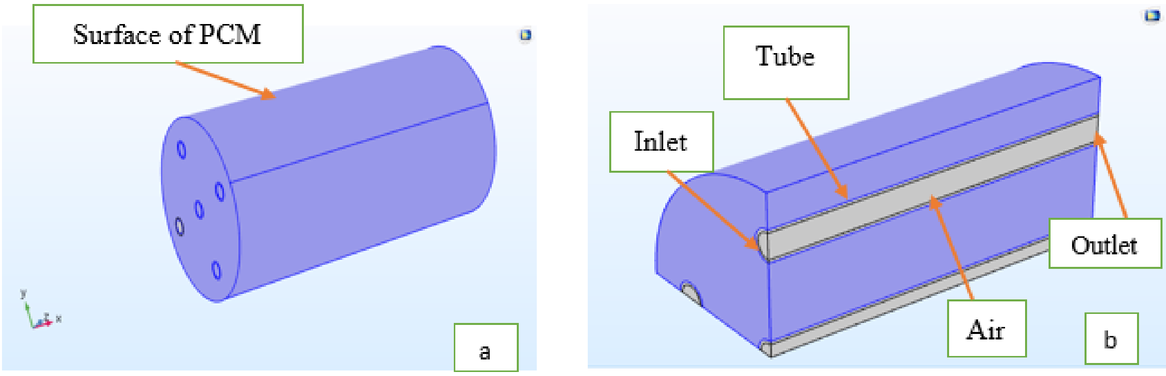

Figure 4. 14: View of the latent heat storage a) isometric b) Section

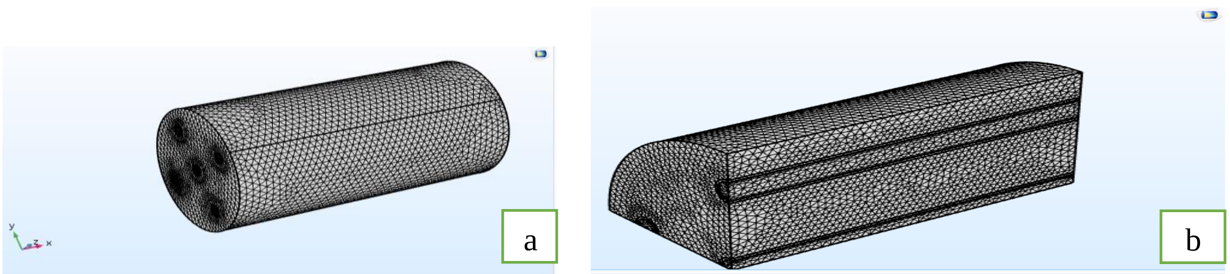

Figure 4. 15: Meshed view of the latent heat storage a) isometric b) section

2. Numerical treatment

A finite element-based software, COMSOL Multiphysics 5.3a which uses Galerkin method as a discretization technique is used to solve the governing equations of the LHS. PARDISO, a time dependent solver, is used to solve the equations and time stepping is done based on the backward differential formula (BDF) which has an initial minimum time step and a maximum time step. The minimum time step is set to 0.01 s and to solve the problem in the least possible run, the maximum time step is not set to automatically maximize the time step.

Governing equations for the latent heat storage

The thermal energy storage behavior of a latent heat storage can be studied by simulating four physical processes, HTF flow, phase change, convection and conduction. The thermal model is developed based on following assumptions: HTF is incompressible and Newtonian.

- HTF flow is laminar and exhibits negligible viscous dissipation.

- The initial temperature of PCM is uniform.
- Phase change during melting/solidification occurs in a temperature interval.
- Thermal losses through the outer wall of the PCM are negligible.
- PCM is homogeneous and isotropic.

A coupled conjugate heat transfer problem which simultaneously solves both the phase change behavior of the PCM and the flow behavior of the air is used to solve the developed LHS model. expressed as (Niyas *et al*., 2017):

$$Cp = \begin{cases} C_{p,s} \quad for\, T < T_s \\ C_{p,EFF} \quad for T_s \le T \le T_l \\ C_{p,l} \quad for\, T > T_l \end{cases} \quad \text{.......} (4.80)$$

$$C_{p,EFF} = \frac{C_{p,s} + C_{p,l}}{2} + \frac{Lh}{T_l - T_S} \quad \text{.......} (4.81)$$

The energy and continuity equations given in Eqns. (4.78) and (4.80) are used to simulate the model. To include the effect of buoyancy ($\vec{F}$) and Darcy law's source term and reduce the complexity in solving the Naiver-Stokes equations, Boussinesq approximation is added to the momentum equation, which is given by (Niyas *et al*., 2017):

$$\frac{\partial \vec{v}}{\partial t} + (\vec{v}.\nabla)\vec{v} = \frac{1}{\rho}\left(-\nabla P + \mu \nabla^2 \vec{v} + \vec{F} + \vec{S}\right) \quad \text{.......} (4.82)$$

$$\vec{F} = \rho g \beta (T - Tm) \quad \text{.......} (4.83)$$

$$\vec{S} = \frac{(1-\theta)^2}{(\theta^3 + \varepsilon)} A_{mush} \vec{v} \quad \text{.......} (4.84)$$

Where, β is thermal expansion of the PCM, θ is melt fraction, A_{mush} is mushy zone constant and ε is a constant value of 0.001. Phase change problems occur during a temperature interval and they are often called mushy region problems. The mushy zone constant defines the transition of velocity in the mushy region and values between 10^3 and 10^7 are recommended for most computations (Niyas *et al*., 2017).

CHAPTER FIVE

5. EXPERIMENTAL SETUP AND PROCEDURE

5.1 Introduction

This chapter presents the conceptual model, working principle, manufacturing process, experimental setup and procedure followed while testing the prototype of a mixed mode, forced convection greenhouse dryer integrated with enhanced solar collector. The conceptual model of the system was developed using **solid works 2018**. The working principle of the system is explained in detail. Manufacturing process of each component for preparing the prototype is presented with descriptive photos. Finally, the measuring and testing devices used are presented.

5.2 Conceptual Model

The system diagram of greenhouse forced convection dryer enhanced with solar collector drawn using Solid Works 2018. The system consists of a flat plate double pass solar collector coated black cooper oxide, back reflector, greenhouse, thermal storage unit, blower, frame, and support. The conceptual design of the dryer is shown in Figure 5. 1.

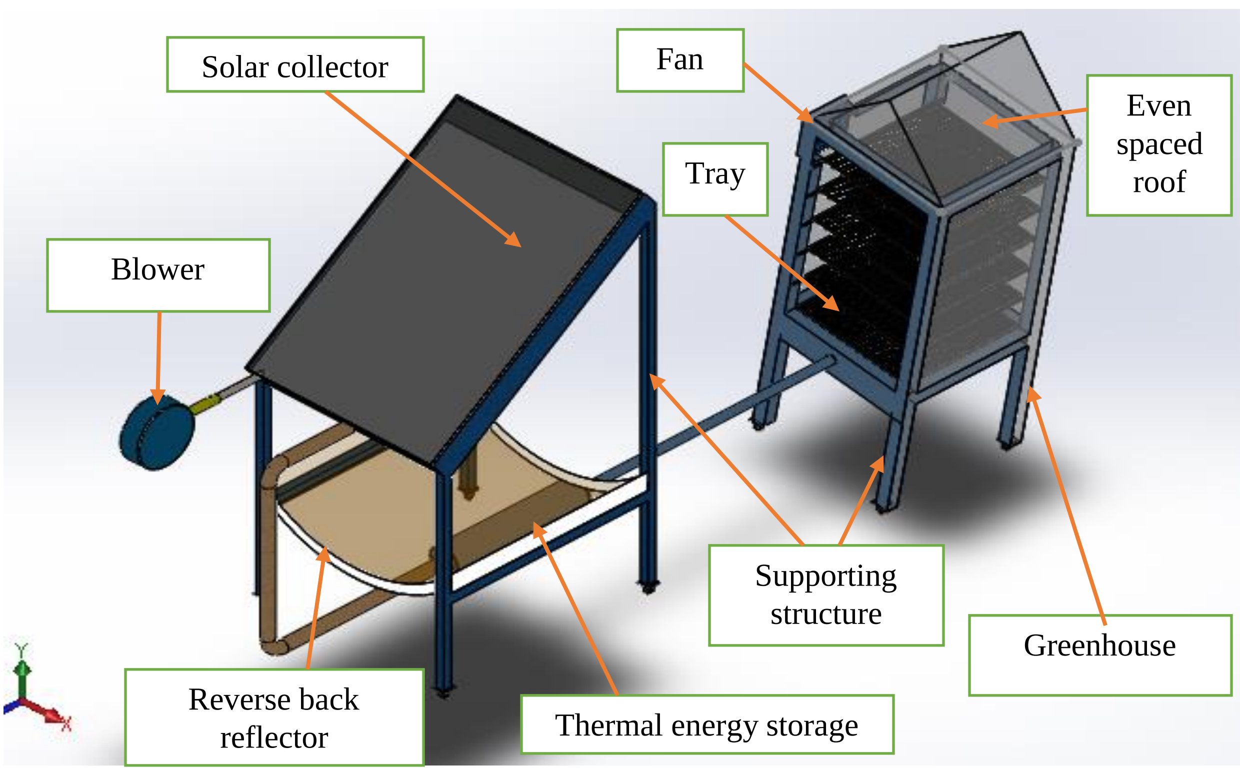

Figure 5. 1: Conceptual schematic of the designed system

5.2.1 Working Principle

The constricted system consists of a double pass flat plate solar collector with cooper oxide coat of absorber plate, greenhouse, thermal storage unit, reverse back reflector and a blower as illustrated in Figure 5.2. In this system, a double pass flat plate solar collector and greenhouse will absorb sun's radiant energy and transfer it to the air. The greenhouse receives heated air exiting from the solar air heater and from the sun, having temperature sufficiently higher than the ambient air. When temperature increases the excess heat will be absorbed and stored for later purpose by energy storage medium, which is filled by paraffin wax, in between the greenhouse and enhanced solar collector.

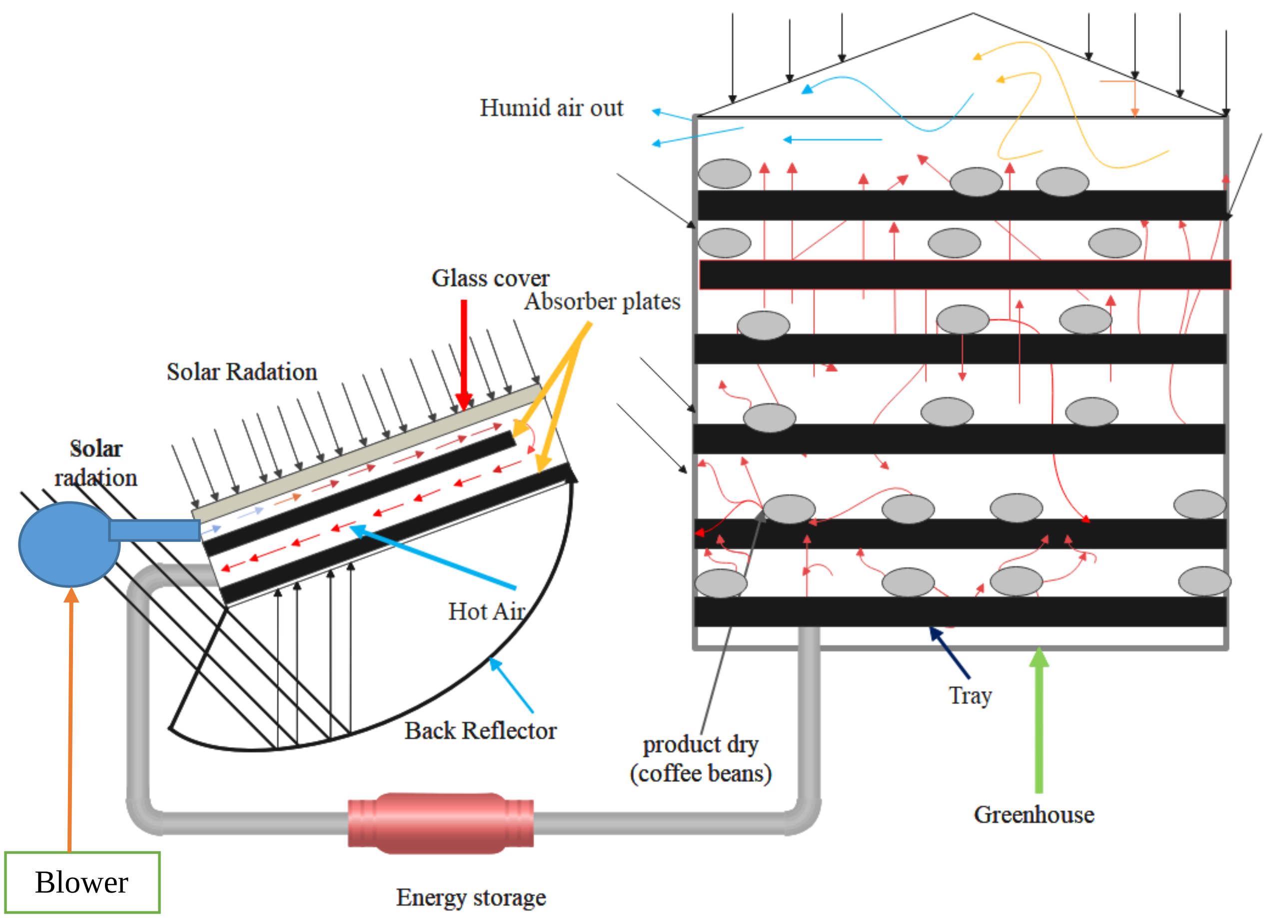

Figure 5. 2: Overall schematic diagram of the proposed solar coffee drier system

During charging, when the temperature of the air leaving the solar air heater is higher than the temperature of the PCM, heat will be transferred from the air to the PCM. Considering that during the discharge period, when the temperature of the air leaving the solar air heater is lower than the

PCM, the stored heat will be released from the PCM, causing the air temperature to rise. Then, the air passes through three drying trays to dry the product and ventilates to the atmosphere through air outlet after removing the moisture from the surface of the products. A blower system which helps in accelerating the heated air from solar collector to the drying chamber is integrated as an active mode.

5.3 Manufacturing Process

The components of the drying systems are the greenhouse, enhanced solar air heater, and latent heat storage. Each step used to construct components of the dryer and its assembly is shown, described, and discussed in this section as follows.

5.3.1 Construction of the Flat Plate Solar Air Heater

The collector is the part of the system that collects the useful energy (solar energy) that comes from the sun and transfers the heat to the air that comes from the ambient air and passes through it. A rectangular box, having a size of 1.4 m x 0.72 m x 0.107 m (length x width x height) was constructed from wood thickness 0.02 m as demonstrated in Figures 5.3. Additionally, the solar air heater contains an upper and lower absorber plate, insulation in side, reverse back reflector and a glass cover. The base plate is a 1.4m × 0.72 m galvanized iron sheet with 0.8 mm thickness. A 15 mm thick foam is placed side direction the collector. Reverse back reflector is placed below absorber plates to reduce bottom heat loss; the reflector has aperture length of 1.3m, aperture width of 1.23 m, rim angle of 66.3 ^{O}C, focal length 0.47m, and aperture area 1.6 m^2 and concentration ratio 0.63. It is covered with gift warp/ holographic paper having reflectivity of 0.95.

Black ink mixed with cooper oxide painted steel sheet of 1.4 m × 0.72 m and 1.0 mm thick is used as back absorber plate and placed at a gap of 80 mm from the glass cover and another black ink

Figure 5. 3: view of solar collector from bottom direction

mixed with coper oxide painted iron sheet of 1.3 m x 0.7 m x 1 mm thick is used as absorber plate and placed at 40 mm below glass cover. The glazing is a 1.4 m × 0.7 m and 4 mm thick plain glass and placed in the top of flat plate collector. The collector is mounted facing south tilted at an angle of 24° as shown in Figure 5.3. Then to reduce leakage silica gel is used to fill the gaps.

5.2.2 Construction of the Greenhouse

The greenhouse receives heat from sun and from enhanced solar collector. The body structure is made up of square steel having dimensions of 0.6 x 0.6 m^2 base area and 2.2 m height with 6 equally spaced trays. And the it is covered with glass having 4 mm thickness in all side except at bottom insulated. The top part of greenhouse is covered with Gable-even-span shape made of glass having slant height of 40 cm and height of 26 cm. the greenhouse has door in one side (backside) which is used for loading and unloading.

As discussed in the previous chapter this dryer has six trays used to carry the drying product. The trays are made of wired mashed (Figure 5.6) with very tiny holes used to transfer heat throughout the dryer. They have a dimension of 0.6 m x 0.6 m. The gap between the trays is 20 cm from one another. Each tray was kept on an angle iron fixed to the inner side of the greenhouse.

Figure 5. 4: Construction of the greenhouse

5.2.3 Construction of Latent Heat Storage Container

Thermal energy storage is done by using phase change material (PCM) as latent heat storage. Tube and shell are used as thermal storage container. The shell was manufactured from steel metal pipe having diameter of 140 mm and length of 76 cm. steel tubes were used to make five tubes with a length of 71 cm and the two ends are welded with flat iron of diameter 138 mm and finally welded with tube the assembled tube and shell. The tube is drilled in order to allow paraffin wax to be filled and finally the hole is welded with steel pipe. The tube and shell is filled with 9 kg of paraffin wax to store the excess heat of the daytime. The paraffin wax modules were first crushed into smaller pieces and melted using the wood firing and finally poured into the container through the PCM filling hole. To prevent leakage, epoxy mixed with hardener is applied to any possible openings in the shell, as well as both sides of the tubes inlet and outlet connections. The shell is covered with a 20 mm thick foam insulation.

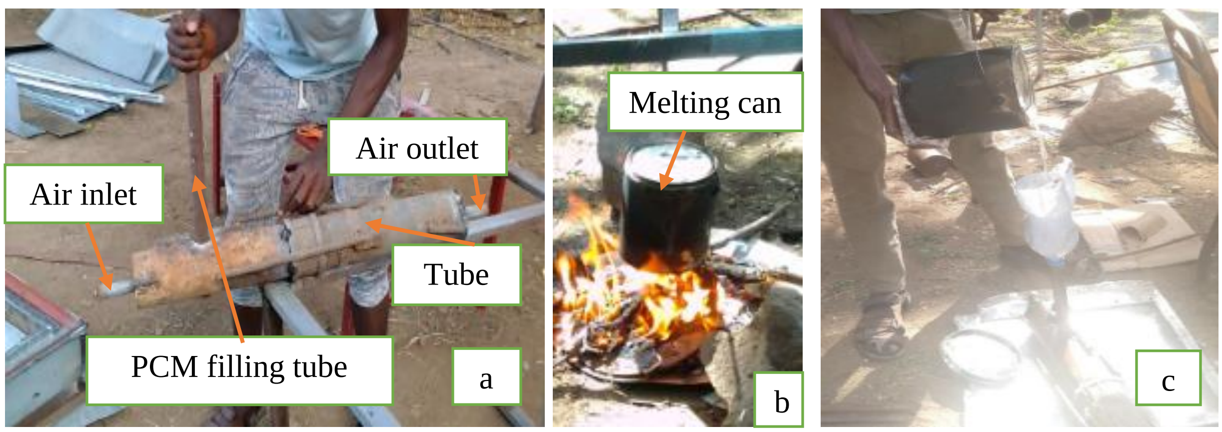

Figure 5. 5 Thermal energy storage ; a) construction of tube, b) melting of paraffin c) filling of tube

5.2.4 Construction of Supporter Structure

The supporting was prepared using welding process to hold the wooden casing of the collector, blower support and PCM container; It provides the rigidity and desired inclination to the solar radiations. The collector is mounted on a 1.42m × 0.72 m frame constructed from a square metal pipe and angle iron at an angle equal with the collector tilt angle of 24° as shown in Figure 5.6 and the reverse back reflector is mounted in it. The PCM is placed on frame constructed from square metal pipe and angle iron as shown in Figure 5.6. The whole supporting structure is painted varnish to improve its life as it always remains in the open environment.

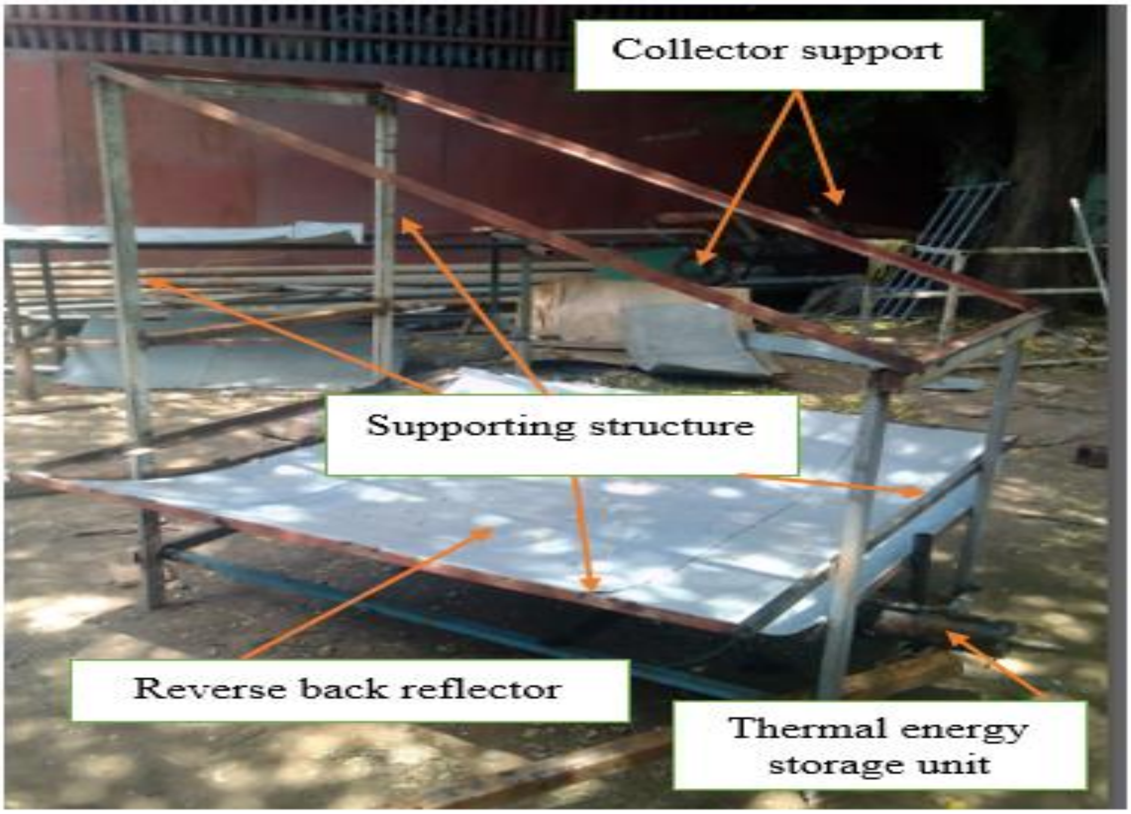

Figure 5. 6 Construction of Supporter Structure

5.3 Experimental Setup

Greenhouse assisted with enhanced solar air dryer in forced convection mode with PCM between greenhouse and enhanced solar collector designed, developed, and installed at Adama Science and Technology University, in front of mechanical workshop, in Adama, Ethiopia. The system facing south and tilted at an angle of 24°. Photograph of the complete experimental setup of the system used for the present experimental investigation is shown in Figure 5.7.

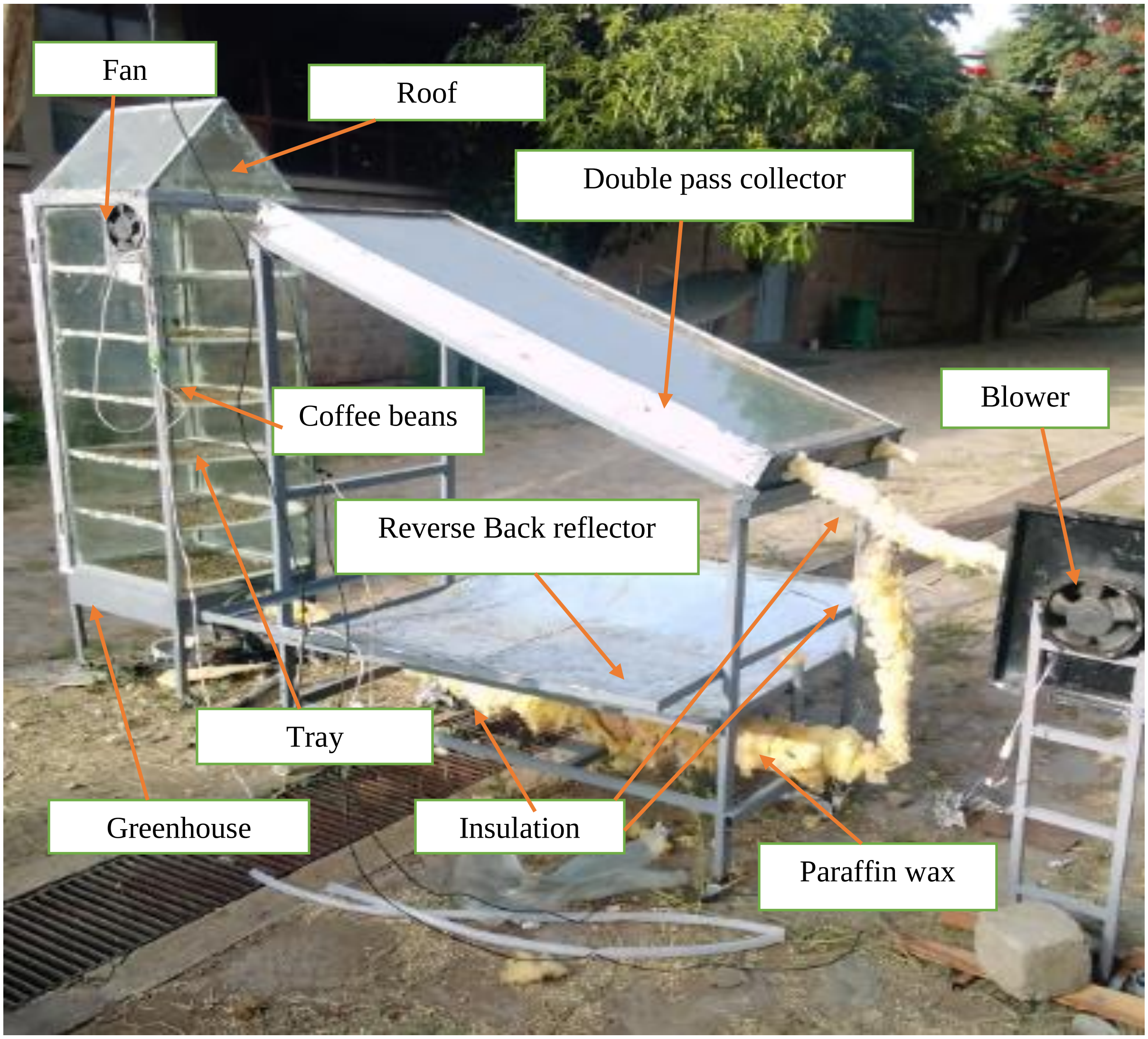

Figure 5. 7 Experimental setup of the system

The experimental setup consists of different parts assembled as one system which are double pass solar air collector, fan, reverse back reflector, greenhouse and tube and shell to keep paraffin inside it. The heat source for the installed dryer is obtained from the solar air collector and greenhouse using air as heat transfer fluid which is derived into the collector with the help of fan connected at the outlet of the greenhouse. A fan facilitates to drive out the moist air from the system to atmosphere and pulls atmospheric air into enhanced solar air collector and helps in accelerating the heated air from solar collector to the greenhouse. Paraffin wax in the form of PCM was placed in the PCM container as thermal storage system. The six drying trays of same size are mounted in side greenhouse demonstrated in Figure 5.7.

5.3.1 Experimental Procedure

The experimental study was carried out for fore different conditions:

1. Solo greenhouse
2. Enhanced collector
3. Greenhouse assisted with enhanced solar collector and PCM.

The first experiment is done on Solo Greenhouse, four thermocouples were placed at the inlet, outlet, ground and in tray of product inside greenhouse. The four thermocouples mounted are used to measure temperature at inlet, outlet, ground and product and then to evaluate the performance of Solo greenhouse. The second experiment was carried out to investigated the performance of enhanced solar air collector and PCM, in addition to the 1st experiment several additional thermocouples are installed in the solar collector at inlet and exit of the solar collector and tube and shell and performance of, collector and PCM is studied. The third experiment conducted to perform the performance of greenhouse enhanced with (nanoparticles coat, double pass, and reverse back reflector) solar collector connected with PCM. In this experiment the overall system performance of drying 5 kg coffee beans was evaluated. In each experiment, the inlet and outlet temperature of the solar air heater, greenhouse, and temperature of air after it passes the thermal energy storage was recorded every 30 minutes' interval.

5.3.2 Experimental measuring Instruments

Instruments used in this experiment are temperature sensor and weight sensor.

Temperature sensor

Thermocouple use to measure temperature of the system during experimentation which are located at different parts of the system. K-type thermocouple wires are used in the setup. A data reader (Thermocouple 1) is used to read the temperature sensed by thermocouples and the values are recorded manually. The thermocouples can read values between -200 to 1350 °C. Thermocouple 2 is used to measure ambient temperature.

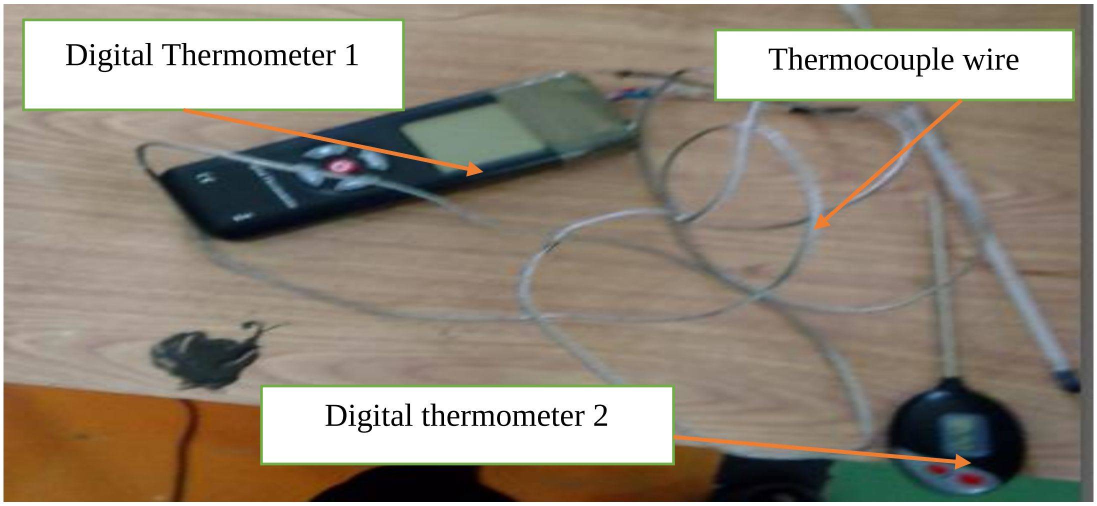

Figure 5. 8 Temperature measuring device

Weight measurement

Digital weight balance is used to measure the weight of the PCM, nanoparticles, and coffee beans.

Figure 5. 9 : Digital weight balance during measurement a) measuring mass of copper oxide b) measuring mass of coffee beans

5.4 Preparation of Nanofluids

Nanofluids are prepared by dispersing nanoparticles in the base fluid. Good dispersion is prerequisite for the application of nanofluids. Hence surfactants are used sometimes which enhance the stability of nanofluids. Besides, surface modification of the dispersed particles and application of strong force on the clusters of the dispersed nanoparticles may increase the stability of nanofluids.

Chemical process is another emerging technology in preparation of nanofluids. The percentage of volumetric concentration is calculated from the Equation 5.1.

$$volume\,concentrtion, \phi = \left[\frac{\frac{w_{np}}{\rho_{np}}}{\frac{w_{np}}{\rho_{np}} + \frac{w_{bf}}{\rho_{bf}}} \right] \qquad (5.1)$$

where w_{np} is weight of nanoparticles, w_{bf} is weight of base fluid, ρ_{np} is density of Nano fluid, and ρ_{bf} is density of the base fluid.

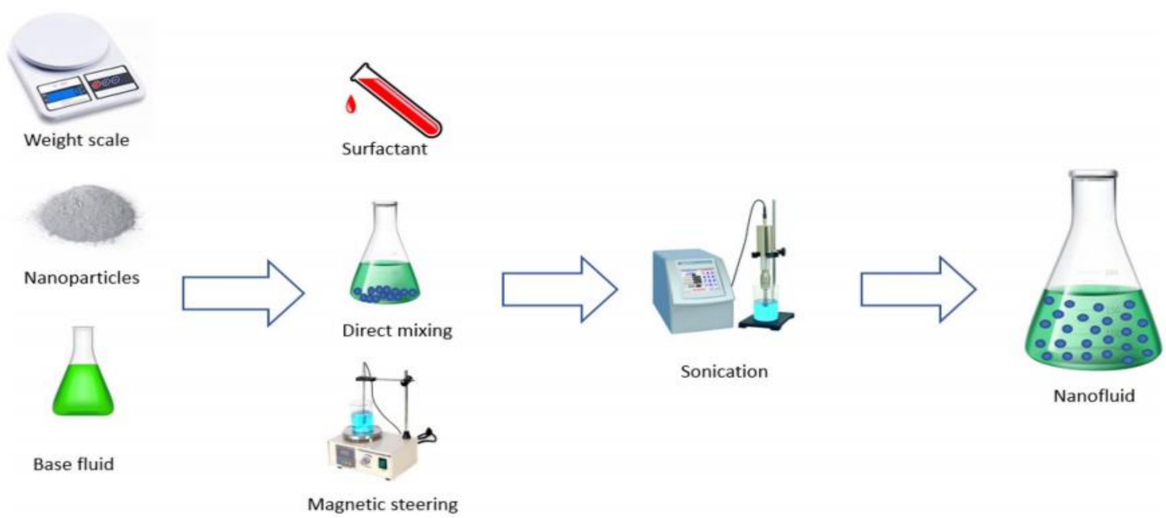

Figure 5. 10: Preparation procedure of nanofluids in laboratory (Abu and Bodius, 2020)

Stability of nanofluids is important to get constant thermos physical properties. Stability analysis can be done by Sedimentation photograph method, Centrifugation method, Zeta potential, and Electron microscopy method are used. Stability can be enhanced with Dispersant, Magnetic stirring, and Sonication.

Dispersant

Addition of dispersants or surfactants is the common method in enhancing the stability of nanofluids which prevents the agglomeration of nanoparticles by reducing the surface tension of the base fluid. But excess use of dispersant may deteriorate the thermos physical properties of nanofluids including decrease in thermal conductivity as well as degradation of chemical stability

Magnetic stirring

stirrer is employed in laboratory which use rotating magnetic field to increase the homogeneity of nanofluids by reducing sediment

Sonication

Sonication method gives better dispersion which has less probability of particle agglomeration than magnetic stirring. Ultrasonic waves are applied in sonication method through the nanofluids. Sonication helps to make more homogenized suspension. To provide uniform dispersion, sonication is better than magnetic stirrer.

5.4.1 X-Ray Diffraction (XRD) Characterization of Cuo Nanofluid

It is an easy tool to determine the size and the shape of the unit cell for any compound using XRD. Diffraction pattern gives information on translational symmetry size and shape of the unit cell from Peak Positions and information on electron density inside the unit cell, namely where the atoms are located from Peak Intensities.

Figure 5.11 shows the XRD pattern of CuO Nanoparticle. The XRD test was conducted in Materials Engineering department, ASTU. All the peaks in diffraction pattern shows monoclinic structure of CuO, and the Peaks. XRD results confirmed that the CuO nanoparticle were crystalline. The y-axis shows the numbers of nanoparticle exist at each peak with respective diffraction angle and x-axis indicates the diffraction peaks with respective nanoparticle. The diffraction peaks of nanoparticle are important to estimate the average particle size.

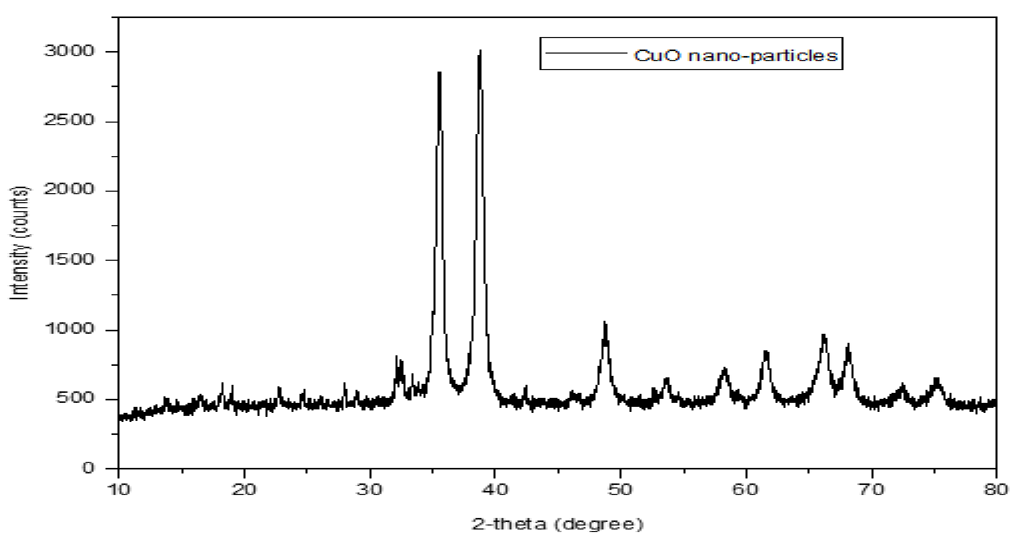

Figure 5. 11: XRD pattern of CuO nanoparticle

CHAPTER SIX

6. RESULT AND DISCUSSION

6.1 Introduction

In this chapter, the experimental results obtained from the designed greenhouse integrated with enhanced solar dryer is presented. Performance of greenhouse and performance of solar collector components and essential points that obtained from the results are discussed in detail. Finally, the economic analysis of the solar dryer is presented.

6.2 Solar Radiation

Solar irradiance affects the performance of the system, since the collector temperature, fluid outlet temperature, greenhouse temperature, and others are directly related to solar irradiance. Thus, as solar radiation increases these temperature results also increase proportionally. The solar radiance increases to a maximum value at noontime and starts to falls in the afternoon. Figure 6.1 at 9:00 am, the solar intensity is 585.4 W/m^2, and as time passes, the intensity starts to rise until reaching the peak with a value of 911.2W/m^2 around 12:00 pm. Average solar radiation observed was 581.4W/m^2 After that time, the intensity decreases to approximately 26.96 W/m^2 at 18:00 pm.

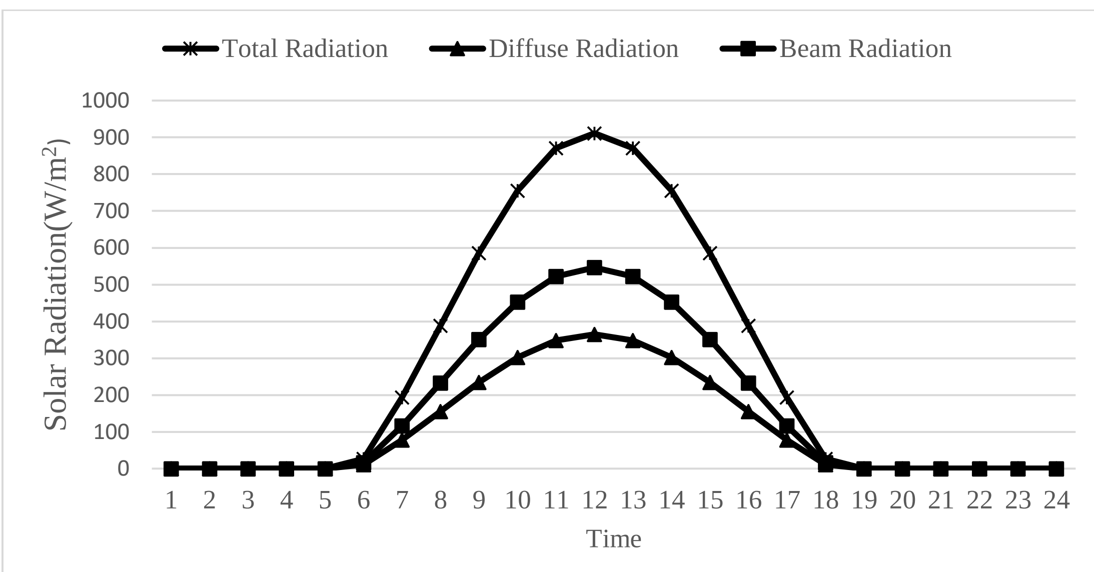

Figure 6. 1: Estimated hourly variation of solar radiation of Adama may

6.3 Ambient Temperature Profile

The ambient temperature of Adama measured during the test period were presented in the figure 6.2. The ambient temperature is the maximum value after noontime and starts to decline in the afternoon. The maximum ambient temperature measured between 12:00 to 14:00 is found to be 36.6 ^{O}C. The minimum temperature measured during the experiment was 27.1 ^{O}C, at 9:00 and average ambient temperature seen was 30.1 ^{O}C. The figure shows experimental temperature is higher than numerical result this is due to rise in temperature in all over Ethiopia above predicted.

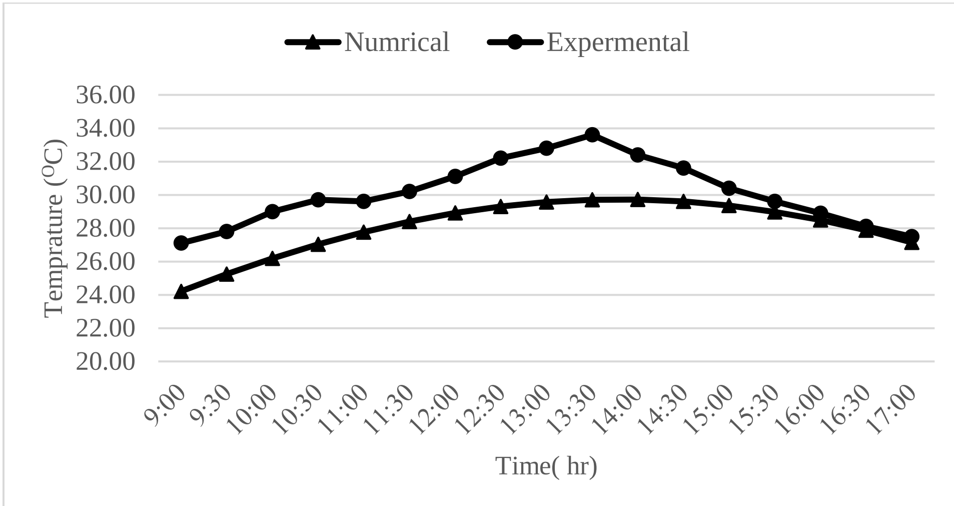

Figure 6. 2: Ambient Temperature

6.4 Experimental Results of Solo Greenhouse

To examine the performance of solo greenhouse experimental tests were performed on May 15th, 16th, and 17th, 2022. After adjusting the experimental setup, several parameters were measured using thermocouples mounted at various points throughout the system. The next subsection presents and discusses the various results obtained.

6.4.1 Greenhouse Outlet and Product Temperature Variation

Figure 6.3 exhibit the inlet and outlet temperature variations of the greenhouse with time. The Figure illustrates, the outlet temperature of the greenhouse varied from 33.9 to 70.9 ℃. The outlet temperature of the greenhouse increases with increase in solar radiation intensity. The maximum outlet air temperature of the greenhouse was 70.9 ℃ recorded in the day of the experiment at 13:00 h and the minimum was 33.9 ℃ at 9:00 h.

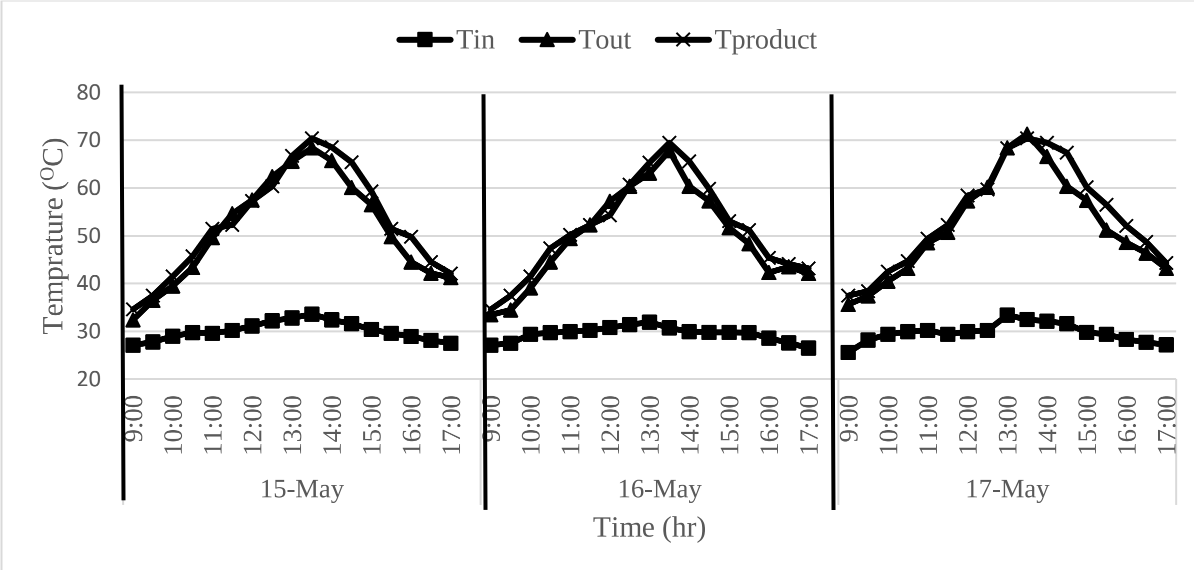

Figure 6. 3: Temperature variation of solo Greenhouse

6.4.2 Useful Heat Gain solo greenhouse

Useful heat gain is calculated from the inlet and outlet air temperatures and mass flow rate. Figures 6.4 show the useful heat gain of solo greenhouse. The experiments were carried out from 9:00 am to 17:00 pm for several days. However, the useful heat gains first increase, reach a peak value around solar noon, and then decline. This is due to the fact that the useful heat gain is strongly dependent on the incident solar radiation so do change of temperature. The maximum useful heat gain seen in May 17 at 13:30 was found 701.9 W and the minimum seen was 95.8 at May 15 at 9:00.

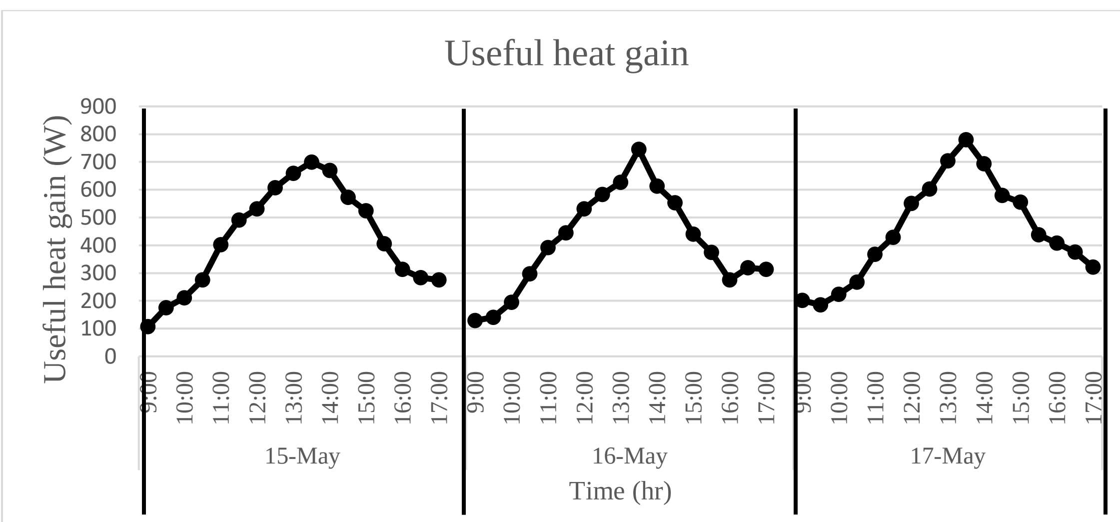

Figure 6. 4: Useful heat gain of solo greenhouse

6.4.3 Thermal Efficiency of Solo Greenhouse

Thermal efficiency of the greenhouse as a function of time for three consecutive days are shown in Figure 6.5. The average thermal efficiencies of the greenhouse from day 1 to day 3 were found as 21.18, 20.69, and 22.59%, respectively. The graph showed that the instantaneous thermal efficiency increases rapidly during the time interval between 9:00 and 12.00 am. After that, further increase is at a slower rate relative to the previous one until it reaches its peak from 14:00 -15:00 h, and then it starts decreasing. The pattern of efficiency is related with change in temperature of air in the greenhouse and solar radiation intensity. The efficiency of the greenhouse ranged from 5 % to 38.99 % with an average value of 21.5% at a drying air flow rate of 0.02 kg/s

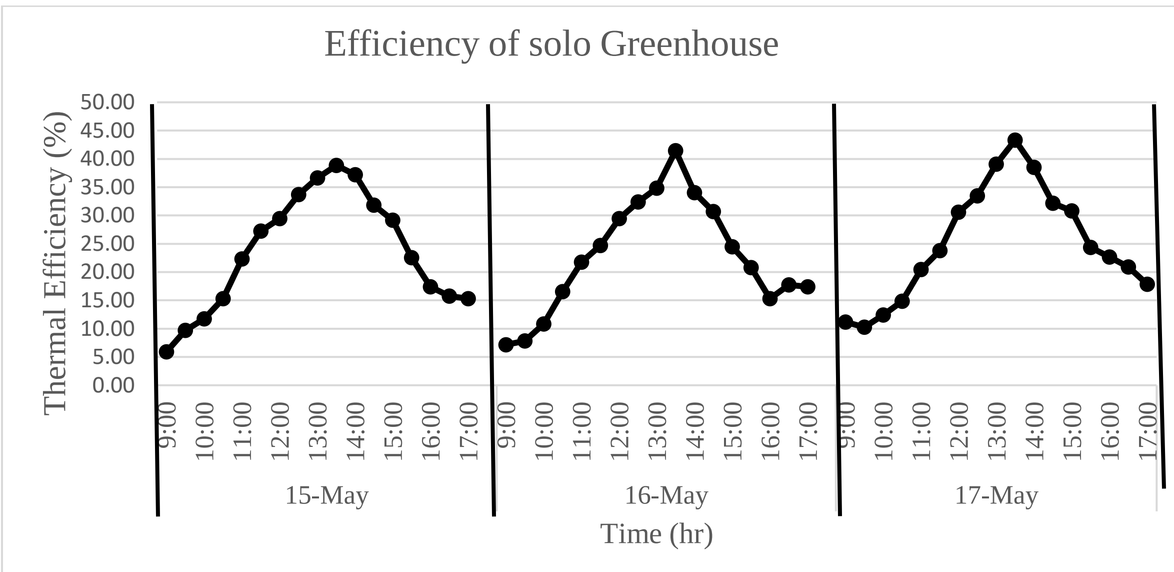

Figure 6. 5: Thermal Efficiency of solo greenhouse

6.4.4 The exergy efficiency of Solo Greenhouse

Exergy efficiency is amount of heat converted into useful work, increase exergy of fluid flow, is a measure of true performance of system. The variation of the exergy efficiency of the greenhouse with time are depicted in Figure 6.6. The exergy efficiency is highly dependent on the outlet temperature of the greenhouse and increases when it increases. The maximum exergy efficiency was found during experiment was 2.97 % at 14:00 h in May 17and the minimum is 0.06% found at 9:00 h in May 15. The average exergy efficiency of the solar air heater was 1.58 %. The average exergy efficiency determined during experiment was 0.75,0.65, and 0.81 in May 15,16, and 17 respectively and the average exergy efficiency was 0.74.

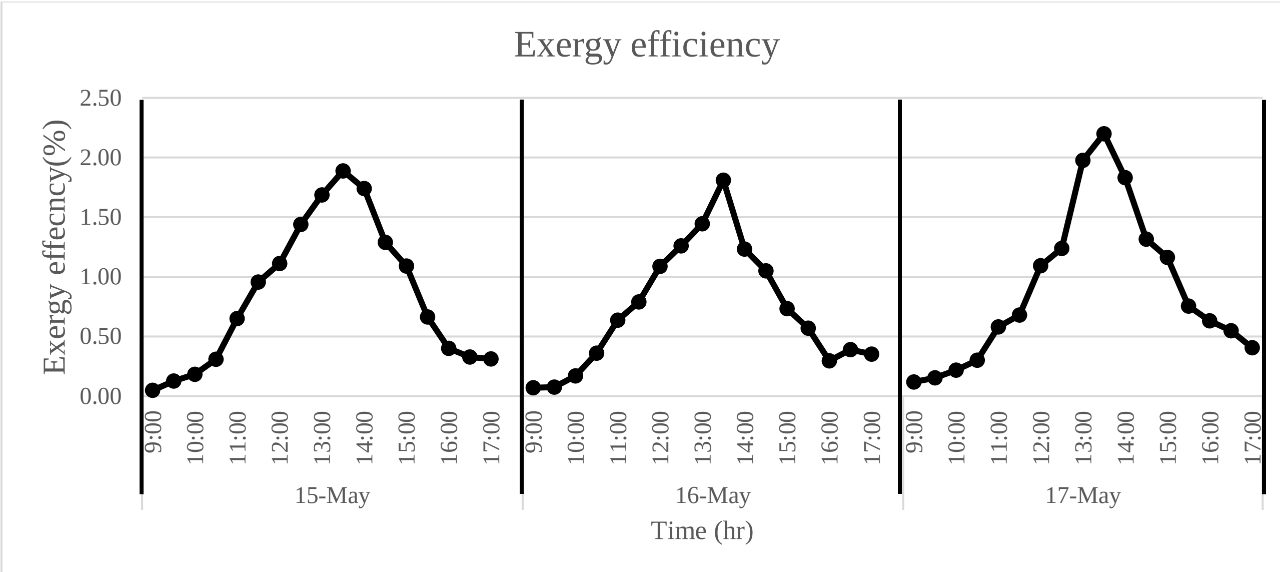

Figure 6. 6: Exergy efficiency of Solo Greenhouse

6.5 Experimental Results of Enhanced Solar Collector

To examine the performance of enhanced solar collector experimental tests were performed on May 15th, 16th, and 17th, 2022. After adjusting the experimental setup, several parameters were measured using thermocouples mounted at various points throughout the system. The next subsection presents and discusses the various results obtained.

6.5.1 Temperature Variation

Figure 6.7 exhibit the plate 1, plate 2, inlet, outlet, fluid and glass temperature variations of the solar air heater with time. The Figure illustrates, the average temperature observed was 73.1, 63, 29.7, 59.2, 60.1and 48.3 for plate 1, plate 2, inlet, outlet, fluid and glass temperature respectively. The out let temperature of the enhanced solar collector varied from 43.2 to 76.5℃. The temperature of the enhanced collector increases with increase in solar radiation intensity except for temperature of plate 2; temperature decreases when sun is at overhead that is due to the shading effect of the collector. The maximum temperature of the was 97.1, 81.4, 33.4, 79.6, 80.2 and 57.6 ℃ plate 1, plate 2, inlet, outlet, fluid and glass temperature respectively.

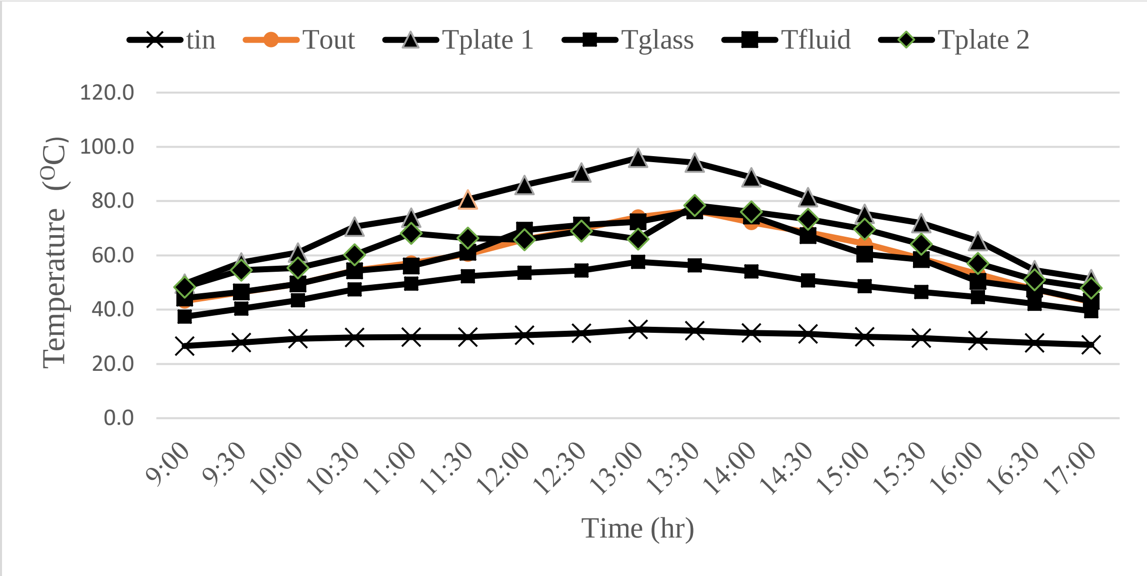

Figure 6. 7: Average Temperature Variation of enhanced solar collector

6.5.2 Useful Heat gain of enhanced solar collector

The experiments were carried out from 9:00 to 17:00 hr. for three days (May 15,16, and 17) and average useful heat gain as shown in Figure 6.8. The useful heat gains first increase, reach a peak value after solar noon, and then decline. This is due to the fact that the useful heat gain is strongly dependent on the incident solar radiation so do change of temperature. The maximum useful heat gain seen was found 889.76 W and the minimum seen was 316.91 W. the average useful heat gain was 590 W.

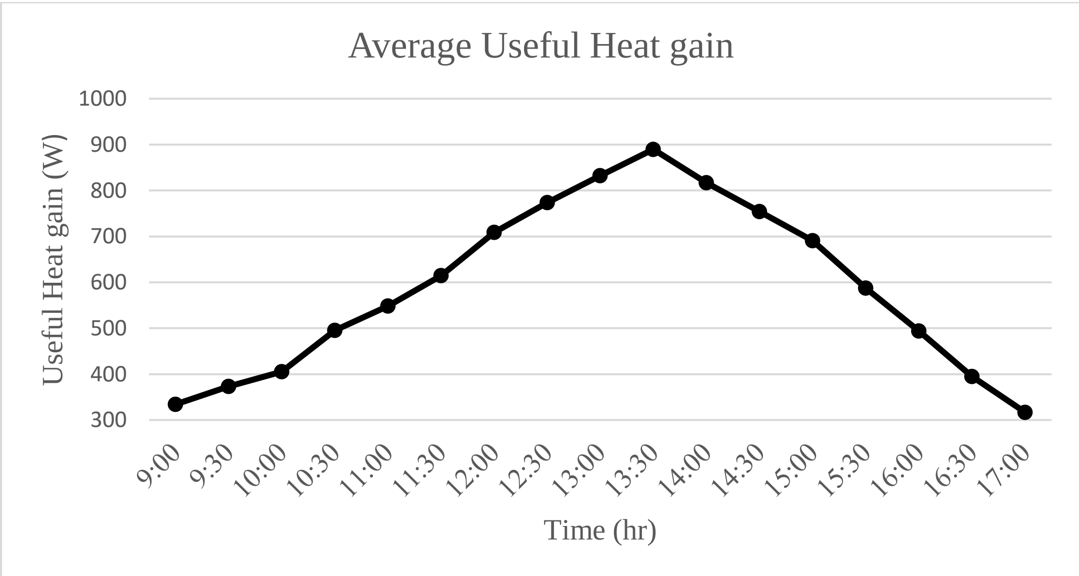

Figure 6. 8: Useful Heat gain of enhanced solar collector

6.5.3 Thermal Efficiency of Enhanced Solar Collector

Figure 6.9 shows the average thermal efficiencies of the collector during experimental days. From experimental day the average thermal efficiency was found 42.1%. The graph showed that the instantaneous thermal efficiency increases up to 13:30 and then it starts decreasing. The pattern of efficiency is related with change in temperature of air in the collector and solar radiation intensity. The efficiency of the collector ranged from 22.64 to 63.55 % having mass flow rate 0.02kg/s

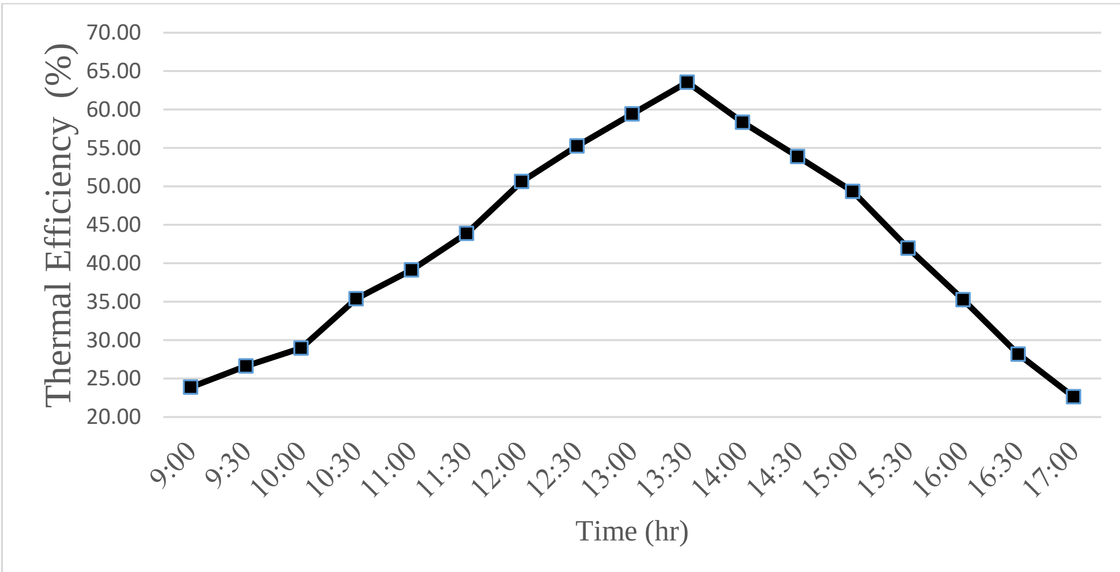

Figure 6. 9 The average thermal efficiency of enhanced solar collector

6.5.4 The Exergy Efficiency of Enhanced Solar Collector

The variation of the exergy efficiency of the collector with time are shown in Figure 6.10.

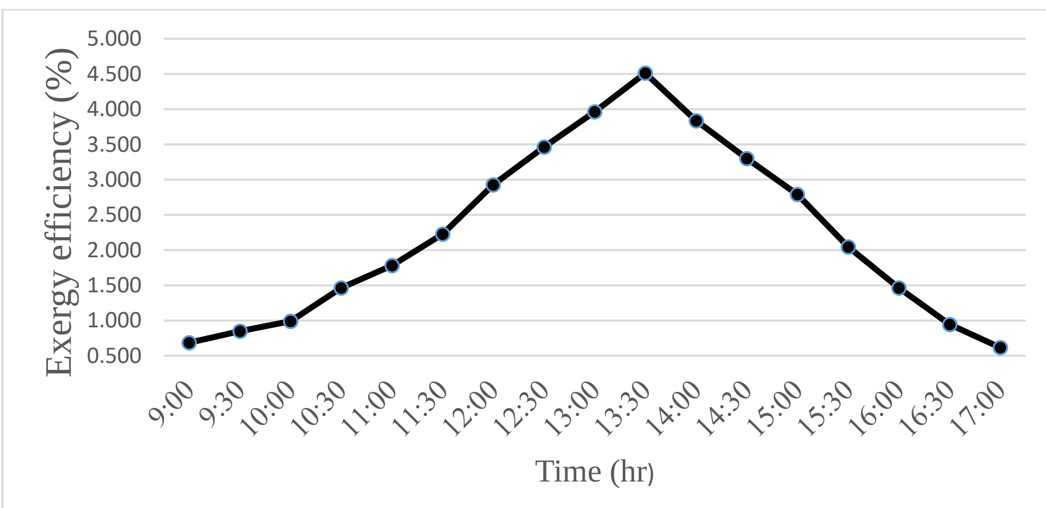

Figure 6. 10: exergy efficiency of enhanced solar collector

The exergy efficiency is highly dependent on the outlet temperature of the collector and increases when it increases. The average maximum exergy efficiency was found during experiment was 4.51% at 13:30 h and the minimum is 0.61% found at 17:00 h during experimental days. The average exergy efficiency was 2.51%.

6.6 Experimental Results of Greenhouse Integrated with Enhanced Solar Collector

To examine the performance of enhanced solar collector in a greenhouse experimental tests were performed on May 18th, 19th, and 20th, 2022. After adjusting the experimental setup, several parameters were measured using thermocouples mounted at various points throughout the system. The next subsection presents and discusses the various results obtained.

6.6.1 Outlet and Inlet Temperature Variation of Greenhouse Integrated with Enhanced Solar Collector

Figure 6.11 exhibit the inlet and outlet temperature variations of the greenhouse enhanced with solar collector heater with time. The Figure illustrates, the outlet temperature of the greenhouse varied from 49.8 to 84.5 ℃. The outlet temperature of the greenhouse increases with increase in solar radiation intensity. The maximum outlet air temperature of the greenhouse was 84.5 ℃ in May 20 recorded in the day of the experiment at 12:30 hr. and the minimum was 49.8 ℃ in May 18 at 9:00 h. the inlet temperature of the greenhouse increases almost in uniform manner expect for May 19 at 11:00 to 12 there is high wind causes conviction heat transfer causes decreasing inlet temperature of the greenhouse. In the afternoon the rate of decreasing in the inlet temperature of greenhouse that is due to charging of paraffin wax.

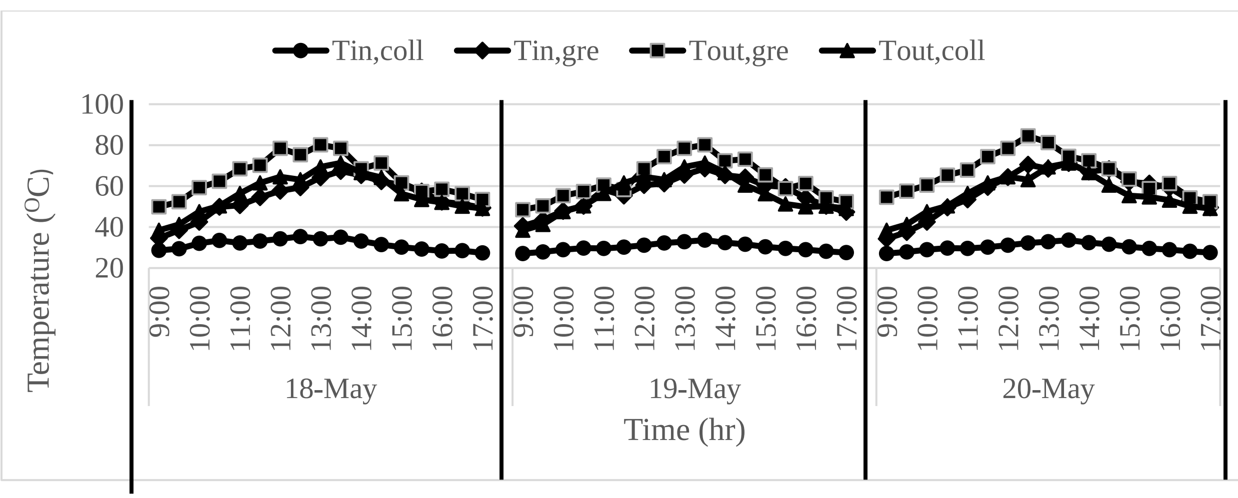

Figure 6. 11 Outlet and Inlet Temperature Variation of greenhouse integrated with enhanced solar collector

6.7 Comparison of Various Performance Parameters for Greenhouse with and Without Enhanced Collector

In this sub section, effect of adding enhanced collector parameter's (reverse back reflector, nanoparticles coat, double pass, and using Paraffin wax) on the performance of greenhouse is investigated and discussed. Inlet and outlet temperature of the greenhouse were recorded in 30 minutes' interval for three consecutive days (15-17 May 2022) without enhanced collector and after integrating enhanced collector into the greenhouse for three consecutive days (18-20 May, 2022) during the drying process. In the next sub section detail information will be presented.

6.7.1 Comparison of Outlet and Inlet Temperature of Greenhouse with and without Enhanced Solar Collector

Figure 6.12 shows the effects of adding enhanced collector on outlet in air temperature of the greenhouse. The maximum outlet temperature of the greenhouse was 84.5 and 70.9 ^{O}C for with and without enhanced solar collector, respectively. It is also observed that, the change in air temperature of greenhouse with enhanced collector is 6.8 to 18.6 ℃ higher than that of without enhanced collector. The average increment of 13.6 ℃. This temperature increment is obtained due to accumulation of solar energy inside solar collector. The inlet temperature of greenhouse varies from to 9.3 to 35.5 ℃ higher than that of without enhanced collector. The average increment of 25.6 ℃

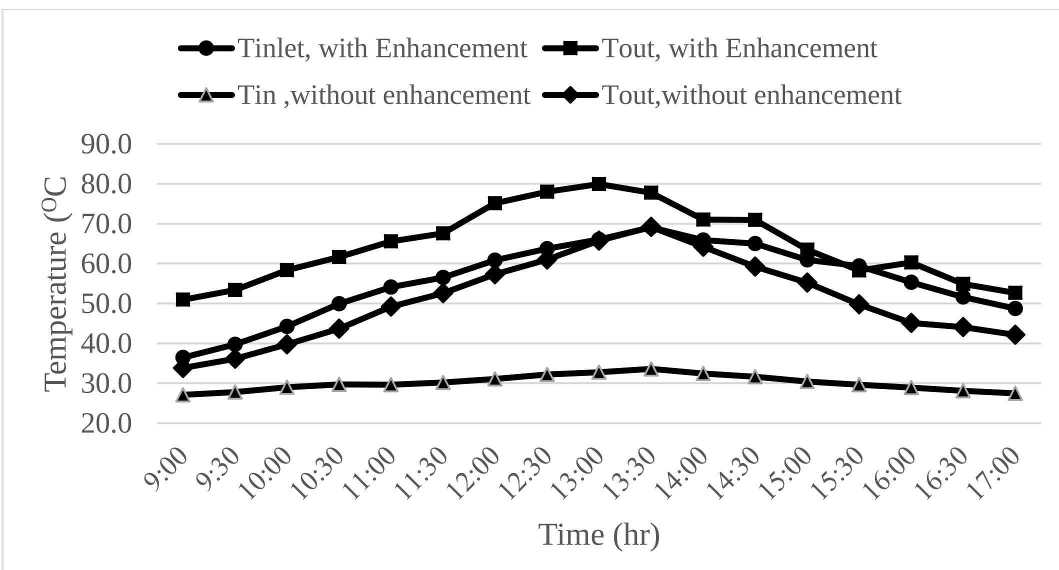

Figure 6. 12: Comparison of outlet Temperature of greenhouse with and without enhanced solar collector

6.7.2 Comparison of Thermal Efficiency Greenhouse with and without Enhanced Solar Collector

Figure 6.13 illustrates the effect of enhanced solar collector in the thermal efficiency of greenhouse. The maximum efficiency was 45.5 and 38.86% with and without enhancement Average thermal efficiency of the greenhouse with and without enhanced collector were found to be 33.12 and 23.5 %, respectively. It is clearly observed that, the thermal efficiency of the greenhouse with enhanced collector is 2.31 to 16.89 % higher than that of without enhanced solar collector with an average value of 9.73%.

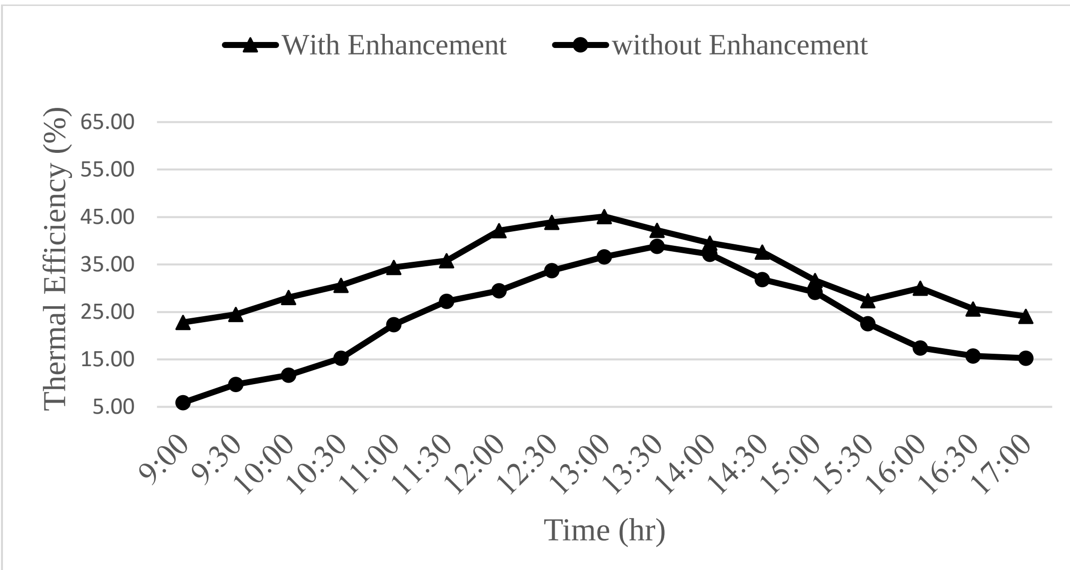

Figure 6. 13: Comparison of Energy Efficiency greenhouse with and without enhanced solar collector

6.7.3 Comparison of Exergy Efficiency of Greenhouse with and without Enhanced Solar Collector

Figure 6.14 shows exergy efficiency of the system with and without enhanced solar collector.

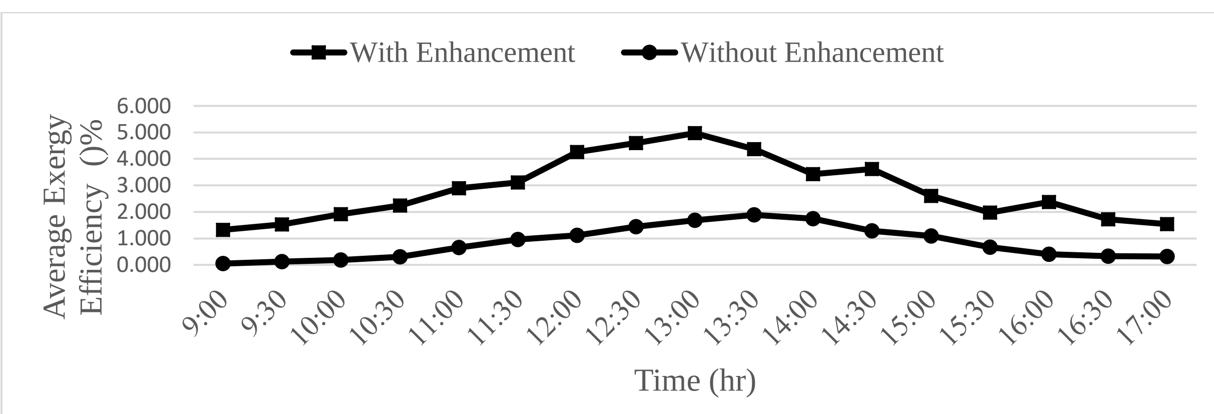

Figure 6. 14: Comparison of Exergy Efficiency of greenhouse with and without enhanced solar collector

For both cases the exergy efficiency is dependent on the intensity of solar radiation falling on the enhanced collector and greenhouse. The maximum exergy efficiency of 4.97 and 1.86% were achieved for greenhouse with and without enhanced collector, respectively. It is observed that, the addition of enhanced collector enhances the exergy efficiency of the greenhouse and an average exergy value of 2.85 and 0.86 % were found during the experimental investigation with and without enhanced collector, respectively.

6.8 Experimental Results of the Thermal Energy Storage

Thermocouples mounted at three different locations i.e. at inlet and outlet of the tube and the temperature of the paraffin wax are used to measured temperature and the results are presented as follows.

6.8.1 Variation of Inlet and Outlet Temperatures of the Energy Storage

Figure 6.15 shows the variation of the inlet and outlet air temperatures of the thermal energy storage during the charging and discharging process. It is observed that, the outlet air temperature varied between 37.6℃ and 70.5 ℃ whereas the inlet temperature varies between 48.6 ℃ and 73.2 ℃. The inlet temperature of the storage varied with the change in solar intensity. It starts increasing and becomes maximum between 12:00 and 14:30 hr. and starts decreasing. However, the outlet air temperature remains 4.5 to 11 ℃ higher than the inlet after charging. During the charging process, a highest drop in air temperature of 14.9 ℃ between the inlet and outlet of the storage is observed and during the discharging process, a rise in air temperature of 10 ℃ is observed. When temperature of the air does not change while passing through the energy storage, the PCM is assumed as completely melted.

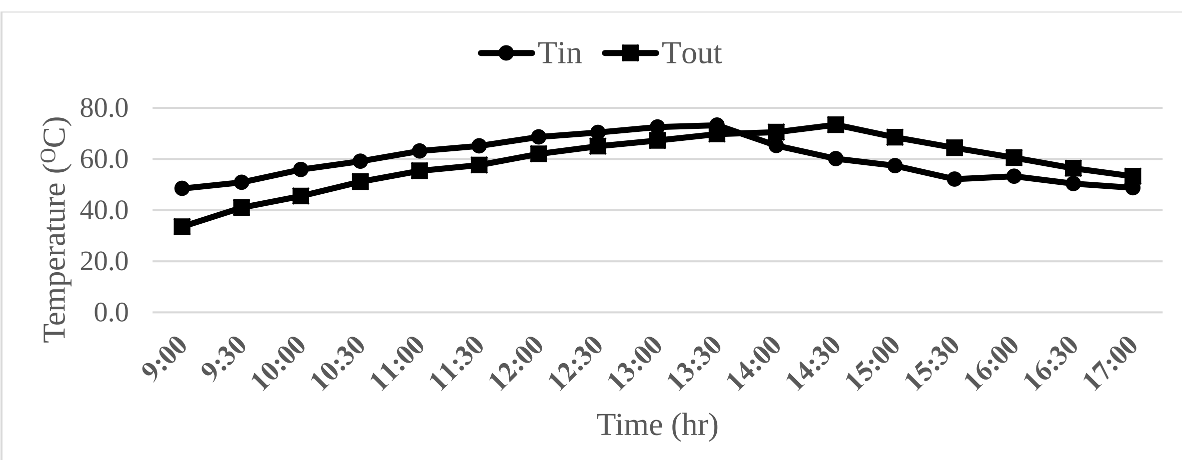

Figure 6. 15:The average Inlet and outlet temperature variation of the energy storage.

6.8.2 Heat Stored/Released and melt fraction during the charging and discharging process

Heat stored/ released is the cumulative sum of both sensible and latent heat. When temperature of paraffin wax is less than T-Solidus it only exhibits latent heat and further increase in temperature results in both sensible and latent heat when it is between T-solidus and T-liquids temperature. Finally, when temperature greater than T-liquids it only exhibits sensible heat. Figure 6.16 shows the total amount of heat released/recovered and average melt fraction during charging and discharging. The maximum amount of heat released /stored during charging was 6.32MJ occurs at 13:30 and the maximum amount of heat recovered during discharging is 2.58 MJ.

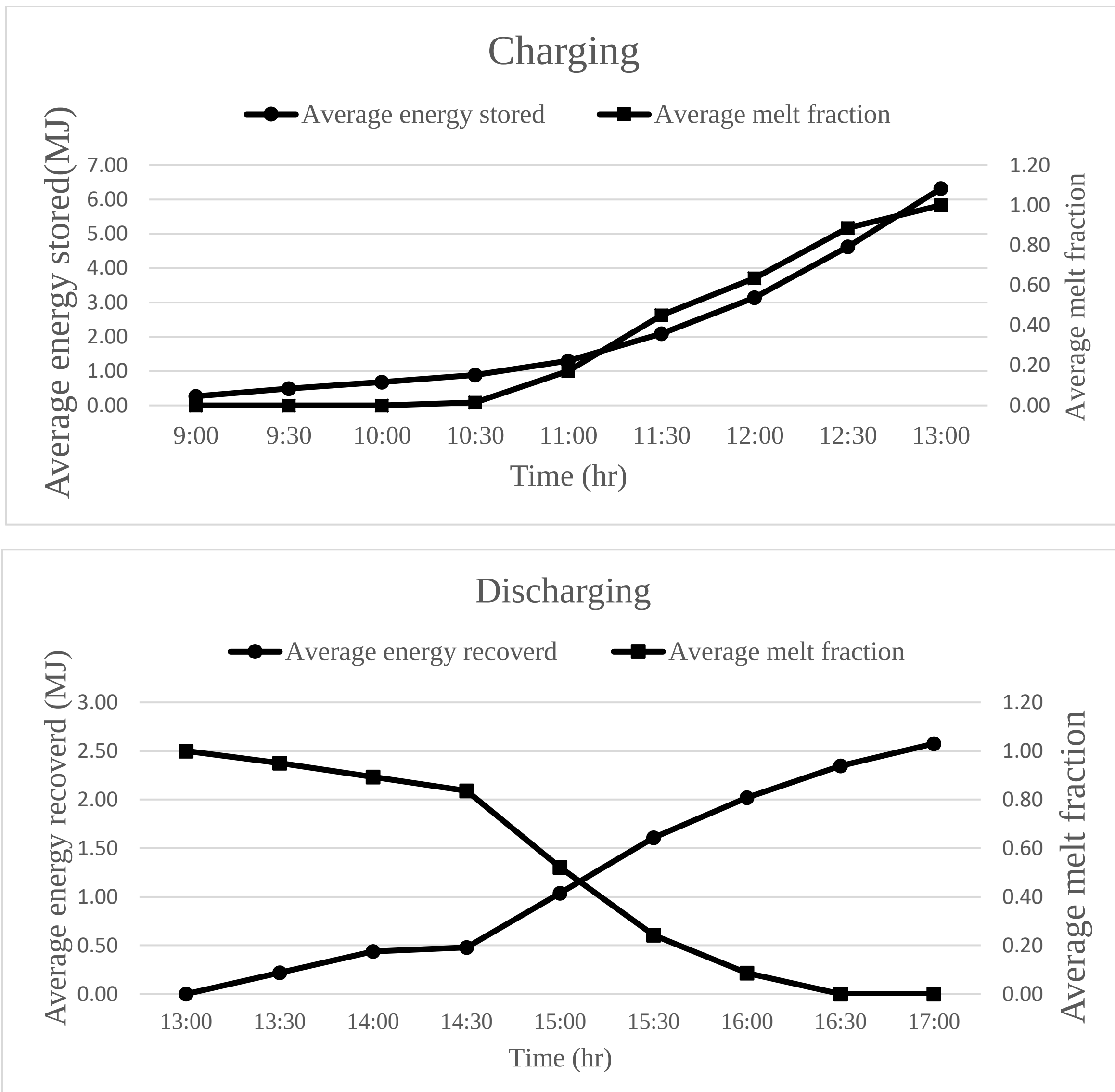

Figure 6. 16: Heat Stored/Released and melt fraction during the charging and discharging process during experimental days

6.9 Moisture Removed from The Sample

The variation in moisture of content of the dried washed coffee beans with drying time for greenhouse with and without enhanced collector is presented in Figure 6.17. The moisture content of the coffee was determined by measuring its weight and calculating the weight loss within two hours' interval. The moisture content of the red chilli sample was reduced from the initial value of 61 % (w.b.) to the final value of 11.7 % (w.b) in 16 h (two days) in the greenhouse integrated with enhanced collector and in 24 hr. (three days) in the solo greenhouse without enhanced collector drying.

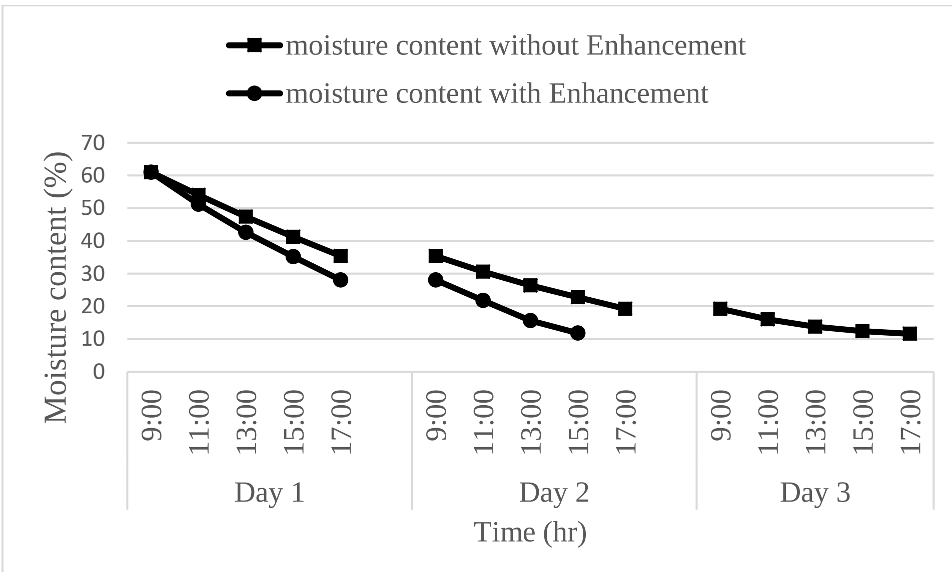

Figure 6. 17 : Moisture content (w.b.)

It is clearly observed that, the highest moisture removal was achieved during the first day of the drying process and the moisture removal rate decreased toward the end of drying process. This was happened due to reduction in moisture to be removed toward the end. The change in the drying rates with the drying time is shown in Figure 6.17. It is observed that the drying rate of the coffee beans dried in the greenhouse enhanced collector is faster than that of solo greenhouse drying, and it decreases continuously as the number of drying days advanced. The maximum drying rate was visible during the peak sunshine hour of the day when the solar radiation intensity and the drying air temperature were maximum. The drying rate of the coffee beans dried is maximum till the first 8 h of the drying period, and afterwards, the drying rate became low due to low moisture content.

6.10 Overall system efficiency of the system

The mass of evaporated moisture from 5 kg of coffee beans while reducing the moisture content from an initial value of 61 to 11.7 % in wet basis was 2.78 kg. The average intensity of the solar radiation incident on the surface of the solar collector was estimated to be 645 W/m^2 and the total area of the system was 3 m^2 (1 m^2collector area plus 2m^2 greenhouse). The power consumed by the blower and fan was 80 W, and the dryer was operated daily for 8 h. The latent heat evaporation of water is 2382.12 kJ/kg. The heat required to evaporate 2.78 kg of moisture was 6.622 MJ. The total energy input to the drying system during the entire drying period was 116.1 MJ and 169.776 MJ with and without enhancement respectively. The specific energy consumption of the dryer was found to be 11.6 and16.96 kWh per kg of moisture with and without enhancement respectively. The electrical energy consumption of blower per kg of moisture removal was 0.69 kWh which was only 4.1 % of the total specific energy consumption. Thus, 95.9 % of the total energy used for drying the product in the newly developed dryer was harvested from the free and eco - friendly solar energy. The overall efficiency of the drying system was found to be 6% and 4% with and without enhancement respectively.

6.11 CFD Results

CFD model is studied for the location of Adama for May 2022 from 9 to 17 hr. by giving ambient air temperature as inlet air temperature for solar collector and exit of solar collector for greenhouse measured for 0.5 hour (30 min) time interval. As blower is used to insert air at inlet of double pass solar air heater, outlet condition of pressure outlet has been applied to validate CFD model with experimental model. Figure 18 shows plane temperature contour showing maximum and minimum temperatures of collector and greenhouse components at time different time. Figure 6.18 shows temperature contours at mid plane of double pass solar air heater fluid zone i.e. at plane parallel to length of solar air heater. Temperature variation from upper right side from where ambient air is entering solar air heater traveling from right to left and coming in second pass and traveling from left to right towards air outlet can be easily visualized with the help of figure 6.18

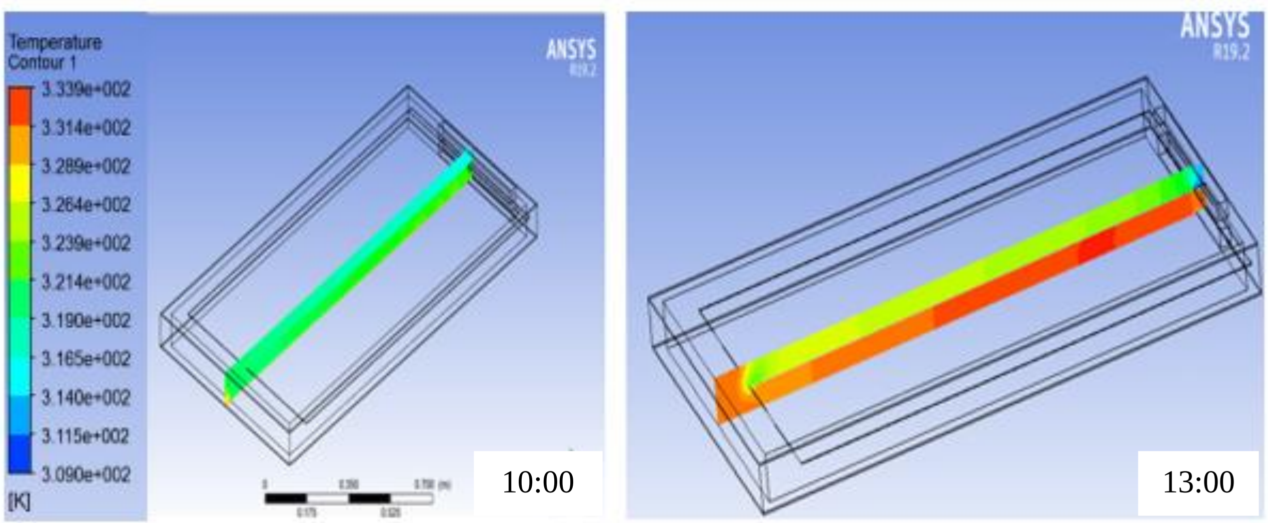

Figure 6. 18: Temperature contours at mid plane of double pass solar air heater fluid zone at different time

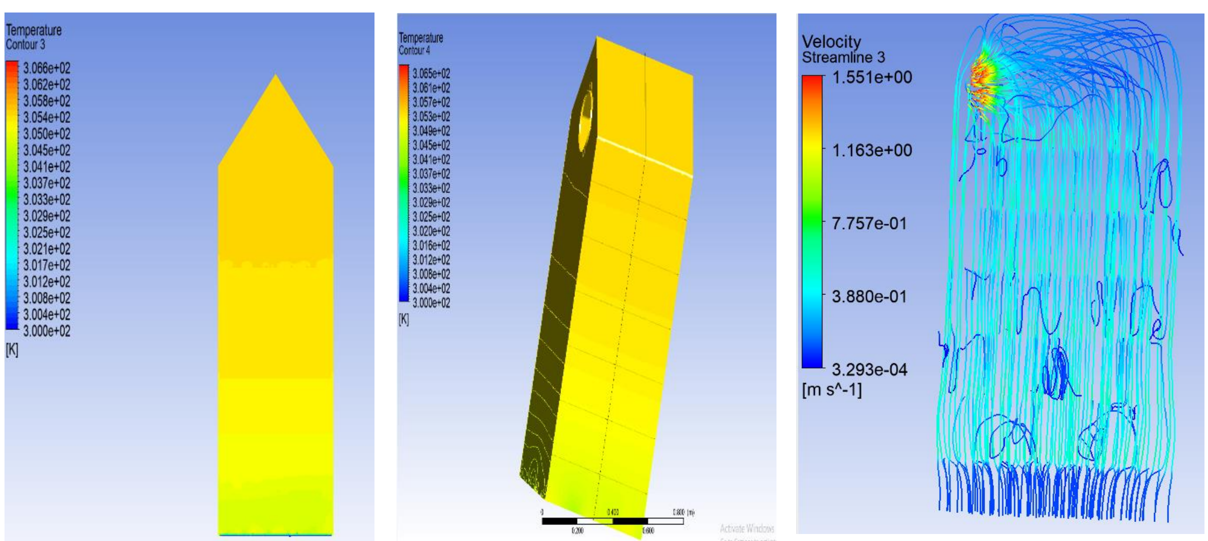

Figure 6. 19: Simulation result inside greenhouse at 9:00 a) mid plane temperature b) all air contour c) velocity streamline

6.11.1 CFD model validation

Experimental study of double pass enhanced solar air heater and greenhouse is performed on May 2022. Results obtained through experimental study are compared with results obtained through CFD simulation.

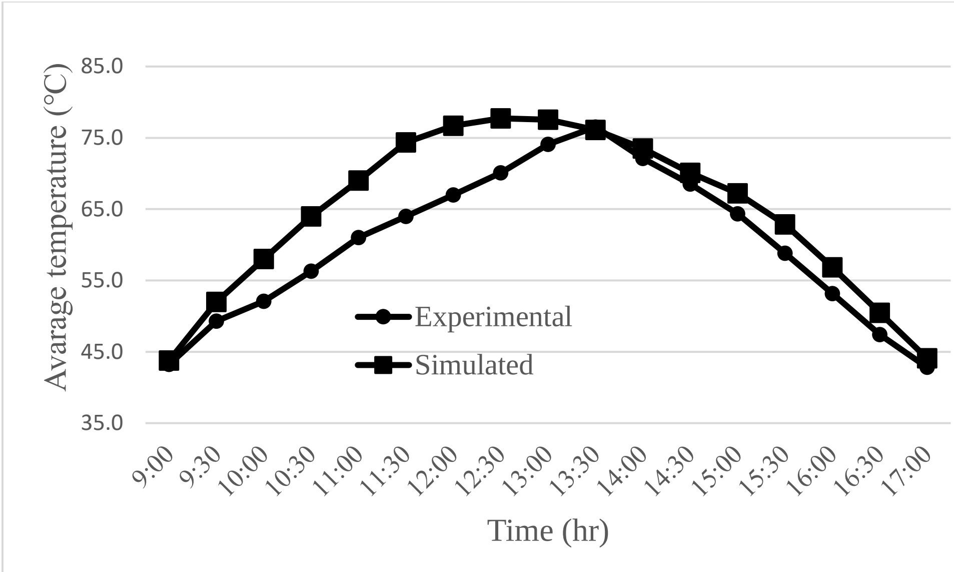

Figure 6. 20: Comparison between outlet air temperature of CFD simulation and experimental study

Figure 6.19 shows comparison between outlet air temperatures of CFD simulation study and experimental study. Variation of readings is within acceptable limit for afternoon.

6.12 Simulation results of the thermal energy storage

Average temperature variation of the PCM, the charging and discharging time and amount of melt fraction are predicted with simulation on COMSOL Multiphysics 5.3a and presented as follows.

6.12.1 Temperature variation of the PCM

Figure 6.20 represents the volumetric average temperature variation of the latent heat storage during the charging and discharging process. Initially the storage is at 28/71 ℃ during the charging and discharging process. When the heat transfer fluid at 71/28 ℃ passes through the tubes, heat transfer takes place between the heat transfer fluid and the PCM. From Figure 6.20, it is observed that the initial part of the curve shows a steady increase/decrease of temperature due to the higher heat transfer potential available during the initial period of the charging/discharging process. After 4000 s, the storage stores/discharges a large amount of heat and the slope of the curve starts decreasing

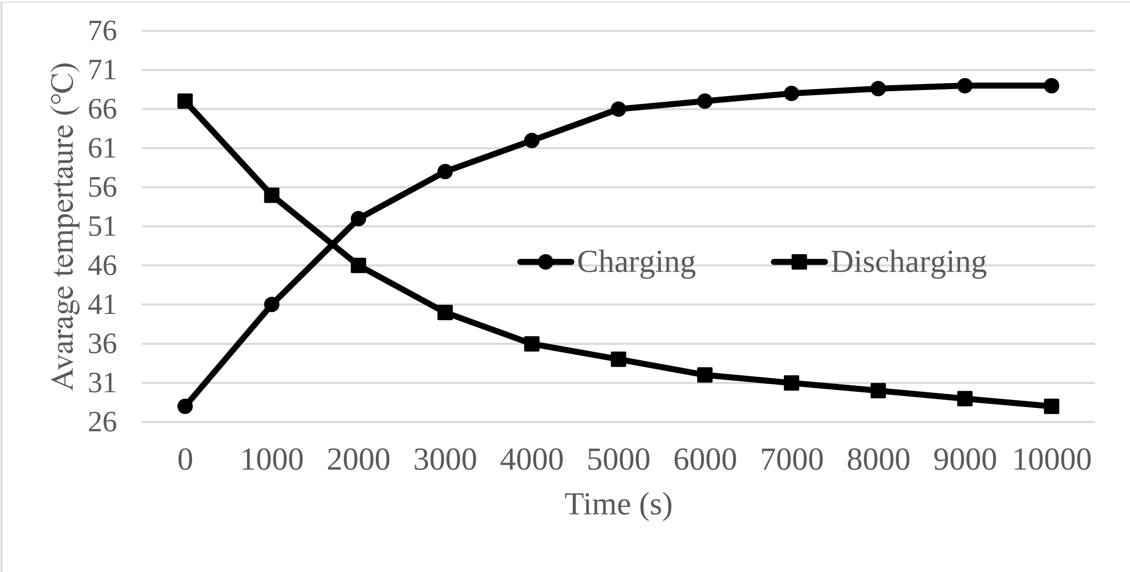

Figure 6. 21: Average temperature of the PCM

6.12.2 Charging and discharging time

Figure 6.21 shows the volumetric average melt fraction variation of the latent heat storage during the charging and discharging process. Melt fraction only shows the latent heat storing and discharging characteristics of a latent heat storage during the charging and discharging periods. It is observed that there is a faster rise/fall of melt fraction at the beginning of each process due to the higher heat transfer rate between the PCM and the air.

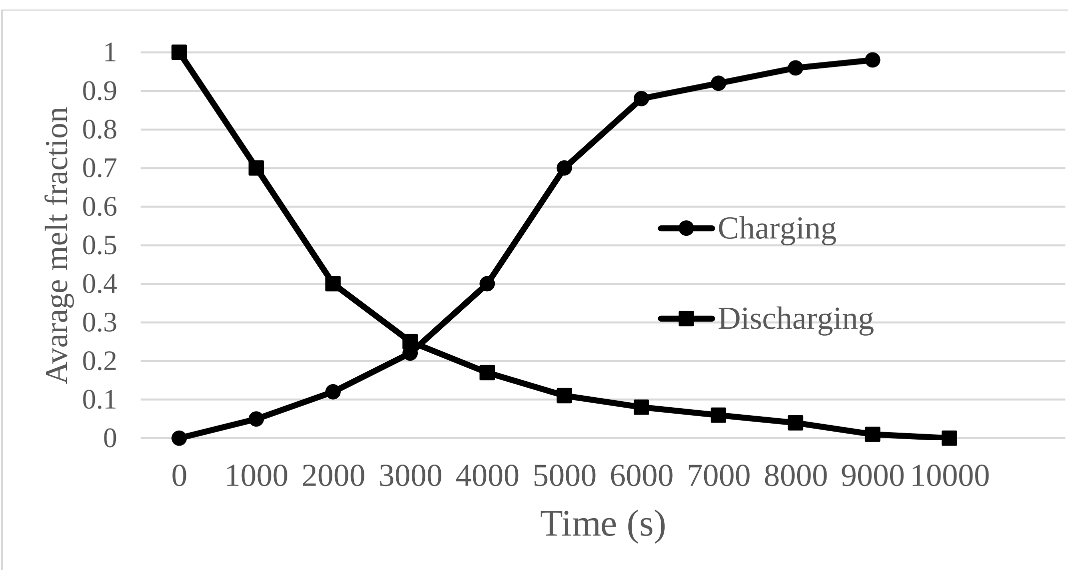

Figure 6. 22 :Average melt fraction of PCM

6.12.3 Contours of average melt fraction

Figure 6.22 shows some contours of average melt fraction during the charging process. At the beginning of the charging process (t = 0 s), the average melt fraction of the PCM is 0 and at the end of the process it becomes 1.

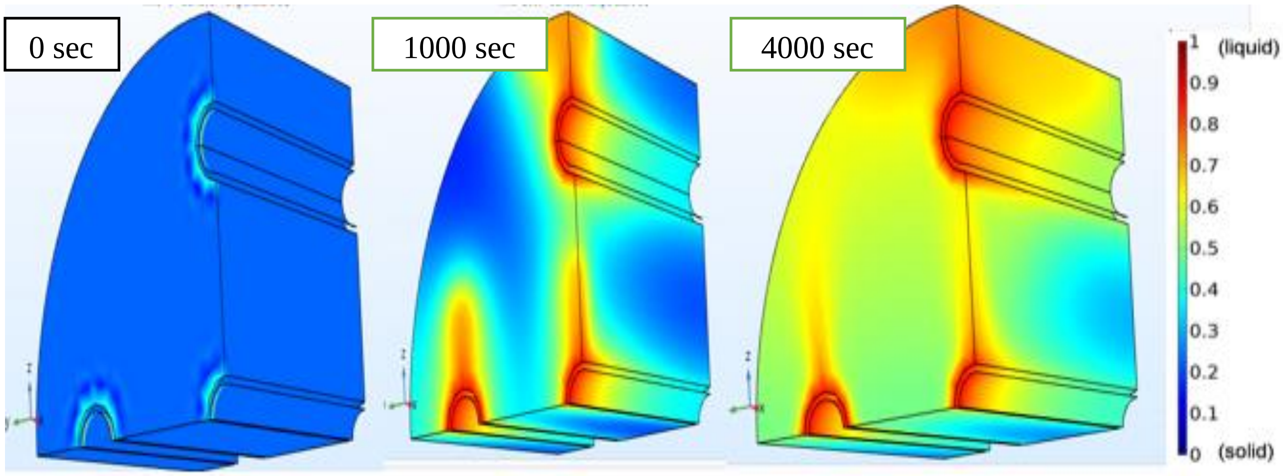

Figure 6. 23: some contours of average melt fraction during the charging process

6.12.4 Model validation

The predicted charging time of the PCM with the simulated model is 2 h and 47 min with inlet air temperature of 71 ℃. This result is validated with the experimental result of the energy storage. During the experiment, charging starts from 9:30 h and completed at 13:00 h. Between 9:30 h and 11:00 h, only sensible heating takes place and the PCM starts melting after 11:00 h. The inlet temperature of the energy storage becomes 5 to 9 ℃ higher than the melting temperature of the PCM from 11:00 to 14:00 h (3 h) and the average temperature of the PCM within this time interval is between 53 and 62 ℃. Therefore, complete melting of the PCM is insured within the 3hrs and agrees with the predicted results of the simulation.

6.13 Economic Analysis

Economic analysis includes fixed cost, drying cost, and payback period. Fixed costs are expenses that are not dependent on the level of products. Fixed cost (FC) includes of costs of all components, including solar air heater, PCM storage unit, greenhouse, trays, insulation, fan, and manufacturing cost. Table 6.1 presents construction cost of the system component with component price.

Table 6. 1 Capital cost of the drying system

No.	Component	Cost(ETB)
1	Glass	3600
2	Nanoparticle	1800
3	Galvanized iron sheet and plate	1500
4	Wood	200
5	Paraffin wax	1500
6	Fan	900
7	Supporting structure	1200
8	Steel pipes of different diameters	1200
9	Tray	520
10	Manufacturing Cost	1500
Total fixed cost		13920

The annualized cost of the dryer C_{ad} can be calculated as (Elkhadraoui *et al*., 2015):

$$C_{ad} = C_{ac} + C_m - SV_a + C_{ec} \qquad (6.1)$$

Where, C_{ac} is annual capital cost, C_m is maintenance cost, SV_a is annual salvage value and C_{ec} is annual electricity cost for running the fan.

The annual capital cost and salvage value are calculated using Equation (6.2) and (6.3), respectively:

$$C_{ac} = C_{ccd} F_c \qquad (6.2)$$

$$SV_a = SVF_s \qquad (6.3)$$

Where, C_{ccd} is capital cost of the dryer, F_c is capital recovery factor, SV is the salvage value of the dryer taken as 10 % of the capital cost of the dryer and F_s is the salvage fund factor.

The capital recovery factor and the salvage fund factor are given by Equation (6.4) and (6.5), respectively as follow:

$$Fc = \frac{i(1+i)^n}{(1+i)^n - 1} \qquad (6.4)$$

$$Fs = \frac{i}{\left(1+i\right)^{n} - 1} \quad (6.5)$$

Where, is the interest rate assumed to be 11 % and is the life period assumed to be 10 years.

Annual electric cost of Fan and blower

The annual running cost of electricity for the dryer consumed by the fan is given by:

$$C_{ec} = P_{bl}\, x\, t_{y}\, x\, C_{ue} \quad (6.6)$$

Where, P_{bl} is the power consumed by the fan, t_y is the number of hours the blower run each year and C_{ue} the unit charge for electricity.

The cost of drying per kilogram of dried product (C_d)is then calculated by (Elkhadraoui *et al.*, 2015):

$$C_d = \frac{C_{ad}}{M_y} \quad (6.7)$$

Where, M_y is the amount of dried product removed from the solar dryer per year and defined as:

$$M_y = \frac{m_{p,b} n_{d,y}}{n_{d,b}} \quad (6.8)$$

Where, $m_{p,b}$ is the mass of the product dried per batch, $n_{d,y}$ is the number of days of operation of the dryer per year and $n_{d,b}$ is the number of days of operation of the dryer per batch.

The cost of fresh product per kilogram of the dried product ($C_{fp,d}$)is evaluated using Equation (6.9) as:

$$C_{fp,d} = C_{fp}\left(\frac{m_{fp}}{m_{p,b}}\right) \quad (6.9)$$

Where, C_{fp} is the cost of fresh product per kg and m_{fp} is mass of fresh product loaded in the solar dryer per batch in kg.

Therefore, the cost of 1 kg of dried product (C_{dc})for the solar air dryer is the summation of the cost of fresh product per kilogram of the dried product($C_{fp,d}$) and the cost of drying per kilogram of dried product (C_d). Mathematically expressed as

$$C_{dc} = C_{fp,d} + C_d \quad (6.10)$$

The saving per kilogram of dried product (S_{ky})in the base year due to use of the solar dryer is calculated using:

$$S_{ky} = S_p - C_{dc} \quad (6.11)$$

Where, S_p is selling price of dried product.

Then, the saving per batch (S_b) and the saving per day(S_d) in the base year are evaluated using equation (6.12) and (6.13), respectively.

$$S_b = S_{kg} m_{p,b} \quad (6.12)$$

$$S_d = \frac{S_b}{n_{d,b}} \quad (6.13)$$

For the life of the system, the annual savings (S_j) for drying the typical product in the j^{th} year is obtained as (Elkhadraoui *et al*., 2015):

$$S_j = S_d n_{d,y} \left(1+d\right)^{j-1} \quad (6.14)$$

Payback period (PP)

Payback period is the investment cost per average annual net income. The returns indicate recovered invested capital of the system. It is computed as (Elkhadraoui *et al*., 2015):

$$pp = \frac{\ln\left[1 - \frac{C_{ccd}}{S_j}\left(i-d\right)\right]}{\ln\left(\frac{1+d}{1+i}\right)} \quad (6.15)$$

Where, d is depreciation and can be calculated by subtracting salvage value from capital cost and divide this amount by its life span (in year) and found to be 9 %.

Table 6. 2 Summary of economic analysis

No.	**Particulars**	Symbol	Cost (ETB)
1	Capital cost(ETB)	Cc	13,920.00
2	Annual capital cost	C_{ac}	2,366.40
3	Maintenance cost	Cm	236.64
4	Salvage value	SV	1,392.00
5	Annual salvage value	SV_a	83.52
6	Annual electric cost	C_{ec}	640.00
7	Annual cost of the dryer	$C_{fp,d}$	3159.52
8	Cost of drying per kilogram of dried product	$C_{fp,d}$	60.00
9	Cost of 1 kg of dried product	C_{dc}	350.00
10	Saving per kilogram of dried product	S_{ky}	53.00
11	Saving per batch	S_b	62.00
12	Saving per day	S_d	20.00
13	Annual savings	S_j	6,875.60
14	Payback period (years)	pp	2.14

CHAPTER SEVEN

7. CONCLUSIONS AND RECOMMENDATIONS

7.1 Conclusions

In this study greenhouse integrated with an enhanced solar collector and latent heat storage filled with 9kg paraffin wax with melting temperature of 58 ℃ is developed and experimentally tested. The components of the dryer have been sized based on the energy and mass of air required for drying 5 kg shaded and washed coffee beans. The drying system is fabricated from locally available materials and the performance of the components of the system and the performance of the overall drying system is evaluated using energy and exergy analysis. No load testing is done on 15th, 16th and 17th May,2022 to evaluate the performance of the Enhanced SAH and the energy storage and the effect of integrating the energy storage on the inlet temperature of the Greenhouse in meantime the performance of greenhouse is takes place to evaluate the performance of solo greenhouse. Then 5kg loaded greenhouse with washed coffee beans system is integrated with enhanced SAH and LHS to study the performance of integration three consecutive days (18th, 19th and 20th May, 2022). CFD analysis was carried out for solar air heater and greenhouse and results are compared with experimental results and the model validation was in accepted range. Finally, economic analysis of the system is calculated.

The following conclusions are drawn from this study:

- The minimum useful heat gains of the whole enhanced system obtained during experimentation was 316.91 W and 896.4 and 590 W found as maximum and average useful heat gain respectively.
- The maximum thermal efficiency obtained was 63.55%. average and minimum was found 41.1 and 26.64% respectively
- The energy and exergy efficiency of the SAH increases with increasing solar radiation intensity and the average energy and exergy efficiency of the enhanced double pass SAH was 41.1 and 2.15 %, respectively
- Integration of the energy storage reduces the fluctuations in the outlet air temperature of the SAH and extends the drying process beyond the sunny hours.

- The specific energy consumption was 11.6 and 16.96 kWh per kilogram of moisture with and without enhanced SAH and the electrical energy consumption of the blower was 0.6 kWh per kilogram of moisture which was 4.1 % of the total energy consumption and the remaining 95.9 % energy was harvested from solar energy.
- 2.78 kg water was removed from 5 kg washed coffee while drying the it from an initial moisture content of 61% (w.b.) to a final moisture content of 11.7% (w.b.) within 24h and 16h of drying preserving the color and texture of the product inside greenhouse without and with integration of enhanced SAH respectively, and the overall efficiency of the drying system was 6 and 4% with and without enhanced SAH.
- CFD simulation was performed using ANSYS FLUINT and the result obtained was found was acceptable range.
- Cost analysis shows the pay back period was 2.14 year.

7.2 Recommendations for future work

Experimental instigation of greenhouse integrated with enhanced SAH and LHS system for drying coffee beans application has been carried out in this research. It tremendously provides a solution to reduce drying time. However, there is still a sufficient scope to improve the system performance. Some of future scopes to study are:

- According to the data recorded the outlet temperature of the greenhouse is higher than the ambient air temperature. therefore; recirculating this hot air can be studied further.
- In this study, the dryer was designed for 5 kg of coffee beans Thus, the dryer can be investigated further for large scale application.
- Since electricity is not available throughout the Ethiopia, integrating/ changing the electric supply by solar panel minimize cost and increase efficiency when electricity is off.
- Due to time experimental performance of nanofluid is not examined for various concentration therefore further study can be studied on variation of nanofluid concentration.

REFERENCES

Abubakar, S., Umaru, S., Anafi, F. O., Abubakar, A. S., & Kulla, D. M. (2018). Design and performance evaluation of a mixed-mode solar crop dryer. *FUOYE J Eng Technol*, *3*(1), 22-26.

Aghbashlo, M., Mobli, H., Rafiee, S., & Madadlou, A. (2013). A review on exergy analysis of drying processes and systems. *Renewable and Sustainable Energy Reviews*, *22*, 1-22.

Aklilu Tesfamichael. (2004). Experimental Analysis for Performance Evaltuation of Solar Dryer. *Department of Mechanical Engineering, AAU*.

Alam, T., & Kim, M. H. (2017). Performance improvement of double-pass solar air heater–A state of art of review. *Renewable and Sustainable Energy Reviews*, *79*, 779-793.

Alam, T., & Kim, M. H. (2017). Performance improvement of double-pass solar air heater–A state of art of review. *Renewable and Sustainable Energy Reviews*, *79*, 779-793.

Aldabbagh, L. B. Y., Egelioglu, F., & İlkan, M. (2010). Single and double pass solar air heaters with wire mesh as packing bed. *Energy*, *35*(9), 3783-3787.

Ali, S. (2019). Design, Optimization and CFD analysis on the thermal performance of solar coffee dryer with jet impingement on corrugated absorber plate

Amer, B. M., Gottschalk, K., & Hossain, M. A. (2018). Integrated hybrid solar drying system and its drying kinetics of chamomile. *Renewable Energy*, *121*, 539-547.

Asmare, E., Tewabe, D., Mohamed, B., & Hailu, B. (2015). Pre-Scaling Up of Solar Tent Fish Drier in Northern and North Western Part of Lake Tana, Ethiopia. *International Journal of Aquaculture and Fishery Sciences*, *1*(2), 48-53.

Assefa, A., Abunna, F., Biset, W., & Leta, S. (2018). Assessment of post-harvest fish losses in two selected lakes of Amhara Region, Northern Ethiopia. *Heliyon*, *4*(11), e00949.

Assis, E., Katsman, L., Ziskind, G., & Letan, R. (2007). Numerical and experimental study of melting in a spherical shell. *International Journal of Heat and Mass Transfer*, *50*(9-10), 1790-1804.

Atalay, H. (2019). Comparative assessment of solar and heat pump dryers with regards to exergy and exergoeconomic performance. *Energy*, *189*, 116180.

Ayyappan, S., & Mayilsamy, K. (2012). Solar tunnel drier with thermal storage for drying of copra. *International journal of energy technology and policy*, *8*(1), 3-13.

Bahrehmand, D., Ameri, M., & Gholampour, M. (2015). Energy and exergy analysis of different solar air collector systems with forced convection. *Renewable Energy*, *83*, 1119-1130.

Baniasadi, E., Ranjbar, S., & Boostanipour, O. (2017). Experimental investigation of the performance of a mixed-mode solar dryer with thermal energy storage. *Renewable energy*, *112*, 143-150.

Barbés, B., Páramo, R., Blanco, E., & Casanova, C. (2014). Thermal conductivity and specific heat capacity measurements of CuO nanofluids. *Journal of Thermal Analysis and Calorimetry*, *115*(2), 1883-1891.

Barbés, B., Páramo, R., Blanco, E., Pastoriza-Gallego, M. J., Pineiro, M. M., Legido, J. L., & Casanova, C. (2013). Thermal conductivity and specific heat capacity measurements of Al2O3 nanofluids. *Journal of Thermal Analysis and Calorimetry*, *111*(2), 1615-1625.

Bhardwaj, A. K., Chauhan, R., Kumar, R., Sethi, M., & Rana, A. (2017). Experimental investigation of an indirect solar dryer integrated with phase change material for drying valeriana jatamansi (medicinal herb). *Case studies in thermal engineering*, *10*, 302-314.

Bolaji, B. O., & Olalusi, A. P. (2008). Performance evaluation of a mixed-mode solar dryer.

Borém, F. M., Marques, E. R., and Alves, E. (2008). Ultrastructural analysis of drying damage in parchment Arabica coffee endosperm cells. *Biosystems Engineering*, *99*(1), 62-66.

Çebi, Ü. K., Aydin, B., Cakir, R., and Altintas, S. (2019). Energy use efficiency and economic analysis of greenhouse cucumber farming in Turkey: case of Thrace Region. *Cust. Agronegocio*, *15*(2), 2-21.

César, L. V. E., Lilia, C. M. A., Octavio, G. V., Isaac, P. F., & Rogelio, B. O. (2020). Thermal performance of a passive, mixed-type solar dryer for tomato slices (Solanum lycopersicum). *Renewable Energy*, *147*, 845-855.

Çomakli, Ö., Bayramoğlu, M., and Kaygusuz, K. (1996). A thermodynamic model of a solar assisted heat pump system with energy storage. *Solar Energy*, *56*(6), 485-492.

Cossu, M., Yano, A., Solinas, S., Deligios, P. A., Tiloca, M. T., Cossu, A., and Ledda, L. (2020). Agricultural sustainability estimation of the European photovoltaic greenhouses. *European Journal of Agronomy*, *118*, 126074.

Da Cunha, J. P., & Eames, P. (2016). Thermal energy storage for low and medium temperature applications using phase change materials–a review. *Applied energy*, *177*, 227-238.

Dawit, G. D. (2018). Thermal Analysis of Solar Flat Plate Collector Coupled with Heat Storage (Doctoral dissertation).

Delgado, M., Lázaro, A., Mazo, J., & Zalba, B. (2012). Review on phase change material emulsions and microencapsulated phase change material slurries: materials, heat transfer studies and applications. *Renewable and Sustainable Energy Reviews*, *16*(1), 253-273.

Dhiman, P. (2014). Performance modelling and analysis of double-pass packed-bed solar air heaters: an analytical framework. *International Journal of Sustainable Energy*, *33*(4), 811-826.

Duffie, J. A., Beckman, W. A., & Blair, N. (2020). *Solar engineering of thermal processes, photovoltaics and wind*. John Wiley & Sons.

Duffie, J. A., Beckman, W. A., and Blair, N. (2020). *Solar engineering of thermal processes, photovoltaics and wind*. John Wiley & Sons.

Esen, H. (2008). Experimental energy and exergy analysis of a double-flow solar air heater having different obstacles on absorber plates. *Building and Environment*, *43*(6), 1046-1054.

Gorjian, S., Calise, F., Kant, K., Ahamed, M. S., Copertaro, B., Najafi, G., and Shamshiri, R. R. (2021). A review on opportunities for implementation of solar energy technologies in agricultural greenhouses. *Journal of Cleaner Production*, *285*, 124807.

Günther, M., Joemann, M., Csambor, S., Guizani, A. and Krüger, D. (2011). Parabolic trough technology. Advanced CSP teaching materials, pp.1 -106.

Habtamu Tkubet. (2007). Simulation of Solar Cereal Dryer using TRNSYS. *Department of Mechanical Engineering, AAU*.

Hauer, A. (2007). Adsorption systems for TES—Design and demonstration projects. In *Thermal energy storage for sustainable energy consumption* (pp. 409-427). Springer, Dordrecht.

Hernandez, A. L., & Quiñonez, J. E. (2013). Analytical models of thermal performance of solar air heaters of double-parallel flow and double-pass counter flow. *Renewable Energy*, *55*, 380-391.

Hernández-Díaz, W. N., Hernández-Campos, F. J., Vargas-Galarza, Z., Rodríguez-Jimenes, G. C., and García-Alvarado, M. A. (2013). Coffee grain rotary drying optimization. *Revista Mexicana de ingeniería química*, *12*(2), 315-325.

Kalbande, S. R., Jadhav, P., Khambalkar, V. P., & Deshmukh, S. (2017). Design of solar dryer assisted with reflector for drying of medicinal crops. *International Journal of Current Microbiology and Applied Sciences*, *6*(2), 170-184.

Kaleemullah, S., & Kailappan, R. (2005). Drying kinetics of red chillies in a rotary dryer. *Biosystems Engineering*, *92*(1), 15-23.

Kalogirou, S. A. (2013). *Solar energy engineering: processes and systems*. Academic press.

Khawale, V. R., & Thakare, S. B. (2018). Modeling and Experimental Studies on Solar Crop Dryer Coupled with Reversed Absorber Type Solar Air Heater. *International Journal of Energy and Power Engineering*, *12*(3), 207-212.

Malekjani, N., & Jafari, S. M. (2018). Simulation of food drying processes by Computational Fluid Dynamics (CFD); recent advances and approaches. *Trends in Food Science & Technology*, *78*, 206-223.

Martin, S., Silva, J. N. D., Zanatta, F. L., Galvarro, S. F. S., and Volk, M. B. D. S. (2011). Evaluation of coffee drying costs: pre-drying on concrete terrace and complementary drying in co-current and counter-current flow dryer.

Motahayyer, M., Arabhosseini, A., Samimi-Akhijahani, H., and Khashechi, M. (2018). Application of computational fluid dynamics in optimization design of absorber plate of solar dryer. *Iranian Journal of Bio System Engineering*, *49*(2), 285-294.

Neira, M. J. M., Roa, M., and Correa, R. (2018). Thermal analysis of coffee hulls and their effect on the drying process in conventional ovens. *Indian Journal of Science and Technology*, *11*(36), 1-13.

Niyas, H., Prasad, S., & Muthukumar, P. (2017). Performance investigation of a lab–scale latent heat storage prototype–Numerical results. *Energy Conversion and Management*, *135*, 188-199.

Niyas, H., Rao, C. R. C., & Muthukumar, P. (2017). Performance investigation of a lab-scale latent heat storage prototype–experimental results. *Solar Energy*, *155*, 971-984.

Ozgen, F., Esen, M., & Esen, H. (2009). Experimental investigation of thermal performance of a double-flow solar air heater having aluminium cans. *Renewable Energy*, *34*(11), 2391-2398.

Pardhi, C. B., & Bhagoria, J. L. (2013). Development and performance evaluation of mixed-mode solar dryer with forced convection. *International journal of energy and environmental engineering*, *4*(1), 1-8.

Purohit, P., Kumar, A., and Kandpal, T. C. (2006). Solar drying vs. open sun drying: A framework for financial evaluation. *Solar energy*, *80*(12), 1568-1579.

Rohsenow, W. M., Hartnett, J. P., and Cho, Y. I. (1998). Handbook of heat transfer (Vol.3). New York: McGraw-Hill.

Rohsenow, W. M., Hartnett, J. P., and Ganic, E. N. (1985). Handbook of heat transfer applications.

Romdhane, S. B., Amamou, A., Khalifa, R. B., Said, N. M., Younsi, Z., & Jemni, A. (2020). A review on thermal energy storage using phase change materials in passive building applications. *Journal of Building Engineering*, *32*, 101563.

Sacilik, K. (2007). Effect of drying methods on thin-layer drying characteristics of hull-less seed pumpkin (Cucurbita pepo L.). *Journal of food engineering*, *79*(1), 23-30.

Sarbu, I., & Sebarchievici, C. (2018). A comprehensive review of thermal energy storage. *Sustainability*, *10*(1), 191.

Sfredo, M. A., Finzer, J. R. D., and Limaverde, J. R. (2002). Study of the drying process of Arabica coffee cherries using vibrated trays driers in the fine drink attainment. In *Proceedings of the 13th international drying Symposium (IDS 2002), Beijing China. B* (pp. 1342-1351).

Sfredo, M. A., Finzer, J. R. D., and Limaverde, J. R. (2005). Heat and mass transfer in coffee fruits drying. *Journal of Food Engineering*, *70*(1), 15-25.

Shanmugam, V., & Natarajan, E. (2007). Experimental study of regenerative desiccant integrated solar dryer with and without reflective mirror. *Applied thermal engineering*, *27*(8-9), 1543-1551.

Sharma, A., Tyagi, V. V., Chen, C. R., & Buddhi, D. (2009). Review on thermal energy storage with phase change materials and applications. *Renewable and Sustainable energy reviews*, *13*(2), 318-345.

Soodmand-Moghaddam, S., Sharifi, M., & Zareiforoush, H. (2019). Investigation of fuel consumption and essential oil content in drying process of lemon verbena leaves using a continuous flow dryer equipped with a solar pre-heating system. *Journal of cleaner production*, *233*, 1133-1145.

Swami, V. M., Autee, A. T., & Anil, T. R. (2018). Experimental analysis of solar fish dryer using phase change material. *Journal of Energy Storage*, *20*, 310-315.

Thakar, M. A., Jha, S. S., Phasinam, K., Manne, R., Qureshi, Y., & Babu, V. H. (2022). X ray diffraction (XRD) analysis and evaluation of antioxidant activity of copper oxide nanoparticles synthesized from leaf extract of Cissus vitiginea. *Materials Today: Proceedings*, *51*, 319-324.

Tian, Y., & Zhao, C. Y. (2013). A review of solar collectors and thermal energy storage in solar thermal applications. *Applied energy*, *104*, 538-553.

Wikipedia contributors. (2021, September 29). Rotary dryer. In *Wikipedia, The Free Encyclopedia*. Retrieved 07:51, November 28, 2021

Yang, J., Yang, L., Xu, C., & Du, X. (2016). Experimental study on enhancement of thermal energy storage with phase-change material. *Applied Energy*, *169*, 164-176.

Zalba, B., Marın, J. M., Cabeza, L. F., & Mehling, H. (2003). Review on thermal energy storage with phase change: materials, heat transfer analysis and applications. *Applied thermal engineering*, *23*(3), 251-283.

Zhou, D., Zhao, C. Y., & Tian, Y. (2012). Review on thermal energy storage with phase change materials (PCMs) in building applications. *Applied energy*, *92*, 593-605.

Zomorodian, A., Zare, D., & Ghasemkhani, H. (2007). Optimization and evaluation of a semi-continuous solar dryer for cereals (Rice, etc). *Desalination*, *209*(1-3), 129-135.

Zoukit, A., El Ferouali, H., Salhi, I., Doubabi, S., & Abdenouri, N. (2019). Simulation, design and experimental performance evaluation of an innovative hybrid solar-gas dryer. *Energy*, *189*, 116279.

APPENDIXES

Appendix-A: Experimental results of temperature during experimentation

Table A- 1: Average experimental result of solo greenhouse

Time	T-in	T-out	T-product	T-glass
9:00	27.6	32.4	34.6	37.4
9:30	28.3	36.5	37.5	40.4
10:00	30.0	39.5	41.5	43.5
10:30	30.9	43.4	45.7	47.5
11:00	30.5	49.6	51.5	49.6
11:30	31.2	54.6	52.3	52.3
12:00	32.2	57.5	57.3	53.6
12:30	33.3	62.4	60.4	54.4
13:00	33.3	65.6	66.7	57.6
13:30	34.1	68.4	70.4	56.3
14:00	32.7	65.7	68.5	54.1
14:30	31.5	60.1	65.4	50.8
15:00	30.3	56.5	59.3	48.7
15:30	29.5	49.8	51.5	46.5
16:00	28.7	44.5	49.8	44.6
16:30	28.2	42.2	44.5	42.1
17:00	27.5	41.2	42.1	39.4

Table A- 2: ***Average experimental Temperature of the combined system***

	Greenhouse Temperature				Enhanced collectors Temperature					Thermal storage		
Time	T-in	T-out	T-pro	T-gl	Tp1	Tp2	Tgl	Tin	Tout	Tin	Tout	Tpcm
9:00	36.4	50.9	34.6	37.4	50.5	48.3	37.4	27.1	45.6	48.4	33.5	43.2
9:30	39.8	53.4	37.5	40.4	58.5	54.6	40.4	27.8	47.9	50.9	41.0	45.3
10:00	44.3	58.3	41.5	43.5	62.6	55.4	43.5	29	50.4	55.8	45.5	47.5
10:30	49.9	61.7	45.7	47.5	70.1	60.2	47.5	29.7	56.7	59.2	51.1	48.2
11:00	54.1	65.6	51.5	49.6	75.1	68.1	49.6	29.6	59.4	63.1	55.3	50.4
11:30	56.5	67.6	52.3	52.3	81.2	66.4	52.3	30.2	62.5	65.1	57.7	54.3
12:00	60.8	75.1	57.3	53.6	89.3	65.8	53.6	31.1	68.6	68.6	62.0	56.9
12:30	63.7	78.0	60.4	54.4	91.5	69.0	54.4	32.2	72.5	70.4	64.9	60.4
13:00	66.0	79.9	66.7	57.6	97.1	66.0	57.6	32.8	76.4	72.5	67.2	63.5
13:30	69.1	77.7	70.4	56.3	94.5	78.4	56.3	33.6	79.6	73.2	69.7	67.3
14:00	65.9	71.0	68.5	54.1	88.6	76.0	54.1	32.4	74.5	65.3	70.5	60.5
14:30	65.0	70.9	65.4	50.8	80.4	73.3	50.8	31.6	70.6	60.1	73.4	59.7
15:00	60.9	63.5	59.3	48.7	76.3	69.7	48.7	30.4	66.4	57.3	68.5	55.3
15:30	59.4	58.2	51.5	46.5	71.4	64.1	46.5	29.6	60.5	52.1	64.3	51.4
16:00	55.3	60.3	49.8	44.6	65.4	57.0	44.6	28.9	54.3	53.2	60.5	49.2
16:30	51.6	54.9	44.5	42.1	54.9	51.0	42.1	28.1	48.4	50.3	56.4	47.5
17:00	48.7	52.7	42.1	39.4	49.2	47.9	39.4	27.5	43.2	48.7	53.2	45.3

Appendix-B: Descriptions and calibration of instruments

Instruments used in this experimentation are digital thermocouple, digital thermometer digital thermometer and U-tube manometer. Their accuracy and calibration as follow.

Table B- 1: Instruments and their accuracy

Instruments	Type	Range	Accuracy	Error	Used to measure
Digital thermocouple	k-type	0 to 800 ^{O}C	±0.5 ^{O}C	2%	System component temperature using thermocouple wires
Digital thermometer	k-type	-50 to +200 ^{O}C	±0.1 ^{O}C	0.25%	Ambient temperature and calibration
Digital weight balance		0.01 g to 10 kg	±0.01 g	0.05%	Mass of coffee beans and mass of copper oxide nanoparticle
U-tube manometer		Xx to xx mm	±0.02mm	0.5%	Measure pressure difference of blower and fan

Digital weight balance calibration was made by pressing calibration button mounted on digital weight balance.

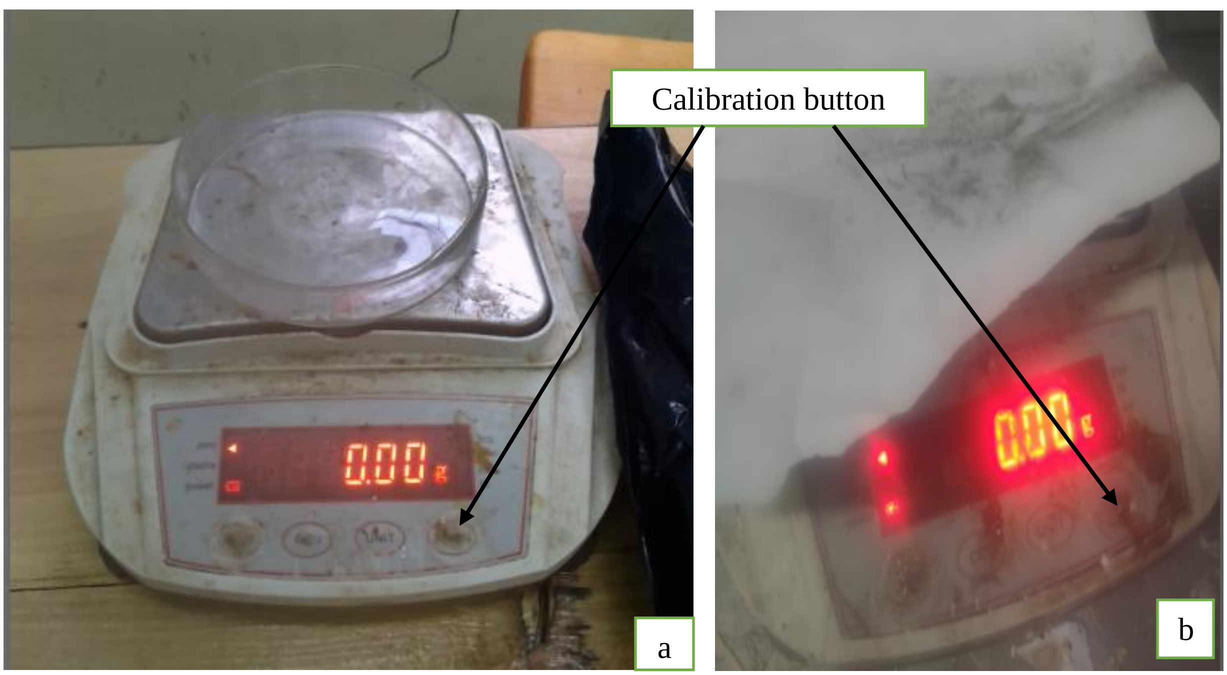

Figure B- 1: Digital weight balance calibration ; a) calibration of Petri dish, b) calibration of paper

Calibration of thermometers can be carried out using a reference thermometer in a temperature calibration test by comparing both measurement values of a reference thermometer and other thermometers. Calibration test for four channel digital k-type thermocouple was conducted in thermal laboratory with standard laboratory thermocouples (WL362 model) by using 0.2kg water boiling and cooling test for 31 minutes in 2-minute gap.

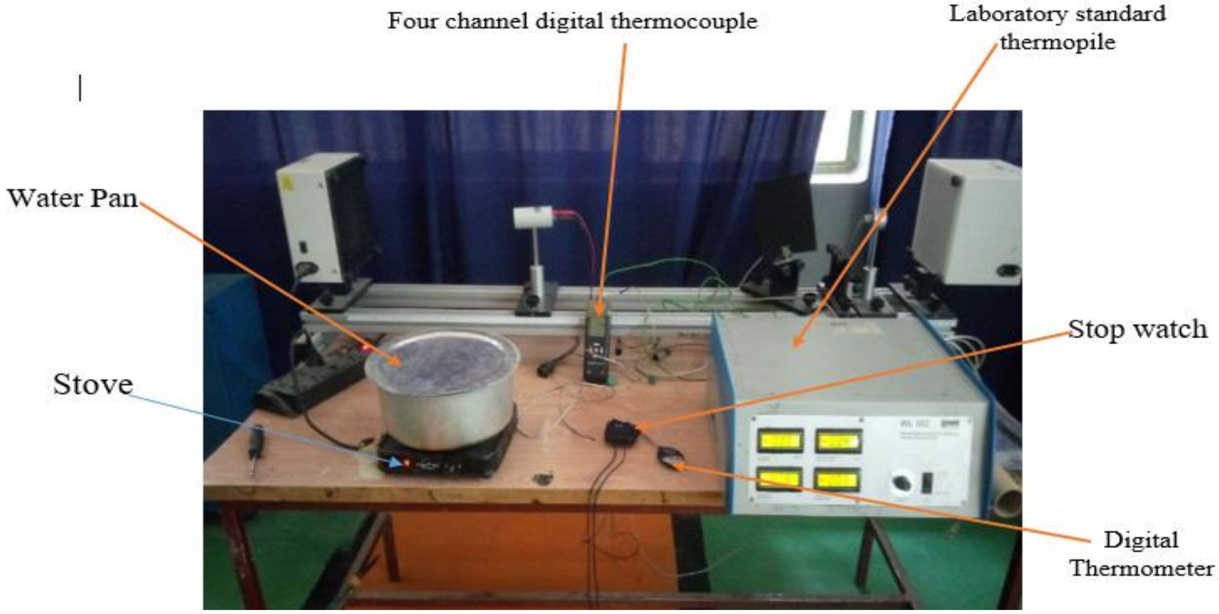

Figure B- 2: Calibration of thermocouple set up

Table B- 2: Water temperature measuring test by using k-type thermocouples

Time (minute)	TR(Reference thermometer)(^{O}C)	TM (Digital four channel Thermocouple)(^{O}C)
1	29.8	30.1
3	35.4	35.6
5	42.1	46.3
7	49.8	53.1
9	54.9	58.3
11	64.1	64.6
13	69.4	69.8
15	74.2	74.8
17	77.1	77.9
19	79.5	79.3

21	82.2	82.6
23	84.8	84.1
25	87.1	87.5
27	89.9	90.2
29	92.3	92.5
31	93.4	94.2

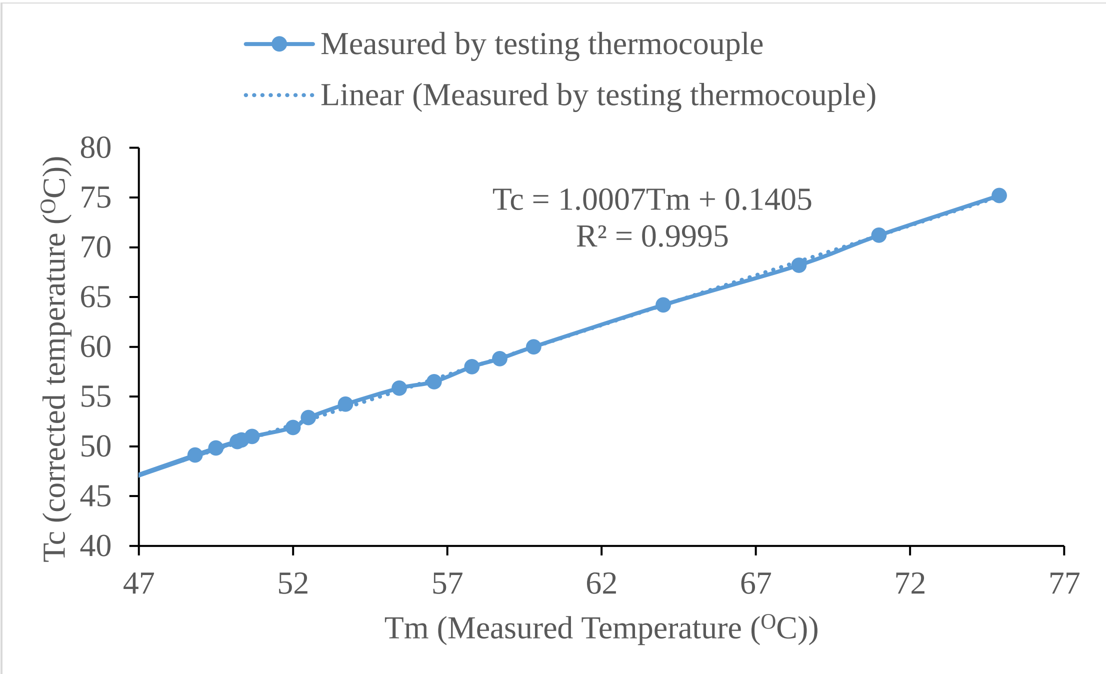

Figure B- 3: Calibration of Thermocouple; measured vs corrected temperature